Effective Neural Approximations for Geometric Optimization Problems

Samantha Chen
Computer Science and Engineering
University of California, San Diego
sac003@ucsd.edu

Oren Ciolli
Computer Science and Engineering
University of California, San Diego
ociolli@ucsd.edu

Anastasios Sidiropolous
Computer Science and Engineering
University of Illinois, Chicago
sidiropo@uic.edu

Yusu Wang
Halıcıoğlu Data Science Institute
University of California, San Diego
yusuwang@ucsd.edu

Abstract

Neural networks offer a promising data-driven approach to tackle computationally challenging optimization problems. In this work, we introduce neural approximation frameworks for a family of geometric "extent measure" problems, including shape-fitting descriptors (e.g. minimum enclosing ball or annulus). Central to our approach is the *alignment* of our neural model with a new variant of the classical ε-kernel technique from computational geometry. In particular, we develop a new relaxed-ε-kernel theory that maintains the approximation guarantees of the classical ε-kernels but with the crucial benefit that it can be implemented with *bounded model complexity* (i.e, constant number of parameters) by the simple SumFormer neural network. This leads to a simple neural model that approximate quantities such as the directional width of any input point set and empirically shows good out-of-distribution generalization. Many geometric extent measures, such as the minimum enclosing spherical shell, cannot be directly captured by ε-kernels. To this end, we show that an encode-process-decode framework with our kernel-approximating NN used as the "process" module can approximate such extent measures, again, with bounded model complexity where parameters scale only with the approximation error ε and not the size of the input set. Empirical results on diverse point-cloud datasets demonstrate the practical performance of our models.

1 Introduction

Using neural networks to solve optimization problems in a data-driven manner has received great attention in recent years [9, 45, 19, 30]. However, one challenge in using neural networks to solve optimization problems is that their architectures often grow with problem size [23]. The key question we consider is the design of practical neural models that both have the capacity to approximate solutions to specific optimization problems with *bounded model complexity* (i.e. number of parameters is independent of the size of input), and perform well in practice. A direction that has shown promise both theoretically and practically is *neural algorithmic alignment* [37, 38, 44, 36], which intuitively informs architecture design via loosely imitating ("alignment" with) certain algorithmic frameworks to achieve improved accuracy and out-of-distribution (OOD) generalization.

Our overall motivation is to design efficient and practical neural models to solve problems in a data-driven manner. In this paper, we study this problem in the context of a particular family of

39th Conference on Neural Information Processing Systems (NeurIPS 2025).

geometric optimization problems and demonstrate that biasing the model architecture towards some algorithmic flow yields more efficient and accurate approximations. In particular, we aim to compute a variety of point cloud descriptors, such as convex hulls, bounding volumes (e.g. minimum enclosing ball or ellipsoids), or best shapes fitting an input point set (e.g, the minimum-width slabs or spherical shells that cover an input set of points). These problems are called *extent measure problems* and are well-studied in computational geometry; e.g, [10, 2, 1, 46, 21, 16, 6, 11]. We show how biasing our model architectures towards a particularly well-known approximation technique known as the ε-kernel [3, 27, 2, 11] results in neural networks which can approximate the aforementioned point cloud descriptor with *bounded model complexity*, or a constant number of parameters which is independent to input size.

New work. In the high level, the type of geometric problems we consider have the following form: Given an arbitrary set of points P in $\mathbb{R}^d$, the goal is to compute a certain geometric descriptor $\mu(P)$ for P. We want to train a suitable neural network model that can approximate $\mu(P)$ efficiently for *any* input point set P. We draw inspiration from an elegant line of work in computational geometry that approximately solves these problems using the ε-coreset framework via ε-kernels; see Section 2 for detailed descriptions. Our contributions can be summarized as follows.

Neural approximation of ε-kernels. An ε-kernel Q of a set of points P is a subset of P that approximately preserves the projection of P along any direction in $\mathbb{R}^d$. Once Q is given, one can approximate a family of geometric descriptors (e.g, the convex hull of P) by computing them using Q in time dependent only on $|Q|$ and not on $|P|$. However, computing the ε-kernel is not naturally aligned with common neural models for point clouds. We instead introduce an alternative theory of *relaxed-ε-kernels*, which retain the same approximation guarantees while aligning naturally with the simple Sumformer [5] (a variant of DeepSets [47]). This leads to an efficient neural model that approximates relaxed ε-kernels with *bounded model complexity* independent of size of input point set P.

Neural approximations of extent measures. Among the so-called *unfaithful extent measures* which cannot be directly approximated by ε-kernels, a family of them can nevertheless be approximated via the *linearization* technique [4]. In Section 4, we show that our relaxed-ε-kernel can still be combined with the linearization technique to approximate such extent measures. We further employ an *encode-process-decode* framework (introduced by [37] to solve algorithmic tasks) where our relaxed ε-kernel neural network will be used as the processor module. See Figure 1. This framework can approximate both faithful and a family of unfaithful extent measures using only bounded model complexity.

Empirical performance. Importantly, we empirically demonstrate the accuracy (both in and out of distribution) and efficiency of the proposed neural models both for approximating ε-kernels and several (faithful and unfaithful) extent measures (e.g, minimum enclosing balls / annulus) in comparison to both natural neural baselines and algorithmic approaches. Our Sumformer instantiated neural model consistently exhibits much stronger OOD generalization than Transformer-instantiated neural models for these tasks, which we think is partially due to the alignment of the Sumformer model with our relaxed-ε-kernel algorithm.

In summary, the encode-process-decode framework instantiated with our relaxed ε-kernel NN as the processor network is both practical and theoretically sound, and can solve a family of geometric optimization problems accurately. Importantly, our models offer the advantage of being differentiable, enabling them to be used in downstream ML pipelines. Our neural approach also provides greater flexibility in comparison to classical algorithmic techniques: our framework can tackle tasks where the objective is hidden and only implicitly given via labeled examples. In contrast to classical algorithms which can not be used without knowing the target objective, our model can still efficiently learn the objective in a data-driven manner, as long as the underlying goal corresponds to a variant of the shape-fitting problem (even when unknown).

Related work. This paper discusses efficient neural approximations of a certain family of geometric optimization problems on point clouds. As such, we will discuss relevant work related to neural point cloud processing and neural network approximations of general optimization problems. In particular, deep learning on geometric data – especially point clouds – has advanced rapidly. Two foundational permutation-equivariant models are DeepSets [47] and PointNet [29, 28]. Both DeepSets and PointNet have universal approximation guarantees; however, general universal approximation of permutation

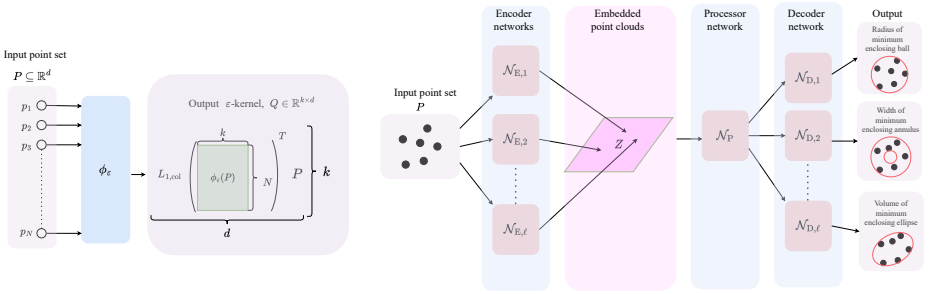

(a) (b)

Figure 1: Illustration of (a) our kernel-approx-NN, and (b) our encode-decode-process framework for approximating various extent measures. The processor module $\mathcal{N}_{\text{P}}$ can be frozen as a pre-trained kernel-approx-NN, and only encoder / decoder needs to be trained in a task-dependent manner.

invariant functions requires the internal latent dimension *depend on the size of the input point set* [40, 12]. In geometric deep learning, it is also common to use geometry-enhanced graph neural networks to process point clouds; see the proto-book [8] for a comprehensive discussion. Recent work has seen a shift to Transformer based architectures for point cloud processing [48, 41, 42, 24, 14].

In recent years there have been great interest in using ML to help tackle combinatorial optimization problems; e.g, [39, 19, 22, 32, 13, 31], and surveys [7, 9]. Theoretically, there are also several works on the best possible approximation guarantees one can get from these neural network approaches [23, 31, 45, 30, 17]. However, bounded model complexity usually is not guaranteed, other than [18, 25], which use hybrid neural-algorithmic models. Our work uses neural algorithmic alignment ideas [37, 38, 44] to develop practical neural networks with bounded model complexity.

2 Preliminaries

Transformers. A standard Transformer is the composition of multiple Transformer blocks, each of which models a sequence-to-sequence permutation equivariant function using a specific attention mechanism. For simplicity, below we introduce the formulation using just a single attention head: Given a sequence $X \in \mathbb{R}^{n \times d}$ (a length-n sequence of vectors in $\mathbb{R}^d$), the output of a single attention block $\mathcal{T}$ is another length-n sequence $\mathcal{T}(X) \in \mathbb{R}^{n \times d}$ defined by

$$\mathcal{T}(X) = \text{MLP}(X + \text{Attn}(X)XW_V), \quad \text{where} \quad \text{Attn}(X) = \text{softmax}(XW_Q(XW_K)^T).$$

Here, $W_Q, W_K, W_V \in \mathbb{R}^{d \times d}$ are matrices and $\text{MLP} : \mathbb{R}^d \to \mathbb{R}^d$ operates element-wise on each of the n elements. (We fix the internal dimension to be d for simplicity of presentation.) Sequences for language tasks typically use positional encodings, e.g rotary PEs [33], to encode ordering information. However, since we are concerned with processing point clouds, each point in an input point cloud P has its coordinates in $\mathbb{R}^d$; hence we omit positional encodings. For a Transformer with *bounded complexity*, i.e, total number of parameters is a constant independent of n, it still takes $O(n^2)$ time per forward pass when processing an input point set of size n.

Sumformers. A Sumformer [5] is a sequence-to-sequence permutation equivariant model formed by composition of blocks defined as follows:

Definition 2.1 (Sumformer Block)**.** *A* Sumformer block *is a sequence-to-sequence function $\mathcal{S} : \mathcal{X}^n \to \mathcal{Y}^n$, such that for any length-n sequence $X = [x_1, \ldots, x_n] \in \mathcal{X}^n$, the output is another length-n sequence in $\mathcal{Y}^n$ defined by $\mathcal{S}(X) = \mathcal{S}([x_1, \ldots, x_n]) = [\psi(x_1, Z), \ldots, \psi(x_n, Z)]$, where $Z := \sum_{i=1}^n \phi(x_i)$, $\phi : \mathcal{X} \to \mathbb{R}^{d'}$, and $\psi : \mathcal{X} \times \mathbb{R}^{d'} \to \mathcal{Y}$. Usually, both the input and output feature spaces are Euclidean: $\mathcal{X} = \mathbb{R}^{d_1}$ and $\mathcal{Y} = \mathbb{R}^{d_2}$.*

Intuitively, at each layer, a Sumformer block first computes a global representation of the input sequence via sum-aggregation (the quantity Z above), and then computes the individual representation of each input token from its initial encoding and the global representation Z via the function ψ (i.e, $\mathcal{S}(X)[i] = \psi(x_i, Z)$). Conceptually, it is similar to the DeepSet architecture [47], but each layer is not necessarily a linear equivariant layer. Unlike the Transformer, the SumFormer takes linear

time per forward pass as computing Z takes $\Theta(n)$ time while computing each $\psi(x_i, Z)$ takes only constant time, assuming d' and the dimensions of $\mathcal{X}$ and $\mathcal{Y}$ are constant.

ε-kernels and coresets. A classical technique in developing approximation algorithms for geometric problems is via the extraction of a certain small representative subset of the input object, called ε-coresets, and solving the problem only on the small subset. A popular coreset construction is via the ε-kernels. First, given a set of points P and a direction $u \in \mathbf{S}^{d-1}$ with $\mathbf{S}^{d-1}$ denoting the unit-sphere in $\mathbb{R}^d$, the **directional interval** $\overrightarrow{\mathsf{w}}_u(P)$ and **directional width** $\mathsf{w}_u(P)$ w.r.t. u are defined as:

$$\overrightarrow{\mathsf{w}}_u(P) = \left[\min_{p\in P}\langle u, p\rangle, \max_{p\in P}\langle u, p\rangle\right]; \text{ and } \mathsf{w}_u(P) = \max_{p\in P}\langle u, p\rangle - \min_{p\in P}\langle u, p\rangle = \text{length of } \overrightarrow{\mathsf{w}}_u(P).$$

Definition 2.2 (ε-kernel)**.** *Given a set of point $P \subseteq \mathbb{R}^d$, an ε-kernel for P is* **a subset of points** *$Q \subseteq P$ such that for any $u \in \mathbf{S}^{d-1}$, $w_u(Q)$ is an ε-approximation of $w_u(P)$; i.e., $(1-\varepsilon)w_u(P) \leq w_u(Q)$.*

Hence, an ε-kernel Q of P approximates the width of P along any direction u. In this paper, we assume that any input point set P is contained within a bounded compact set in $\mathbb{R}^d$; in fact, w.l.o.g., assume each P is contained in the d-D hypercube $\mathbb{C}_d = [-1, 1]^d$. Let $\mathrm{CH}(P)$ denote the *convex hull* of P consisting of all convex combinations of points in P. Our theoretical results in this paper will assume that each point set P is not too "skinny", in the sense that it is "fat": A point set $P \subseteq \mathbb{R}^d$ is α**-fat** if there exist $0 < \alpha \leq 1$ and $\vec{o} \in \mathbb{R}^d$ such that $\vec{o} + \alpha\mathbb{C}_d \subseteq \mathrm{CH}(P) \subseteq \vec{o} + \mathbb{C}_d$.

We now explain the utility of ε-kernels for extent measures. An **extent measure** μ is a function that maps any point set $P \subset \mathbb{R}^d$ to a real value such that $\mu(P') \leq \mu(P)$ for all $P' \subset P$. Examples include the diameter of point set P, the minimum radius of any ball covering P (i.e, the radius of the minimum enclosing ball of P), the minimum width of any slab (parallel hyperplane) containing P, and the minimum width of any spherical or cylindrical shells containing P.

Definition 2.3 (Coresets and faithful extent measures)**.** *$Q \subseteq P$ is an ε-**coreset for** P **w.r.t.** μ if $\mu(P) \leq (1+\varepsilon)\mu(Q)$. An extent measure μ is **faithful** if there exists $c > 0$ such that every ε-kernel Q of P is a $c\varepsilon$-coreset for μ.*

Note that ε-kernel is defined w.r.t. directional width; while ε-coreset is defined for a target extent measure. Intuitively, μ is a faithful measure if any ε-kernel of P serves as a valid ε-coreset for P w.r.t. this measure μ. Examples of faithful measures include diameter, smallest enclosing-ball radius, min-width of any enclosing slab, and bounding-box volume. For a faithful measure μ, once an ε-kernel Q is computed for P, evaluating $\mu(Q)$ yields a ε-approximation to $\mu(P)$ in time *depending only on* $|Q|$. In short, computing ε-kernels leads to approximations of faithful extent measures. In the next Section 4, we will discuss approximations of *unfaithful extent measures*.

Motivating example. Before introducing our neural architecture, we provide a motivating example: the minimum enclosing ball. Given a set of points $P \subseteq \mathbb{R}^d$, the minimum enclosing ball is the smallest-radius ball that contains all of P. In Figure 2, we compare two natural end-to-end neural network approaches, one using a *Sumformer* and the other a *Transformer*, to directly predict the radius of the minimum enclosing ball from the input point set. We also compare with the algorithmically aligned encoder-processor-decoder network that we propose later in the paper. Each model is trained with point clouds of size 100 sampled uniformly from $[-5, 5]^2$ and tested on point clouds of increasing sizes and bounding boxes (see Appendix for details).

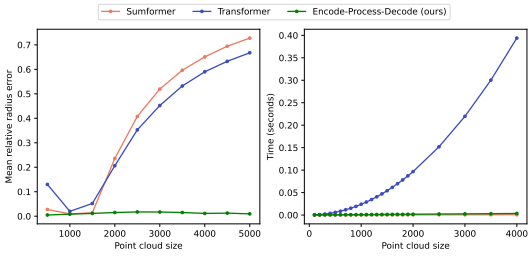

Figure 2: Comparison of error (left) and inference time (right) of the Transformer, Sumformer, and encode-process-decode approaches for estimating the radius of the minimum enclosing ball.

The error is shown on the left side of Figure 2 and we see that *neither* end-to-end approach generalize across sizes since the error grows rapidly as the size of the point cloud increases. In contrast, our encode-process-decode approach maintains low error across sizes as its error rate remains flat. On the right side of Figure 2, we see that our new encode-process-decode approach is as efficient as Sumformer (time complexity grows linearly), while Transformer grows quadratically. In what follows, we show how the encode-process-decode aligns with the ε-kernel and can therefore approximate extent measures with bounded model complexity.

3 Neural approximations of relaxed-ε-kernels

The previous section states that for faithful measures, computing ε-kernels leads to their approximation for any input point-set P. Hence intuitively, we wish to have a neural architecture to compute ε-kernels. It turns out that existing algorithms to construct ε-kernels all require being able to identify the exact extreme point(s) in various projects, which does not easily align with Transformer nor SumFormer. Instead, we will propose a variant of the classical ε-kernels, called *the relaxed-ε-kernel*, which shares similar theoretical guarantees as ε-kernels. We then develop a simple Sumformer-based neural model that can efficiently approximate a relaxed-ε-kernel with *bounded model complexity*.

Algorithm 1 Relaxed-ε-kernels

Require: $P = \{p_1, \ldots, p_n\} \subseteq \mathbb{R}^d, k$
1: $\Omega \leftarrow$ set of k directions from $\mathbf{S}^{d-1}$
2: $Q \leftarrow \{\}$
3: **for** $u \in \Omega$ **do**
4: $\quad A_u \leftarrow \{\langle u, p\rangle : p \in P\}$
5: $\quad w(A_u) \leftarrow \max A_u - \min A_u$
6: $\quad$ Compute $\rho_\varepsilon(A_u)$
7: $\quad q_u \leftarrow (\sigma(\rho_\varepsilon(A_u)))^T P$
8: $\quad Q$.append(q_u)
9: **end for**
10: **return** Q

Set $M_{A_u} := \max(A_u) = \max_{p \in P} \langle u, p\rangle$

$$\rho_\varepsilon(A_u) = \begin{pmatrix} \mathrm{ReLU}(\langle u, p_1\rangle + \varepsilon w(A_u) - M_{A_u}) \\ \mathrm{ReLU}(\langle u, p_2\rangle + \varepsilon w(A_u) - M_{A_u}) \\ \vdots \\ \mathrm{ReLU}(\langle u, p_n\rangle + \varepsilon w(A_u) - M_{A_u}) \end{pmatrix}$$

Let $\sigma : \mathbb{R}^n \to \mathbb{R}^n$ such that

$$\sigma(x) = \left[\frac{e^{x_1} - 1}{\sum_i^n (e^{x_i} - 1)} \cdots \frac{e^{x_n} - 1}{\sum_i^n (e^{x_i} - 1)}\right]^T$$

Figure 3: An algorithm for computing relaxed ε-kernels. The functions ρ_ε and σ are defined on the right. Notice that σ is a modified softmax function.

3.1 Relaxed ε-kernels

Definition 3.1 (Relaxed-ε-kernel)**.** *Given a set of points $P \subseteq \mathbb{R}^d$, a relaxed ε-kernel is a set of points $Q \subseteq CH(P)$ such that for any $u \in \mathbf{S}^{d-1}$, we have $(1-\varepsilon)w_u(P) \leq w_u(Q)$.*

Unlike a standard ε-kernel, where the output points must be a subset of P, the relaxed-ε-kernel allows each output to be *convex combinations* of input points (as guaranteed by $Q \subset CH(P)$). See Figure 4 for a visualization. The key is to show the relaxed-ε-kernels can replace ε-kernels in approximating faithful extent measures. Indeed, this is guaranteed by the following theorem (through the relaxed ε-coreset). The proofs are in Appendix A.3.1. In addition to the relaxed-ε-kernel, we define an analogous relaxed-ε-coreset and show that it has the same approximation guarantees for faithful measures μ. Specifically, a **relaxed ε-coreset** of P w.r.t μ is a set of points $Q \subseteq \mathbf{CH}(P)$ (versus $Q \subset P$) such that $(1-\varepsilon)\mu(Q) \leq \mu(P) \leq (1+\varepsilon)\mu(Q)$.

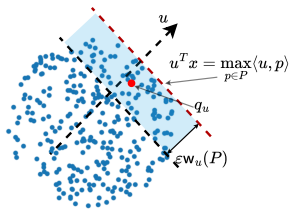

Figure 4: q_u is the convex combination of points in the shaded region.

Theorem 3.2. *Let μ be a faithful measure with constant c. Let $0 < \varepsilon < \frac{1}{6c}$. There exists c' such that for any P, any relaxed ε-kernel Q for P is a relaxed $c'\varepsilon$-coreset for P.*

A NN-aligned relaxed-ε-kernel construction. A relaxed-ε-kernel for P can be computed by Algorithm 1. Intuitively, we pick a fixed set of directions Ω and for each $u \in \Omega$, we output a point $q_u \in \mathbb{R}^d$ which is a convex combination of points in P whose projections onto u are within $\varepsilon w_u(P)$ of the maximum. $\rho_\varepsilon(A_u)$ computes an indicator vector for such points, and $(\sigma(\rho_\varepsilon(A_u)))^T P$ then computes q_u, where σ is the modified softmax function described in Algorithm 1 and q_u is a convex combination of the points in P.

Theorem 3.3 (proof in Appendix A.3.1) below shows that the quality of the output of Algorithm 1 depends on the "fatness" of the input point set P. We also need to choose an appropriate set of

directions Ω: in particular, Ω is a $\frac{\alpha\varepsilon}{4\sqrt{d}}$-net for all possible unit directions $\mathbf{S}^{d-1}$. Note that a set A is a δ-net of a metric space (X, d_X) if $A \subset X$ and for any point $x \in X$, there exists $a \in A$ such that $d_X(x, a) \leq \delta$. It is easy to construct a δ-net of $\mathbf{S}^{d-1}$ of size $O(1/\delta^{d-1})$ where the distance between two directions is measured as the angle between them.

Theorem 3.3. *Let $P \subset [-1, 1]^d$ be a α-fat point set and let $0 < \varepsilon < \frac{1}{3}$. Suppose Ω^+ is an $\frac{\alpha\varepsilon}{4\sqrt{d}}$-net for $\mathbf{S}^{d-1}$ s.t. $|\Omega| = O\Big(\frac{1}{(\frac{\alpha\varepsilon}{4\sqrt{d}})^{d-1}}\Big)$. Let $\Omega^- = \{-u : u \in \Omega^+\}$ and let $\Omega = \Omega^- \cup \Omega^+$ so for all $u \in \Omega$, $-u \in \Omega$. Then the set of points Q constructed via Algorithm 1 is a relaxed-3ε-kernel of P.*

3.2 Relaxed-ε-kernel approximating NN architecture

Given an arbitrary point set $P \subseteq \mathbb{C}_d$, we will represent $P \in \mathbb{R}^{N\times d}$ as a sequence of d-vectors where $N = |P|$. Given $X \in \mathbb{R}^{N\times k}$, let σ_{col} denote column-wise application of the modified softmax normalization described in Algorithm 1 (i.e. we apply σ to each column in X). First, we introduce a general neural framework of a specific form: given $P \in \mathbb{R}^{N\times d}$, it will output k points in $\mathbb{R}^d$; that is, $\mathcal{N}_{\phi_\varepsilon}(P) \in \mathbb{R}^{k\times d}$, as follows:

$$\mathcal{N}_{\phi_\varepsilon}(P) = \sigma_{\text{col}}(\phi_\varepsilon(P))^T P, \tag{1}$$

where ϕ_ε is a sequence-to-sequence permutation equivariant model that maps a sequence of points in $\mathbb{R}^d$ to a sequence of points in $\mathbb{R}^k$. Note that regardless of the length of the input sequence P (i.e., N), the output $\mathcal{N}_{\phi_\varepsilon}(P)$ is always in $\mathbb{R}^{k\times d}$, viewed as k points in $\mathbb{R}^d$. The model ϕ_ε can be instantiated with any permutation equivariant neural network: such as a Sumformer $\mathcal{S}_\varepsilon$ or a Transformer $\mathcal{T}_\varepsilon$. The resulting final model $\mathcal{N}_{\phi_\varepsilon}$ is then denoted by $\mathcal{N}_{\mathcal{S}_\varepsilon}(P) = \sigma_{\text{col}}(\mathcal{S}_\varepsilon(P))^T P$ for the SumFormer instantiation or $\mathcal{N}_{\mathcal{T}_\varepsilon}(P) = \sigma_{\text{col}}(\mathcal{T}_\varepsilon(P))^T P$ for the Transformer instantiation. See Figure 1 (a). We will use the Sumformer implementation $\mathcal{N}_{\mathcal{S}_\varepsilon}$, as the following result shows that this simple model is sufficient to align with the computation of a relaxed-ε-kernel.

Theorem 3.4. *Given any $\varepsilon, \alpha > 0$, there exists a SumFormer $\mathcal{S}_\varepsilon$ with only a single block, and bounded model complexity (depending only on ε, α, and the input dimension d) such that, for any α-fat point clouds $P \subset \mathbb{R}^d$ of arbitrary size, $\mathcal{N}_{\mathcal{S}_\varepsilon}(P)$ is a relaxed-ε-kernel for P.*

Intuitively, the SumFormer $\mathcal{S}_\varepsilon(P) \in \mathbb{R}^{N\times k}$ can easily simulate the computation of the collection of $\rho_\varepsilon(A_u)$'s, for all k number of $u \in \Omega$, as in Algorithm 1. Line 7 of Algorithm 1 is then computed by the outer columnwise-softmax normalization as in Eqn. (1), thereby outputting k points in $\mathbb{R}^d$ which form a relaxed-ε-kernel for input point set P. We refer to the neural network model $\mathcal{N}_{\mathcal{S}_\varepsilon}$ in Theorem 3.4 as our *relaxed-ε-kernel-approximating-neural network*, abbrev. *kernel-approx-NN*.

With our kernel-approx-NN, it is now easy to construct a bounded-complexity neural network to approximate *faithful extent measures*. Consider any faithful extent measure μ: For any input point set P, once we are given a relaxed-ε-kernel Q of P, we can simply compute $\mu(Q)$ as an approximation of $\mu(P)$. By Theorem 3.4, the k points $\mathcal{N}_{\phi_\varepsilon}(P) \in \mathbb{R}^{k\times d}$ form a relaxed-ε-kernel of P, for a suitable ε depending on the output size k. By Definition 2.3, we can compute $\mu(\mathcal{N}_{\phi_\varepsilon}(P))$ as an approximation of $\mu(P)$. Note that μ can be viewed as a **permutation-invariant function** as its output does not change as the ordering of input points change. Hence we can use a DeepSet architecture [47] to approximate μ: in particular, we set our *faithful-measure-approximating NN* as $\mathcal{N}_{\text{faithful}}(P) = \mathcal{N}_{\text{deepset}}(\mathcal{N}_{\phi_\varepsilon}(P))$. Deepset models are universal approximators for permutation-invariant functions where the model complexity depends on the maximum input size (e.g, [40, 34]) – in our case, the input is of size $k \times d$ (k points in $\mathbb{R}^d$ as computed by our kernel-approx-NN $\mathcal{N}_{\mathcal{S}_\varepsilon}$). Hence the model complexity of $\mathcal{N}_{\text{deepset}}$ is also bounded, depending only k, thus only on ε, α and d, and not on the size of original input point set P. Indeed, the following corollary implies that we have a NN with bounded complexity that can approximate extent measures such as diameter, radius of minimum-enclosing ball, and width of minimum-width slab, for input point set of arbitrary size.

Corollary 3.5. *For any $\varepsilon > 0, \alpha > 0$ and a faithful extent measure μ with constant c as in Definition 2.3, there exists a bounded-complexity NN of the form $\mathcal{N}_{\text{faithful}}(P) = \mathcal{N}_{\text{deepset}}(\mathcal{N}_{\phi_\varepsilon}(P))$, such that for any α-fat point set P, the output $\mathcal{N}_{\text{faithful}}(P)$ satisfies that:*

$$(1 - 3c\varepsilon)\mu(P) - \varepsilon \leq \mathcal{N}_{\text{faithful}}(P) \leq (1 + 3c\varepsilon)\mu(P) + \varepsilon$$

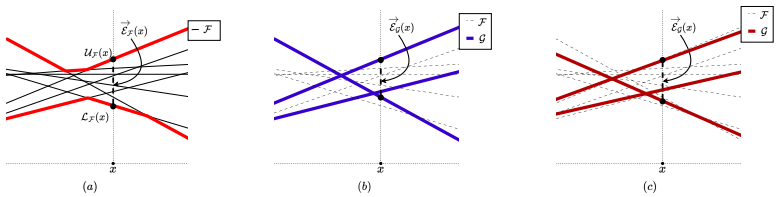

Figure 5: (a) Upper / lower envelopes and the extent vector for a family of linear functions. Thick curves in (b) form an ε-kernel $\mathcal{G}$ of $\mathcal{F}$ and those thick curves in (c) is a relaxed-ε-kernel. Dashed lines are those in $\mathcal{F}$. Note that, unlike (b), a relaxed-ε-kernel does not need to be a subset of $\mathcal{F}$.

4 Neural approximations of unfaithful extent measures

The ε-kernel framework can also be used to derive efficient approximations for a certain family of unfaithful measures via the so-called"linearization" trick [2]. We briefly describe the high-level idea, which follows the same framework as [2]. We will show that our relaxed-ε-kernel can replace the role of ε-kernel in this approach. First, we need to define (relaxed-)ε-kernels for *sets of functions* (instead of points). The way to handle those unfaithful extent measures is to first convert them to higher-dimensional **linear functions** via the linearization technique. Specifically, given a set of real-valued functions $\mathcal{F} = \{f_1, \ldots, f_n : \mathbb{R}^{d-1} \to \mathbb{R}\}$, its *upper envelope* is the function $U_{\mathcal{F}} : \mathbb{R}^{d-1} \to \mathbb{R}$ where $U_{\mathcal{F}}(x) = \max_{f \in \mathcal{F}} f(x)$, while its *lower envelope* is defined by $L_{\mathcal{F}}(x) = \min_{f \in \mathcal{F}} f(x)$.

Definition 4.1. *Given a set of functions $\mathcal{F} = \{f_1, \ldots, f_n\}$, where $f_i : \mathbb{R}^{d-1} \to \mathbb{R}$, its* **extent** *is $\mathcal{E}_{\mathcal{F}}(x) = U_{\mathcal{F}}(x) - L_{\mathcal{F}}(x)$ and its* **extent-interval** *is $\overrightarrow{\mathcal{E}}_{\mathcal{F}}(x) = [L_{\mathcal{F}}(x), U_{\mathcal{F}}(x)]$. An* **$\varepsilon$-kernel** *for $\mathcal{F}$ is a set $\mathcal{G} \subseteq \mathcal{F}$ such that $\mathcal{E}_{\mathcal{G}} \geq (1-\varepsilon)\mathcal{E}_{\mathcal{F}}$.*

See Figure 5. We define analogous concepts for relaxed-ε-kernels. Given two intervals $I_1 = [a, b]$ and $I_2 = [c, d]$, the *Hausdorff distance* between them equals $max\{|a-c|, |b-d|\}$.

Definition 4.2 (Relaxed-ε-kernels for sets of functions)**.** *A* relaxed ε-kernel *for $\mathcal{F}$ is a* **set** *$\mathcal{G}$ of functions (not necessarily subset of $\mathcal{F}$) such that for any $x \in \mathbb{R}^{d-1}$, we have that (i) $\overrightarrow{\mathcal{E}}_{\mathcal{G}}(x) \subseteq \overrightarrow{\mathcal{E}}_{\mathcal{F}}(x)$ and (ii) the Hausdorff distance between $\overrightarrow{\mathcal{E}}_{\mathcal{G}}(x)$ and $\overrightarrow{\mathcal{E}}_{\mathcal{F}}(x)$ is at most $\varepsilon \cdot \mathcal{E}_{\mathcal{F}}(x)$.*

Now consider a linear function $f(x) = a_1 x_1 + \cdots + a_{d-1} x_{d-1} + a_d$, where $x = [x_1, \ldots, x_{d-1}]^T \in \mathbb{R}^{d-1}$: This linear function represents a hyperplane in $\mathbb{R}^d$. Its dual is the point $f^* := [a_1, \ldots, a_d]^T \in \mathbb{R}^d$. Symmetrically, given a point $p = [p_1, \ldots, p_d]^T \in \mathbb{R}^d$, its dual hyperplane is the linear function $p^*(x) = p_1 x_1 + \ldots + p_{d-1} x_{d-1} + p_d$. Given a set of **linear functions** $\mathcal{F} = \{f_1, \ldots, f_n\}$, let $\mathcal{F}^* = \{f_1^*, \ldots, f_n^*\} \subset \mathbb{R}^d$ denote its dual point set. Note that $(f^*)^* = f$ and $(\mathcal{F}^*)^* = \mathcal{F}$.

Theorem 4.3. *$\mathcal{G}$ is a relaxed ε-kernel for the set of linear functions $\mathcal{F}$ if and only if $\mathcal{G}^*$ is a relaxed ε-kernel for the point set $\mathcal{F}^*$.*

Often we want to find the extent or ε-kernels for sets of non-linear functions. Depending on the functions, it is possible to *linearize* them as follows [2]: Suppose $\mathcal{F}$ is a set of $(d+p)$-variate polynomials $\mathcal{F} = \{f_i(x) = f(x, a_i) : i \in [N], x \in \mathbb{R}^d, a_i \in \mathbb{R}^p\}$. We say that $\mathcal{F}$ *admits a linearization of dimension m* if there exist p-variate polynomials $\psi_0, \ldots, \psi_m : \mathbb{R}^p \to \mathbb{R}$ and d-variant polynomials $\varphi_1, \ldots, \varphi_m : \mathbb{R}^d \to \mathbb{R}$ such that for each f_i, we can write it as

$$f_i(x) = f(x, a_i) = \psi_0(a_i) + \psi_1(a_i)\varphi_1(x) + \cdots + \psi_k(a_i)\varphi_m(x).$$

Now define functions $\Psi : \mathbb{R}^p \to \mathbb{R}^{m+1}$ and $\Phi : \mathbb{R}^d \to \mathbb{R}^{m+1}$ as $\Psi(a) = [\psi_0(a), \ldots, \psi_m(a)]^T$ for any $a \in \mathbb{R}^p$ and $\Phi(x) = [1, \varphi_1(x), \ldots, \varphi_m(x)]^T$ for any $x \in \mathbb{R}^d$. Then we can view f_i as a new **linearized form** $f(x, a_i) = \Psi(a_i)^T \Phi(x)$ in space $\mathbb{R}^{m+1}$. For standard ε-kernels, finding the ε-kernel for the dual of the set of linearized functions gives an ε-kernel for the set of original functions. In Theorem 4.4 we prove that we can also construct a relaxed-ε-kernel for a set of functions $\mathcal{F}$ from an ε-kernel of the dual set after linearization.

Theorem 4.4. *Suppose $\mathcal{F}$ is a set of N number of $(d+p)$-variate polynomials which admit a linearization of dimension m; i.e. there is a set of $A = \{a_1, \ldots, a_N\} \subseteq \mathbb{R}^p$, $\Psi : \mathbb{R}^p \to \mathbb{R}^{m+1}$ and $\Phi : \mathbb{R}^d \to \mathbb{R}^{m+1}$, such that $\mathcal{F} = \{f_i(x) = \Psi(a_i)^T \Phi(x) : a_i \in A, i \in [N]\}$, and the dual $\mathcal{F}^* = \{\Psi(a_i) : i \in [N]\}$. Let $\mathcal{Q}_\varepsilon^* \subseteq \mathbb{R}^{m+1}$ be a relaxed-ε-kernel for $\mathcal{F}^*$ of size k computed via Alg. 1. Suppose $\mathcal{Q}_\varepsilon^* = \{\alpha_1^j \Psi(a_1) + \cdots + \alpha_N^j \Psi(a_N) : j \in [k], \sum \alpha_\ell^j = 1, \alpha_\ell^j \geq 0\}$. Then the set of functions $\mathcal{Q}_\varepsilon := \{q^T \Phi(x) : q \in \mathcal{Q}_\varepsilon^*\}$ is a relaxed-ε-kernel for the original set of functions $\mathcal{F}$.*

Finally, as shown in [2], a family of unfaithful extent measures can be transformed to finding the *smallest extent* $\mathcal{E}^*_{\mathcal{F}} = min_x \mathcal{E}_{\mathcal{F}}(x)$ of a set of N functions $\mathcal{F}$(constructed from the input pointset P with $N = |P|$) that admit a linearization, and thereby can be approximated by computing the smallest extent of the relaxed-ε-kernel $\mathcal{Q}_\varepsilon$ as computed in Theorem 4.4. Once $\mathcal{Q}_\varepsilon$ is computed, finding the smallest extent $\mathcal{E}^*_{\mathcal{Q}_\varepsilon}$ takes time only depending on $|\mathcal{Q}_\varepsilon|$ and indepent to the original pointset size P. We provide an example in Appendix A.2 of how relaxed-ε-kernels can be used to approximate the width of the minimum enclosing annulus for a point cloud.

Neural framework for approximating unfaithful extent measures. In order to approximate those unfaithful extent measures that can be solved via linearization, we make use of the encode-process-decode framework proposed in [15]. Given $\mathcal{X}$ which is the space of point clouds, a point cloud $P \in \mathcal{X}$, and an extent measure $\mu : \mathcal{X} \to \mathbb{R}^d$, we define

$$\mathcal{N}_{\text{extent}}(P) = \mathcal{N}_{\text{D}}(\mathcal{N}_{\text{P}}(\mathcal{N}_{\text{E}}(P))) \tag{2}$$

Intuitively, given a size-N pointset $P \in \mathbb{R}^{N\times d}$, the encoder $\widehat{P} = \mathcal{N}_{\text{E}}(P) \in \mathbb{R}^{N\times(m+1)}$ computes the linearization which maps P to a size-N (dual) point set in $\mathbb{R}^{m+1}$. The process-network $\mathcal{N}_{\text{P}}$ then outputs a size-k relaxed-ε-kernel, and the decoder $\mathcal{N}_{\text{D}}$ network computes the final approximation of the extent measure. Importantly, for the process-network $\mathcal{N}_{\text{P}}$, we use our ε-kernel approximating neural network $\mathcal{N}_{\phi_\varepsilon}$ defined in Equation (1), and given $\widehat{P} = \mathcal{N}_{\text{E}}(P)$, the output of processor $\mathcal{N}_{\text{P}}(\widehat{P}) \in \mathbb{R}^{k\times(m+1)}$ is a size-k relaxed-ε-kernel for $\widehat{P}$. See a visualization of this architecture in Figure 1 and note that this is exactly the encode-process-decode framework from our motivating example in Figure 2. Note that the encoder $\mathcal{N}_{\text{E}}$ can be any **permutation equivariant** architecture. In our experiments, we simply apply an MLP to each element of P so $\mathcal{N}_{\text{E}}([p_1, \ldots, p_N]) = [\text{MLP}(p_1), \ldots, \text{MLP}(p_N)]$. The decoder $\mathcal{N}_{\text{D}}$ can be implemented by any universal **permutation invariant** architecture. In our experiments, we use DeepSet as the final decoder, $\mathcal{N}_{\text{D}}$, to compute the final approximation of the extent architecture. Note that we can also use $\mathcal{N}_{\text{extent}}$ to approximate faithful extent measures as $\mathcal{N}_{\text{E}}$ can be set to the identity function. In our experiments, we use this encoder-process-decoder $\mathcal{N}_{\text{extent}}$ to approximate both faithful and unfaithful extent measures.

5 Experiments

We evaluate both our kernel-approx-NN (cf. Eqn. (1)) to approximate relaxed-ε-kernels as well as our encode-process-decode framework (cf. Eqn. (2)) for extent measure approximation tasks (faithful and unfaithful). Throughout this section, we report the best results after a hyperparameter search. All details regarding training and datasets are given in Appendix A.4.

Our experiments use (i) two synthetic datasets 'Gaussian Mixture' (point clouds from 2 to 5 random Gaussian clusters), and 'Mixed Synthetic' (a mixture of synthetically generated point clouds, including 'Ellipse', 'Gaussian Mixture' and more), and (ii) two real datasets, SQUID [26] (2D point clouds generated from boundary contours of fish) and the 3D ModelNet [43]. In the main text, we present average evaluation metrics over all test data; the Appendix provides complete results, including standard deviations, and further experiments demonstrating that fixed-size models continue to perform well on OOD point sets (across varied sampling schemes and sizes).

Relaxed-ε-kernel approximation. We examine the performance of the kernel-approx-NN (cf. Equation (1)) using both Sumformers and Transformers as ϕ_ε in $\mathcal{N}_{\phi_\varepsilon}$; and we denote these different instantiations as $\mathcal{S}_\varepsilon$ and T_ε, respectively. We also compare against a direct neural baseline that directly outputs a coarsened point cloud aggregating encoded point features and passing the result through an MLP to produce the final output point cloud. The Sumformer and Transformer implementations of this baseline are denoted $\mathcal{S}_{\varepsilon,\text{B}}$ and $\mathcal{T}_{\varepsilon,\text{B}}$, respectively. We also include a comparison to the classical ε-kernel and our relaxed ε-kernel algorithms, both with $\varepsilon = 0.1$, denoted $\mathcal{B}_{\varepsilon,E}$ and $\mathcal{B}_{\varepsilon,R}$, respectively. For performance, we use the *directional width error* to measure the error caused by our approximation: $\mathcal{E}_{\text{dir}}(P, \tilde{Q}) = \max_{u\in\Omega} \frac{|\mathsf{w}_u(P) - \mathsf{w}_u(\tilde{Q})|}{\mathsf{w}_u(P,u)}$ where P is the input point set, $\tilde{Q}$ is the output of our kernel-approx-NN, and Ω is a set of 1000 random directions. We report results for datasets in $\mathbb{R}^2$ and in $\mathbb{R}^3$ in Table 1. Additional results for point clouds in $\mathbb{R}^5$, as well as many other experiments including effects of hyperparameters (e.g. width of latent dimension), are given in the Appendix. Overall, using Sumformer instantiation $\mathcal{S}_\varepsilon$ as $\mathcal{N}_{\phi_\varepsilon}$ consistently yields lower error on OOD data than the Transformer-instantiation $\mathcal{T}_\varepsilon$. This gap is most striking on real world datasets: when trained on the synthetic datasets ('Mixed Synthetic or 'Gaussian Mixture'), the $\mathcal{S}_\varepsilon$ has significantly lower error

Table 1: $\mathcal{E}_{\text{dir}}$ for predicted relaxed-ε-kernels of size 16 and 64 respectively, for point clouds in $\mathbb{R}^2$ (left) and $\mathbb{R}^3$ (right) across three different test sets for each train set. 'In-dist.' refers to in-distribution test sets. "Mixed Synthetic" has no "OOD, Synthetic" because the train set contains all types of synthetic data. Similarly, the models trained on SQUID and ModelNet are not OOD on those test sets (so unreported). Since algorithmic baselines do not require training, they have no 'In-dist' error. Boldface indicates the lower error (better accuracy).

		Test Sets		
			OOD	
Train Set	**Method**	In-dist.	Synthetic	SQUID
Gaussian Mixture	$\mathcal{S}_\varepsilon$	**0.014**	**0.043**	**0.028**
	$\mathcal{T}_\varepsilon$	0.027	0.097	0.218
	$\mathcal{S}_{\varepsilon,\text{B}}$	0.146	0.146	0.962
	$\mathcal{T}_{\varepsilon,\text{B}}$	0.190	0.383	0.94
SQUID	$\mathcal{S}_\varepsilon$	**0.028**	0.504	-
	$\mathcal{T}_\varepsilon$	0.061	**0.400**	-
	$\mathcal{S}_{\varepsilon,\text{B}}$	0.421	7.137	-
	$\mathcal{T}_{\varepsilon,\text{B}}$	0.228	14.561	-
Mixed Synthetic	$\mathcal{S}_\varepsilon$	**0.027**	–	**0.065**
	$\mathcal{T}_\varepsilon$	0.032	–	0.296
	$\mathcal{S}_{\varepsilon,\text{B}}$	0.094	-	0.97
	$\mathcal{T}_{\varepsilon,\text{B}}$	0.203	-	0.939
Algorithmic Baselines	$\mathcal{B}_{\varepsilon,R}$	-	0.180	0.228
	$\mathcal{B}_{\varepsilon,E}$	-	0.040	0.062

		Test Sets		
			OOD	
Train Set	**Method**	In-dist.	Synthetic	ModelNet
Gaussian Mixture	$\mathcal{S}_\varepsilon$	**0.047**	**0.039**	**0.064**
	$\mathcal{T}_\varepsilon$	0.054	0.066	0.250
	$\mathcal{S}_{\varepsilon,\text{B}}$	0.274	0.223	1.949
	$\mathcal{T}_{\varepsilon,\text{B}}$	0.357	0.803	5.514
ModelNet	$\mathcal{S}_\varepsilon$	**0.041**	**0.099**	-
	$\mathcal{T}_\varepsilon$	0.049	0.265	-
	$\mathcal{S}_{\varepsilon,\text{B}}$	0.379	0.528	-
	$\mathcal{T}_{\varepsilon,\text{B}}$	0.542	0.581	-
Mixed Synthetic	$\mathcal{S}_\varepsilon$	**0.035**	–	**0.055**
	$\mathcal{T}_\varepsilon$	0.042	–	0.117
	$\mathcal{S}_{\varepsilon,\text{B}}$	0.174	-	2.288
	$\mathcal{T}_{\varepsilon,\text{B}}$	0.289	-	4.356
Algorithmic Baselines	$\mathcal{B}_{\varepsilon,R}$	-	1.016	2.176
	$\mathcal{B}_{\varepsilon,E}$	-	0.062	0.050

than $\mathcal{T}_\varepsilon$ when tested on OOD samples from SQUID (in $\mathbb{R}^2$) and ModelNet (in $\mathbb{R}^3$). While $\mathcal{T}_\varepsilon$ also has the capacity to implement Algorithm 1, we believe that the simple and more direct alignment of $\mathcal{S}_\varepsilon$ with this algorithm leads to faster training (optimization) and better (OOD) generalization.

Approximating extent measures. We train the encode–process–decode model (Eq. 2) to predict three extent measures: radius of minimum enclosing ball (MEB), radii (and therefore area) of minimum enclosing ellipse (MEE), and width of minimum-width annulus (MEA) covering input points. The first two are faithful extent measures, while the last is unfaithful. We compare two instantiations of the general model $\mathcal{N}_{\text{extent}}$: (i) $\mathcal{S}_{\text{extent}}$ when using the Sumformer within the processor model $\mathcal{N}_{\text{P}}$, and (ii) $\mathcal{T}_{\text{extent}}$ when using the Transformer.

To examine the contribution of the relaxed-ϵ-kernel module when used as $\mathcal{N}_{\phi_\varepsilon}$, we compare two training protocols: (1) full end-to-end optimization of the entire pipeline (denoted as 'E2E') and (2) a regime in which the inner kernel-approx-NN is fixed after being pre-trained to output a relaxed-ε-kernel (denoted as 'Frozen'), and then only the encoder and decoder are trained based on the specific task. To understand the effect of mapping input point to a relaxed-ε-kernel in the processor module, we also construct a baseline where we do not use Equation (1) to compute a coreset. Instead, we use the output $\phi_\varepsilon(\widehat{P})$ (where $\widehat{P} = \mathcal{N}_{\text{E}}(P)$) and feed it to the decoder $\mathcal{N}_{\text{D}}$. $\mathcal{S}_{\text{Baseline}}$ and $\mathcal{T}_{\text{Baseline}}$ to denote the Sumformer and Transformer instantiations of this baseline model. Additionally, we also compare against the proposed direct neural approximations described in Section 2, with Sumformer and Transformer implementations denoted as $\mathcal{S}_{\text{Direct}}$ and $\mathcal{T}_{\text{Direct}}$. An extended comparison to classical algorithmic baselines in terms of both accuracy and runtime is also included in Appendix A.4.

The results for all three extent measures are shown in Table 2 and we evaluate the performance as follows: (1) For MEB, we measure the relative error $\mathcal{E}_{\text{r}}$ of predicted minimum-radius over the true optimal. (2) For MEE, we use the relative errors of both predicted major and minor radii (denoted as $\mathcal{E}_{\text{r},maj}$ for the major radius and $\mathcal{E}_{\text{r},min}$ for the minor radius). (3) For the MEA, we use the relative error for the predicted smallest width $\mathcal{E}_{\text{w}}$. To measure the quality of our returned geometric shape, we also compute $\mathcal{E}_{\text{p}}$, the percentage of input points not covered by these approximations. These results are in the Appendix and usually this portion is very small (around 1-2$\%$).

All results in Table 2 are for in-distribution test sets: e.g, if they are trained on SQUID, then the test sets are also from SQUID. The term "Synthetic" in Table 2 refers to different datasets for different tasks (see Appendix A.4 for details). From Table 2, we see that in almost all cases, "$\mathcal{S}_{\text{extent}}$ (Frozen)" achieves the best result (lowest error). In general Sumformer versions outperform corresponding Transformer versions, which is suggestive of the benefit of the alignment (resemblance) of Sumformer-instantiated kernel-approx-NN with Algorithm 1. In the case of Sumformer versions of neural models,

Table 2: Error metrics across MEB, MEE, and MEA (standard deviations in Appendix). $\mathcal{E}_r$: relative radius error of MEB $\mathcal{E}_{r,\min}$ / $\mathcal{E}_{r,\text{maj}}$: minor/major radius errors of MEEs $\mathcal{E}_w$: error in MEA width. Boldface marks the best (lowest) value in each column.

Train Set	Method	MEB	MEE		MEA
		$\mathcal{E}_r$	$\mathcal{E}_{r,\min}$	$\mathcal{E}_{r,\text{maj}}$	$\mathcal{E}_w$
Synthetic	$\mathcal{S}_{\text{extent}}$ (Frozen)	**0.009**	**0.037**	**0.022**	0.050
	$\mathcal{S}_{\text{extent}}$ (E2E)	0.023	0.056	0.047	**0.038**
	$\mathcal{T}_{\text{extent}}$ (Frozen)	0.099	0.041	0.027	0.083
	$\mathcal{T}_{\text{extent}}$ (E2E)	0.024	0.038	0.022	0.077
	$\mathcal{S}_{\text{Baseline}}$	0.048	0.378	0.426	0.674
	$\mathcal{T}_{\text{Baseline}}$	0.030	0.071	0.047	0.417
	$\mathcal{S}_{\text{Direct}}$	0.126	0.033	0.038	0.141
	$\mathcal{T}_{\text{Direct}}$	0.178	0.932	0.887	0.079

Train Set	Method	MEB	MEE		MEA
		$\mathcal{E}_r$	$\mathcal{E}_{r,\min}$	$\mathcal{E}_{r,\text{maj}}$	$\mathcal{E}_w$
SQUID	$\mathcal{S}_{\text{extent}}$ (Frozen)	0.017	**0.056**	0.047	0.073
	$\mathcal{S}_{\text{extent}}$ (E2E)	**0.010**	0.078	0.050	0.087
	$\mathcal{T}_{\text{extent}}$ (Frozen)	0.068	0.058	**0.032**	0.064
	$\mathcal{T}_{\text{extent}}$ (E2E)	0.190	0.093	0.045	0.104
	$\mathcal{S}_{\text{Baseline}}$	0.027	0.322	0.250	0.191
	$\mathcal{T}_{\text{Baseline}}$	0.039	0.357	0.049	0.118
	$\mathcal{S}_{\text{Direct}}$	0.050	0.68	0.05	**0.041**
	$\mathcal{T}_{\text{Direct}}$	0.685	1.269	0.188	0.065

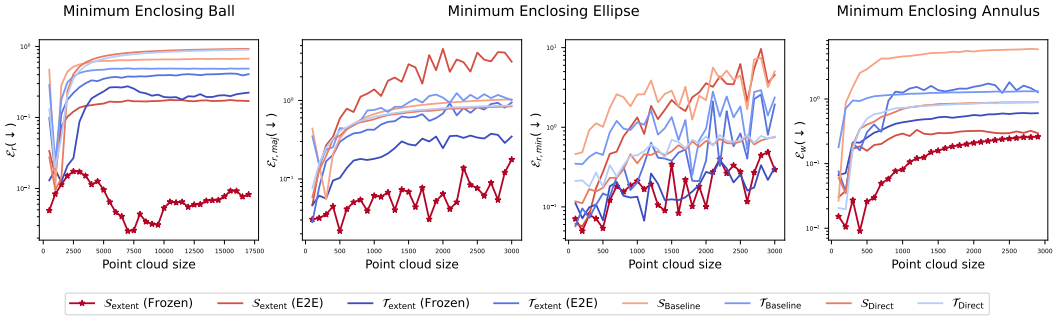

Figure 6: Size generalization across all extent measure tasks. We record the error for each model on extent measure tasks as the size and bounding box of the input point cloud increases. Our frozen $\mathcal{S}_{\text{extent}}$ model consistently outperforms all other neural baselines across every task.

the "Frozen" version (where the processor module is pre-trained then frozen, and only the encoder and decoder will be trained in a task driven manner) is usually much better than the "E2E" version. This advantage, however, is less clear for the Transformer based models. Finally, while the direct models outperform our models in terms of $\mathcal{E}_{\text{w}}$ for MEA on the SQUID dataset, refer to Table 15 in Appendix A.4 to see that our models achieve more geometrically faithful predictions, reducing the proportion of excluded points by approximately one third.

Additionally, we examine how each model's error changes as the size of the input point cloud increases (i.e., its size generalization capability) across all extent-measure problems in Figure 6. Each model in this experiment is trained on synthetic data generated from within the bounding box $[-5, 5]^2$. For the test data, we simultaneously scale both the number of input points and the size of the bounding box from which each point cloud is sampled. Extended details for the experiment set-up are in Appendix A.4. The results in Figure 6 highlight the advantage of the Sumformer-instantiated kernel-approx-NN as the "$\mathcal{S}_{\text{extent}}$ (Frozen)" has much better generalization as compared to all other neural models. Visualizations of the solutions in Figure 14 (Appendix A.4) for in-distribution and out-of-distribution data for each problem even more suggestive of how aligning the processor network explicitly with relaxed-ε-kernel can better adjust to OOD data.

6 Conclusion and Limitations

We introduce an alternative theory of relaxed-ε-kernels which we show naturally aligns with a SumFormer-based architecture to approximate a family of faithful and unfaithful extent measure problems using bounded model complexity. Empirically, we demonstrate the benefits of *alignment* of our SumFormer instantiated models and the effectiveness of our (encoder-process-decoder) architecture, especially in better OOD generalization performance. Some limitations include: The model complexity still depends on the dimension (but not the size) of the input point sets. Also our theoretical results depend on the "fatness" of the input point sets. Nevertheless, our work shows the benefits of neural-algorithmic alignments and opens the door to further explorations of how the interplay between task structure, classical algorithmic approaches, and network design yields better performance, both theoretically and empirically.

7 Acknowledgements

This work is partially supported by NSF (National Science Foundation) by grants CCF-2112665 as well as a NAIRR Pilot Project NAIRR250087.

References

[1] Pankaj K Agarwal, Boris Aronov, and Micha Sharir. Exact and approximation algorithms for minimum-width cylindrical shells. *Discrete & Computational Geometry*, 26:307–320, 2001.

[2] Pankaj K Agarwal, Sariel Har-Peled, and Kasturi R Varadarajan. Approximating extent measures of points. *Journal of the ACM (JACM)*, 51(4):606–635, 2004.

[3] Pankaj K Agarwal, Sariel Har-Peled, Kasturi R Varadarajan, et al. Geometric approximation via coresets. *Combinatorial and computational geometry*, 52(1):1–30, 2005.

[4] Pankaj K. Agarwal and Jirí Matousek. On range searching with semialgebraic sets. *Discrete & Computational Geometry*, 11(4):393–418, 1994.

[5] Silas Alberti, Niclas Dern, Laura Thesing, and Gitta Kutyniok. Sumformer: Universal Approximation for Efficient Transformers. In *Topological, Algebraic and Geometric Learning Workshops 2023*, pages 72–86. PMLR, 2023.

[6] Gill Barequet and Sariel Har-Peled. Efficiently approximating the minimum-volume bounding box of a point set in three dimensions. *Journal of Algorithms*, 38(1):91–109, 2001.

[7] Yoshua Bengio, Andrea Lodi, and Antoine Prouvost. Machine learning for combinatorial optimization: a methodological tour d'horizon. *European Journal of Operational Research*, 290(2):405–421, 2021.

[8] Michael M. Bronstein, Joan Bruna, Taco Cohen, and Petar Velickovic. Geometric Deep Learning: Grids, Groups, Graphs, Geodesics, and Gauges. *CoRR*, abs/2104.13478, 2021.

[9] Quentin Cappart, Didier Chételat, Elias B Khalil, Andrea Lodi, Christopher Morris, and Petar Veličković. Combinatorial optimization and reasoning with graph neural networks. *Journal of Machine Learning Research*, 24(130):1–61, 2023.

[10] Timothy M Chan. Approximating the diameter, width, smallest enclosing cylinder, and minimum-width annulus. In *Proceedings of the sixteenth annual symposium on Computational geometry*, pages 300–309, 2000.

[11] Timothy M Chan. Faster core-set constructions and data stream algorithms in fixed dimensions. In *Proceedings of the twentieth annual symposium on Computational geometry*, pages 152–159, 2004.

[12] Nadav Dym and Steven J Gortler. Low-dimensional invariant embeddings for universal geometric learning. *Foundations of Computational Mathematics*, pages 1–41, 2024.

[13] Maxime Gasse, Didier Chételat, Nicola Ferroni, Laurent Charlin, and Andrea Lodi. Exact combinatorial optimization with graph convolutional neural networks. *Advances in Neural Information Processing Systems*, 32:15580–15592, 2019.

[14] Meng-Hao Guo, Jun-Xiong Cai, Zheng-Ning Liu, Tai-Jiang Mu, Ralph R Martin, and Shi-Min Hu. PCT: Point cloud transformer. *Computational visual media*, 7:187–199, 2021.

[15] Jessica B. Hamrick, Kelsey R. Allen, Victor Bapst, Tina Zhu, Kevin R. McKee, Joshua B. Tenenbaum, and Peter W. Battaglia. Relational inductive bias for physical construction in humans and machines. In *Proceedings of the Annual Conference of the Cognitive Science Society (CogSci)*, pages 1773–1778, Madison, Wisconsin, USA, 2018.

[16] Sariel Har-Peled and Yusu Wang. Shape fitting with outliers. In *Proceedings of the nineteenth annual symposium on Computational geometry*, pages 29–38, 2003.

[17] Yu He and Ellen Vitercik. Primal-Dual Neural Algorithmic Reasoning. In Aarti Singh, Maryam Fazel, Daniel Hsu, Simon Lacoste-Julien, Felix Berkenkamp, Tegan Maharaj, Kiri Wagstaff, and Jerry Zhu, editors, *Proceedings of the 42nd International Conference on Machine Learning*, volume 267 of *Proceedings of Machine Learning Research*, pages 22743–22766. PMLR, Jul 2025.

[18] Andrew B Kahng, Robert R Nerem, Yusu Wang, and Chien-Yi Yang. NN-Steiner: A mixed neural-algorithmic approach for the rectilinear Steiner minimum tree problem. In *Proceedings of the AAAI Conference on Artificial Intelligence*, volume 38, pages 13022–13030, 2024.

[19] Elias Khalil, Hanjun Dai, Yuyu Zhang, Bistra Dilkina, and Le Song. Learning combinatorial optimization algorithms over graphs. *Advances in neural information processing systems*, 30, 2017.

[20] Diederik P Kingma. Adam: A method for stochastic optimization. *arXiv preprint arXiv:1412.6980*, 2014.

[21] Piyush Kumar and E Alper Yildirim. Minimum-volume enclosing ellipsoids and core sets. *Journal of Optimization Theory and applications*, 126(1):1–21, 2005.

[22] Zhuwen Li, Qifeng Chen, and Vladlen Koltun. Combinatorial optimization with graph convolutional networks and guided tree search. *Advances in Neural Information Processing Systems*, 31:537–546, 2018.

[23] Andreas Loukas. What graph neural networks cannot learn: depth vs width. *arXiv preprint arXiv:1907.03199*, 2019.

[24] Dening Lu, Qian Xie, Mingqiang Wei, Kyle Gao, Linlin Xu, and Jonathan Li. Transformers in 3d point clouds: A survey. *arXiv preprint arXiv:2205.07417*, 2022.

[25] Evan McCarty, Qi Zhao, Anastasios Sidiropoulos, and Yusu Wang. NN-Baker: A Neural-network Infused Algorithmic Framework for Optimization Problems on Geometric Intersection Graphs. In *Advances in Neural Information Processing Systems*, volume 34, 2021.

[26] Farzin Mokhtarian and Sadegh Abbasi. Shape similarity retrieval under affine transforms. *Pattern Recognition*, 35(1):31–41, 2002.

[27] Jeff M Phillips. Coresets and sketches. In *Handbook of discrete and computational geometry*, pages 1269–1288. Chapman and Hall/CRC, 2017.

[28] Charles R. Qi, Li Yi, Hao Su, and Leonidas J. Guibas. PointNet++: Deep Hierarchical Feature Learning on Point Sets in a Metric Space. In *Advances in Neural Information Processing Systems (NeurIPS)*, pages 5099–5108, 2017.

[29] Charles Ruizhongtai Qi, Hao Su, Kaichun Mo, and Leonidas J. Guibas. PointNet: Deep Learning on Point Sets for 3D Classification and Segmentation. In *2017 IEEE Conference on Computer Vision and Pattern Recognition, CVPR 2017, Honolulu, HI, USA, July 21-26, 2017*, pages 77–85. IEEE Computer Society, 2017.

[30] Chendi Qian and Christopher Morris. Towards graph neural networks for provably solving convex optimization problems. *arXiv preprint arXiv:2502.02446*, 2025.

[31] Ryoma Sato, Makoto Yamada, and Hisashi Kashima. Approximation Ratios of Graph Neural Networks for Combinatorial Problems. In *Advances in Neural Information Processing Systems*, volume 32, 2019.

[32] Daniel Selsam, Matthew Lamm, Bunz Benedikt, Percy Liang, Leonardo de Moura, David L Dill, et al. Learning a SAT solver from single-bit supervision. In *Proceedings of the International Conference on Learning Representations (ICLR)*, 2018.

[33] Jianlin Su, Murtadha Ahmed, Yu Lu, Shengfeng Pan, Wen Bo, and Yunfeng Liu. Roformer: Enhanced transformer with rotary position embedding. *Neurocomputing*, 568:127063, 2024.

[34] Puoya Tabaghi and Yusu Wang. Universal representation of permutation-invariant functions on vectors and tensors. In *35th Intl. Conf. Algorithmic Learning Theory (ALT)*, 2024.

[35] The CGAL Project. *CGAL User and Reference Manual*. CGAL Editorial Board, 6.1 edition, 2025.

[36] Petar Veličković, Adrià Puigdomènech Badia, David Budden, Razvan Pascanu, Andrea Banino, Misha Dashevskiy, Raia Hadsell, and Charles Blundell. The CLRS algorithmic reasoning benchmark. In *International Conference on Machine Learning*, pages 22084–22102. PMLR, 2022.

[37] Petar Veličković and Charles Blundell. Neural algorithmic reasoning. *Patterns*, 2(7), 2021.

[38] Petar Veličković, Rex Ying, Matilde Padovano, Raia Hadsell, and Charles Blundell. Neural Execution of Graph Algorithms. In *International Conference on Learning Representations*.

[39] Oriol Vinyals, Meire Fortunato, and Navdeep Jaitly. Pointer networks. *Advances in neural information processing systems*, 28, 2015.

[40] Edward Wagstaff, Fabian B Fuchs, Martin Engelcke, Michael A Osborne, and Ingmar Posner. Universal approximation of functions on sets. *Journal of Machine Learning Research*, 23(151):1–56, 2022.

[41] Changshuo Wang, Meiqing Wu, Siew-Kei Lam, Xin Ning, Shangshu Yu, Ruiping Wang, Weijun Li, and Thambipillai Srikanthan. GPSFormer: A global perception and local structure fitting-based transformer for point cloud understanding. In *European Conference on Computer Vision*, pages 75–92. Springer, 2024.

[42] Xiaoyang Wu, Li Jiang, Peng-Shuai Wang, Zhijian Liu, Xihui Liu, Yu Qiao, Wanli Ouyang, Tong He, and Hengshuang Zhao. Point transformer v3: Simpler faster stronger. In *Proceedings of the IEEE/CVF Conference on Computer Vision and Pattern Recognition*, pages 4840–4851, 2024.

[43] Zhirong Wu, Shuran Song, Aditya Khosla, Fisher Yu, Linguang Zhang, Xiaoou Tang, and Jianxiong Xiao. 3d ShapeNets: A deep representation for volumetric shapes. In *Proceedings of the IEEE conference on computer vision and pattern recognition*, pages 1912–1920, 2015.

[44] Keylu Xu, Jingling Li, Mozhi Zhang, Simon S Du, Ken-ichi Kawarabayashi, and Stefanie Jegelka. What Can Neural Networks Reason About? *ICLR 2020*, 2020.

[45] Morris Yau, Nikolaos Karalias, Eric Lu, Jessica Xu, and Stefanie Jegelka. Are Graph Neural Networks Optimal Approximation Algorithms? In *Advances in Neural Information Processing Systems*, volume 37. Neural Information Processing Systems, 2024.

[46] Hai Yu, Pankaj K Agarwal, Raghunath Poreddy, and Kasturi R Varadarajan. Practical methods for shape fitting and kinetic data structures using core sets. In *Proceedings of the twentieth annual symposium on Computational geometry*, pages 263–272, 2004.

[47] Manzil Zaheer, Sahand Kottur, Anima Ravanbakhsh, Barnabás Poczos, Ruslan Salakhutdinov, and Alex Smola. Deep Sets. In *Advances in Neural Information Processing Systems*, volume 30, 2017.

[48] Hengshuang Zhao, Li Jiang, Jiaya Jia, Philip HS Torr, and Vladlen Koltun. Point transformer. In *Proceedings of the IEEE/CVF international conference on computer vision*, pages 16259–16268, 2021.

NeurIPS Paper Checklist

The checklist is designed to encourage best practices for responsible machine learning research, addressing issues of reproducibility, transparency, research ethics, and societal impact. Do not remove the checklist: **The papers not including the checklist will be desk rejected.** The checklist should follow the references and follow the (optional) supplemental material. The checklist does NOT count towards the page limit.

Please read the checklist guidelines carefully for information on how to answer these questions. For each question in the checklist:

- You should answer [Yes] , [No] , or [NA] .
- [NA] means either that the question is Not Applicable for that particular paper or the relevant information is Not Available.
- Please provide a short (1–2 sentence) justification right after your answer (even for NA).

The checklist answers are an integral part of your paper submission. They are visible to the reviewers, area chairs, senior area chairs, and ethics reviewers. You will be asked to also include it (after eventual revisions) with the final version of your paper, and its final version will be published with the paper.

The reviewers of your paper will be asked to use the checklist as one of the factors in their evaluation. While "[Yes] " is generally preferable to "[No] ", it is perfectly acceptable to answer "[No] " provided a proper justification is given (e.g., "error bars are not reported because it would be too computationally expensive" or "we were unable to find the license for the dataset we used"). In general, answering "[No] " or "[NA] " is not grounds for rejection. While the questions are phrased in a binary way, we acknowledge that the true answer is often more nuanced, so please just use your best judgment and write a justification to elaborate. All supporting evidence can appear either in the main paper or the supplemental material, provided in appendix. If you answer [Yes] to a question, in the justification please point to the section(s) where related material for the question can be found.

IMPORTANT, please:

- **Delete this instruction block, but keep the section heading "NeurIPS Paper Checklist"**,
- **Keep the checklist subsection headings, questions/answers and guidelines below.**
- **Do not modify the questions and only use the provided macros for your answers**.

1. **Claims**

   Question: Do the main claims made in the abstract and introduction accurately reflect the paper's contributions and scope?

   Answer: [Yes]

   Justification: In sections 3 and 4, we introduce our neural frameworks approximating solutions for extent measures of point clouds. We also introduce our relaxed-ε-kernel theory in sections 3 and 4. Finally, we show that our neural networks can produce ε-kernel approximations in the section 5.

   Guidelines:

   - The answer NA means that the abstract and introduction do not include the claims made in the paper.
   - The abstract and/or introduction should clearly state the claims made, including the contributions made in the paper and important assumptions and limitations. A No or NA answer to this question will not be perceived well by the reviewers.
   - The claims made should match theoretical and experimental results, and reflect how much the results can be expected to generalize to other settings.
   - It is fine to include aspirational goals as motivation as long as it is clear that these goals are not attained by the paper.

2. **Limitations**

   Question: Does the paper discuss the limitations of the work performed by the authors?

Answer: [Yes]

Justification: we discuss limitations of the work in the conclusion. In each theorem, we point out the assumptions made on the point clouds (e.g. α-fatness).

Guidelines:

- The answer NA means that the paper has no limitation while the answer No means that the paper has limitations, but those are not discussed in the paper.
- The authors are encouraged to create a separate "Limitations" section in their paper.
- The paper should point out any strong assumptions and how robust the results are to violations of these assumptions (e.g., independence assumptions, noiseless settings, model well-specification, asymptotic approximations only holding locally). The authors should reflect on how these assumptions might be violated in practice and what the implications would be.
- The authors should reflect on the scope of the claims made, e.g., if the approach was only tested on a few datasets or with a few runs. In general, empirical results often depend on implicit assumptions, which should be articulated.
- The authors should reflect on the factors that influence the performance of the approach. For example, a facial recognition algorithm may perform poorly when image resolution is low or images are taken in low lighting. Or a speech-to-text system might not be used reliably to provide closed captions for online lectures because it fails to handle technical jargon.
- The authors should discuss the computational efficiency of the proposed algorithms and how they scale with dataset size.
- If applicable, the authors should discuss possible limitations of their approach to address problems of privacy and fairness.
- While the authors might fear that complete honesty about limitations might be used by reviewers as grounds for rejection, a worse outcome might be that reviewers discover limitations that aren't acknowledged in the paper. The authors should use their best judgment and recognize that individual actions in favor of transparency play an important role in developing norms that preserve the integrity of the community. Reviewers will be specifically instructed to not penalize honesty concerning limitations.

3. **Theory assumptions and proofs**

   Question: For each theoretical result, does the paper provide the full set of assumptions and a complete (and correct) proof?

   Answer: [Yes]

   Justification: All proofs are given in the appendix.

   Guidelines:

   - The answer NA means that the paper does not include theoretical results.
   - All the theorems, formulas, and proofs in the paper should be numbered and cross-referenced.
   - All assumptions should be clearly stated or referenced in the statement of any theorems.
   - The proofs can either appear in the main paper or the supplemental material, but if they appear in the supplemental material, the authors are encouraged to provide a short proof sketch to provide intuition.
   - Inversely, any informal proof provided in the core of the paper should be complemented by formal proofs provided in appendix or supplemental material.
   - Theorems and Lemmas that the proof relies upon should be properly referenced.

4. **Experimental result reproducibility**

   Question: Does the paper fully disclose all the information needed to reproduce the main experimental results of the paper to the extent that it affects the main claims and/or conclusions of the paper (regardless of whether the code and data are provided or not)?

   Answer: [Yes]

   Justification: The entire experimental set-up is given in the appendix and we provide the code as well.

Guidelines:

- The answer NA means that the paper does not include experiments.
- If the paper includes experiments, a No answer to this question will not be perceived well by the reviewers: Making the paper reproducible is important, regardless of whether the code and data are provided or not.
- If the contribution is a dataset and/or model, the authors should describe the steps taken to make their results reproducible or verifiable.
- Depending on the contribution, reproducibility can be accomplished in various ways. For example, if the contribution is a novel architecture, describing the architecture fully might suffice, or if the contribution is a specific model and empirical evaluation, it may be necessary to either make it possible for others to replicate the model with the same dataset, or provide access to the model. In general. releasing code and data is often one good way to accomplish this, but reproducibility can also be provided via detailed instructions for how to replicate the results, access to a hosted model (e.g., in the case of a large language model), releasing of a model checkpoint, or other means that are appropriate to the research performed.
- While NeurIPS does not require releasing code, the conference does require all submissions to provide some reasonable avenue for reproducibility, which may depend on the nature of the contribution. For example
  (a) If the contribution is primarily a new algorithm, the paper should make it clear how to reproduce that algorithm.
  (b) If the contribution is primarily a new model architecture, the paper should describe the architecture clearly and fully.
  (c) If the contribution is a new model (e.g., a large language model), then there should either be a way to access this model for reproducing the results or a way to reproduce the model (e.g., with an open-source dataset or instructions for how to construct the dataset).
  (d) We recognize that reproducibility may be tricky in some cases, in which case authors are welcome to describe the particular way they provide for reproducibility. In the case of closed-source models, it may be that access to the model is limited in some way (e.g., to registered users), but it should be possible for other researchers to have some path to reproducing or verifying the results.

5. **Open access to data and code**

   Question: Does the paper provide open access to the data and code, with sufficient instructions to faithfully reproduce the main experimental results, as described in supplemental material?

   Answer: [Yes]

   Justification: As stated previously, we provide the code as well as all the synthetic benchmark datasets. The real datasets are freely available online.

   Guidelines:

   - The answer NA means that paper does not include experiments requiring code.
   - Please see the NeurIPS code and data submission guidelines (`https://nips.cc/public/guides/CodeSubmissionPolicy`) for more details.
   - While we encourage the release of code and data, we understand that this might not be possible, so "No" is an acceptable answer. Papers cannot be rejected simply for not including code, unless this is central to the contribution (e.g., for a new open-source benchmark).
   - The instructions should contain the exact command and environment needed to run to reproduce the results. See the NeurIPS code and data submission guidelines (`https://nips.cc/public/guides/CodeSubmissionPolicy`) for more details.
   - The authors should provide instructions on data access and preparation, including how to access the raw data, preprocessed data, intermediate data, and generated data, etc.
   - The authors should provide scripts to reproduce all experimental results for the new proposed method and baselines. If only a subset of experiments are reproducible, they should state which ones are omitted from the script and why.

- At submission time, to preserve anonymity, the authors should release anonymized versions (if applicable).
- Providing as much information as possible in supplemental material (appended to the paper) is recommended, but including URLs to data and code is permitted.

6. **Experimental setting/details**

   Question: Does the paper specify all the training and test details (e.g., data splits, hyperparameters, how they were chosen, type of optimizer, etc.) necessary to understand the results?

   Answer: [Yes]

   Justification: The train and test details are given in the beginning of Appendix A.4.

   Guidelines:

   - The answer NA means that the paper does not include experiments.
   - The experimental setting should be presented in the core of the paper to a level of detail that is necessary to appreciate the results and make sense of them.
   - The full details can be provided either with the code, in appendix, or as supplemental material.

7. **Experiment statistical significance**

   Question: Does the paper report error bars suitably and correctly defined or other appropriate information about the statistical significance of the experiments?

   Answer: [Yes]

   Justification: We report error bars in all tables.

   Guidelines:

   - The answer NA means that the paper does not include experiments.
   - The authors should answer "Yes" if the results are accompanied by error bars, confidence intervals, or statistical significance tests, at least for the experiments that support the main claims of the paper.
   - The factors of variability that the error bars are capturing should be clearly stated (for example, train/test split, initialization, random drawing of some parameter, or overall run with given experimental conditions).
   - The method for calculating the error bars should be explained (closed form formula, call to a library function, bootstrap, etc.)
   - The assumptions made should be given (e.g., Normally distributed errors).
   - It should be clear whether the error bar is the standard deviation or the standard error of the mean.
   - It is OK to report 1-sigma error bars, but one should state it. The authors should preferably report a 2-sigma error bar than state that they have a 96% CI, if the hypothesis of Normality of errors is not verified.
   - For asymmetric distributions, the authors should be careful not to show in tables or figures symmetric error bars that would yield results that are out of range (e.g. negative error rates).
   - If error bars are reported in tables or plots, The authors should explain in the text how they were calculated and reference the corresponding figures or tables in the text.

8. **Experiments compute resources**

   Question: For each experiment, does the paper provide sufficient information on the computer resources (type of compute workers, memory, time of execution) needed to reproduce the experiments?

   Answer: [Yes]

   Justification: We specify the type/number of GPUs needed in Appendix A.4.

   Guidelines:

   - The answer NA means that the paper does not include experiments.

- The paper should indicate the type of compute workers CPU or GPU, internal cluster, or cloud provider, including relevant memory and storage.
- The paper should provide the amount of compute required for each of the individual experimental runs as well as estimate the total compute.
- The paper should disclose whether the full research project required more compute than the experiments reported in the paper (e.g., preliminary or failed experiments that didn't make it into the paper).

9. **Code of ethics**

   Question: Does the research conducted in the paper conform, in every respect, with the NeurIPS Code of Ethics `https://neurips.cc/public/EthicsGuidelines`?

   Answer: [Yes]

   Justification: Yes, we believe we have conformed with the NeurIPS code of ethics.

   Guidelines:

   - The answer NA means that the authors have not reviewed the NeurIPS Code of Ethics.
   - If the authors answer No, they should explain the special circumstances that require a deviation from the Code of Ethics.
   - The authors should make sure to preserve anonymity (e.g., if there is a special consideration due to laws or regulations in their jurisdiction).

10. **Broader impacts**

    Question: Does the paper discuss both potential positive societal impacts and negative societal impacts of the work performed?

    Answer: [NA]

    Justification: Our work concerns mainly approximation theory and neural network architectures for computational geometric primitives. We see no mechanism by which neural ε-kernels could cause negative impacts. Our paper is not tied to any applications.

    Guidelines:

    - The answer NA means that there is no societal impact of the work performed.
    - If the authors answer NA or No, they should explain why their work has no societal impact or why the paper does not address societal impact.
    - Examples of negative societal impacts include potential malicious or unintended uses (e.g., disinformation, generating fake profiles, surveillance), fairness considerations (e.g., deployment of technologies that could make decisions that unfairly impact specific groups), privacy considerations, and security considerations.
    - The conference expects that many papers will be foundational research and not tied to particular applications, let alone deployments. However, if there is a direct path to any negative applications, the authors should point it out. For example, it is legitimate to point out that an improvement in the quality of generative models could be used to generate deepfakes for disinformation. On the other hand, it is not needed to point out that a generic algorithm for optimizing neural networks could enable people to train models that generate Deepfakes faster.
    - The authors should consider possible harms that could arise when the technology is being used as intended and functioning correctly, harms that could arise when the technology is being used as intended but gives incorrect results, and harms following from (intentional or unintentional) misuse of the technology.
    - If there are negative societal impacts, the authors could also discuss possible mitigation strategies (e.g., gated release of models, providing defenses in addition to attacks, mechanisms for monitoring misuse, mechanisms to monitor how a system learns from feedback over time, improving the efficiency and accessibility of ML).

11. **Safeguards**

    Question: Does the paper describe safeguards that have been put in place for responsible release of data or models that have a high risk for misuse (e.g., pretrained language models, image generators, or scraped datasets)?

Answer: [NA]

Justification: All of our real world data is already publicly available. The SQUID and ModelNet do not have a high risk for misuse as they have already been highly curated and have no unsafe point clouds/images.

Guidelines:

- The answer NA means that the paper poses no such risks.
- Released models that have a high risk for misuse or dual-use should be released with necessary safeguards to allow for controlled use of the model, for example by requiring that users adhere to usage guidelines or restrictions to access the model or implementing safety filters.
- Datasets that have been scraped from the Internet could pose safety risks. The authors should describe how they avoided releasing unsafe images.
- We recognize that providing effective safeguards is challenging, and many papers do not require this, but we encourage authors to take this into account and make a best faith effort.

12. **Licenses for existing assets**

Question: Are the creators or original owners of assets (e.g., code, data, models), used in the paper, properly credited and are the license and terms of use explicitly mentioned and properly respected?

Answer: [Yes]

Justification: We properly cite ModelNet and SQUID.

Guidelines:

- The answer NA means that the paper does not use existing assets.
- The authors should cite the original paper that produced the code package or dataset.
- The authors should state which version of the asset is used and, if possible, include a URL.
- The name of the license (e.g., CC-BY 4.0) should be included for each asset.
- For scraped data from a particular source (e.g., website), the copyright and terms of service of that source should be provided.
- If assets are released, the license, copyright information, and terms of use in the package should be provided. For popular datasets, `paperswithcode.com/datasets` has curated licenses for some datasets. Their licensing guide can help determine the license of a dataset.
- For existing datasets that are re-packaged, both the original license and the license of the derived asset (if it has changed) should be provided.
- If this information is not available online, the authors are encouraged to reach out to the asset's creators.

13. **New assets**

Question: Are new assets introduced in the paper well documented and is the documentation provided alongside the assets?

Answer: [NA]

Justification: We do not release any new assets.

Guidelines:

- The answer NA means that the paper does not release new assets.
- Researchers should communicate the details of the dataset/code/model as part of their submissions via structured templates. This includes details about training, license, limitations, etc.
- The paper should discuss whether and how consent was obtained from people whose asset is used.
- At submission time, remember to anonymize your assets (if applicable). You can either create an anonymized URL or include an anonymized zip file.

14. **Crowdsourcing and research with human subjects**

    Question: For crowdsourcing experiments and research with human subjects, does the paper include the full text of instructions given to participants and screenshots, if applicable, as well as details about compensation (if any)?

    Answer: [NA]

    Justification: Our paper does not involve crowdsourcing or research with human subjects.

    Guidelines:

    - The answer NA means that the paper does not involve crowdsourcing nor research with human subjects.
    - Including this information in the supplemental material is fine, but if the main contribution of the paper involves human subjects, then as much detail as possible should be included in the main paper.
    - According to the NeurIPS Code of Ethics, workers involved in data collection, curation, or other labor should be paid at least the minimum wage in the country of the data collector.

15. **Institutional review board (IRB) approvals or equivalent for research with human subjects**

    Question: Does the paper describe potential risks incurred by study participants, whether such risks were disclosed to the subjects, and whether Institutional Review Board (IRB) approvals (or an equivalent approval/review based on the requirements of your country or institution) were obtained?

    Answer: [NA]

    Justification: Our research does not involve any research with human subjects.

    Guidelines:

    - The answer NA means that the paper does not involve crowdsourcing nor research with human subjects.
    - Depending on the country in which research is conducted, IRB approval (or equivalent) may be required for any human subjects research. If you obtained IRB approval, you should clearly state this in the paper.
    - We recognize that the procedures for this may vary significantly between institutions and locations, and we expect authors to adhere to the NeurIPS Code of Ethics and the guidelines for their institution.
    - For initial submissions, do not include any information that would break anonymity (if applicable), such as the institution conducting the review.

16. **Declaration of LLM usage**

    Question: Does the paper describe the usage of LLMs if it is an important, original, or non-standard component of the core methods in this research? Note that if the LLM is used only for writing, editing, or formatting purposes and does not impact the core methodology, scientific rigorousness, or originality of the research, declaration is not required.

    Answer: [NA]

    Justification: This paper does not describe the usage of LLMs.

    Guidelines:

    - The answer NA means that the core method development in this research does not involve LLMs as any important, original, or non-standard components.
    - Please refer to our LLM policy (`https://neurips.cc/Conferences/2025/LLM`) for what should or should not be described.

A Technical Appendices and Supplementary Material

A.1 Additional details from Section 2

Here, we provide more details regarding the computation of ε-kernels. One simple algorithm to compute an ε-kernel is given in Algorithm 2. More sophisticated methods can be found in [10] and [46] but we highlight Algorithm 2 as it is most similar to the computation of the relaxed-ε-kernel in Section 3.2. In summary, one may compute an ε-kernel by carefully choosing a set of directions Ω and choose points according to the max-projection in that direction. We show the correctness of this algorithm in Theorem A.3. However, we first provide some auxiliary lemmas which we will use in the proof of Theorem A.3 as well as subsequent proofs.

Lemma A.1. *If P is an α-fat point set, then for any $u \in \mathbf{S}^{d-1}$, $\mathsf{w}_u(P) \geq 2\alpha$.*

Proof. Suppose P is an α-fat point set so $\alpha\mathbb{C} \subseteq \text{CH}(P)$. For any $u \in \mathbf{S}^{d-1}$ and $p \in \text{CH}(P)$, $\langle u, p\rangle \geq \|u\|\|p\|$. Since $\alpha\mathbb{C} \subseteq \text{CH}(P)$, $\|p\| \geq \alpha$ so $\langle u, p\rangle \geq \alpha$ and $\max_{p\in P}\langle u, p\rangle \geq \alpha$. Furthermore, $\min_{p\in P}\langle u, p\rangle = -\max_{p\in P} -\langle u, p\rangle = -\max_{p\in P}\langle -u, p\rangle \leq -\alpha$. Then

$$\mathsf{w}_u(P) = \max_{p\in P}\langle u, p\rangle - \min_{p\in P}\langle u, p\rangle \geq 2\alpha$$

□

Lemma A.2. *Let $S \subseteq \mathbb{C}_d$. Given two unit vectors $u, u' \in$ such that $\|u - u'\| \leq \lambda$, $\mathsf{w}_u(S) \geq \mathsf{w}_{u'}(S) - 2\lambda\sqrt{d}$.*

Proof. Given any $x \in S$,

$$|\langle x, u\rangle - \langle x, u'\rangle| = |\langle u - u', x\rangle| \leq |\|u - u'\|\|x\|| \leq \lambda\sqrt{d}.$$

where the final $\sqrt{d}$ is because $x \in [-1, 1]^d$. Then

$$\begin{aligned}
\mathsf{w}_{u'}(S) &= \max_{s\in S}\langle u', s\rangle - \min_{s,\in S}\langle u', s\rangle \\
&\geq \langle u', \text{argmax}_{s\in S}\langle u, s\rangle\rangle - \min_{s\in S}\langle u', s\rangle \\
&\geq \langle u, \text{argmax}_{s\in S}\langle u, s\rangle\rangle - \lambda\sqrt{d} - \min_{s\in S}\langle u', s\rangle \\
&\geq \langle u, \text{argmax}_{s\in S}\langle u, s\rangle\rangle - \lambda\sqrt{d} - \langle u', \text{argmin}_{s\in S}\langle u, s\rangle\rangle \\
&\geq \langle u, \text{argmax}_{s\in S}\langle u, s\rangle\rangle - \lambda\sqrt{d} - (\langle u, \text{argmin}_{s\in S}\langle u, s\rangle\rangle + \lambda\sqrt{d}) \\
&\geq \mathsf{w}_u(S) - 2\lambda\sqrt{d}.
\end{aligned}$$

□

Theorem A.3. *Let $P \subseteq \mathbb{C} = [-1, 1]^d$ be an α-fat point set and let $0 < \varepsilon < \frac{1}{3}$. Suppose Ω is an $\frac{\alpha\varepsilon}{4\sqrt{d}}$-net for $\mathbf{S}^{d-1}$ so $|\Omega| = O\Big(\frac{1}{(\frac{\alpha\varepsilon}{4\sqrt{d}})^{d-1}}\Big)$, $\forall u, u' \in \Omega$, $\|u - u'\| \leq \frac{1}{(\frac{\alpha\varepsilon}{4\sqrt{d}})^{d-1}}$, and for all $u \in \Omega$, $-u \in \Omega$. Suppose that $\forall u \in \Omega$, $-u \in \Omega$. Then the set of points Q constructed via $Algorithm\ 2$ is an ε-kernel for P.*

Algorithm 2 Computation of ϵ-kernels

Require: $P \subseteq \mathbb{R}^d$, k
  Ω is a set of k directions
  Initialize $Q = \{\}$
  for $u \in \Omega$ **do**
    Q.append($\text{argmax}_{p\in P}\langle u, p\rangle$)
  end for
  return $Q = \{q_u : u \in \Omega\}$

Proof of Theorem A.3. Let $u \in \mathbf{S}^{d-1}$. Let $\lambda = \frac{\alpha\varepsilon}{4\sqrt{d}}$. Since Ω is an λ-net for $\mathbf{S}^{d-1}$, there is a $u' \in \Omega$ such that $\|u - u'\| \leq \lambda$. Therefore, by Lemma A.2,

$$\mathsf{w}_u(Q) \geq \mathsf{w}_{u'}(Q) - 2\lambda\sqrt{d} \geq \mathsf{w}_{u'}(P) - 2\lambda\sqrt{d} \geq \mathsf{w}_u(P) - 4\lambda\sqrt{d}.$$

Therefore,

$$\frac{\mathsf{w}_u(Q)}{\mathsf{w}_u(P)} \geq 1 - \frac{4\lambda\sqrt{d}}{\mathsf{w}_u(P)} \geq 1 - \frac{4\lambda\sqrt{d}}{\alpha} = 1 - \varepsilon$$

where the second inequality comes from Lemma A.1. Thus, $\mathsf{w}_u(Q) \geq (1-\varepsilon)\mathsf{w}_u(P)$.

A.2 Additional details from Section 4

We provide an example of how relaxed-ε-kernels can be used to approximate minimum width enclosing annulus. However, we will first need show in Theorem A.5 how Theorem 4.4 can be used to compute relaxed-ε-kernels for fractional powers of polynomials. Our proof of Theorem A.5 builds on the following lemma, originally proved by [2].

Lemma A.4. *Let $0 < \varepsilon < 1$ be a parameter, $r \geq 2$ and let $\delta = (\varepsilon/2(r-1))^r$. If we have $0 \leq a \leq A \leq B \leq b$ and $B - A \geq (1-\delta)(b-a)$, then*

$$B^{1/r} - A^{1/r} \geq (1-\varepsilon)(b^{1/r} - a^{1/r})$$

Theorem A.5. *Let $\mathcal{F}$ be a family of $(d+p)$ variate polynomials which admit a linearization of dimension m as in Theorem 4.4. Additionally, suppose for every f_i, $f_i(x) \geq 0$ for all $x \in \mathbb{R}^d$. Let $r \geq 2$, $\delta = (\varepsilon/2(r-1))^r$, and let $\mathcal{G} = \{g_i\}$ be a relaxed-δ-kernel of $\mathcal{F}$. Then $\mathcal{G}_{1/\mathrm{r}} = \{g_i^{1/r}\}$ is a relaxed-ε-kernel of $\mathcal{F}_{1/\mathrm{r}} = \{f_i^{1/r}\}$.*

Proof. Let $\delta = (\varepsilon/2(r-1))^r$ where $r \geq 2$ is an integer. Let $\mathcal{G}$ be a relaxed-δ-kernel of $\mathcal{F}$ so $\overrightarrow{\mathcal{E}}_{\mathcal{G}}(x) \subseteq \overrightarrow{\mathcal{E}}_{\mathcal{F}}(x)$ and $\overrightarrow{\mathcal{E}}_{\mathcal{G}}(x)$ is within $\varepsilon \cdot \mathcal{E}_{\mathcal{F}}(x)$-Hausdorff distance of $\overrightarrow{\mathcal{E}}_{\mathcal{F}}(x)$. Since $f \in \mathcal{F}$ is positive, for any $x \in \mathbb{R}^d$, we know that

$$0 \leq \min_{f\in\mathcal{F}}(x) \leq \min_{g\in\mathcal{G}}(x) \leq \max_{g\in\mathcal{G}}(x) \leq \max_{f\in\mathcal{F}}(x).$$

Additionally, by the definition of relaxed-ε-kernels, $\max_{g\in\mathcal{G}} g(x) - \min_{g\in\mathcal{G}} g(x) \geq (1-\varepsilon)(\max_{f\in\mathcal{F}}(x) - \min_{f\in\mathcal{F}}(x))$. Then, we apply Lemma A.4 to get

$$\max_{g\in\mathcal{G}_{1/r}} g(x)^{1/r} - \min g \in \mathcal{G}_{1/r} g(x)^{1/r} \geq (1-\varepsilon)(\max_{g\in\mathcal{F}_{1/r}} f(x)^{1/r} - \min_{f\in\mathcal{F}_{1/r}} f(x)^{1/r}).$$

□

Now, we are prepared to provide an example of Theorem A.5 can be used to approximate minimum enclosing annulus for points in $\mathbb{R}^2$. Given $P = \{p_1, \ldots, p_N\} \subseteq \mathbb{R}^2$ and any $x \in \mathbb{R}^2$, finding the width of the a minimum enclosing spherical annulus centered at x is

$$w(x, P) = \max_{p\in P} \|x - p\| - \min_{p\in P} \|x - p\|.$$

We define the set of functions $\mathcal{F} = \{f_p(x) = \|x - p\| : p \in P\}$. Notice then that $\mathcal{E}_{\mathcal{F}}(x) = w(x, P)$ and the width of the minimum enclosing spherical shell is exactly $\min_{x\in\mathbb{R}^d} \mathcal{E}_{\mathcal{F}}(x)$. Similarly, the optimal center for the minimum enclosing spherical shell is $\operatorname{argmin}_{x\in\mathbb{R}^d}\mathcal{E}_{\mathcal{F}}(x)$. By Theorem A.5, a relaxed-ε-kernel for $\mathcal{F}' = \{\|x - p\|^2 : p \in P\}$ translates to relaxed-ε-kernel for $\mathcal{F}$.

Suppose $x = (x_1, x_2) \in \mathbb{R}^2$ and $p_i = (p_{i,1}, p_{i,2}) \in \mathbb{R}^2$ where $p_i \in P$. Given $f_i \in \mathcal{F}'$, $f_i = x_1^2 + x_2^2 - 2p_{i,1}x_1 - 2p_{i,2}x_2 + p_{i,1}^2 + p_{i,2}^2$. f_i admits a linearization of dimension 3 as follows:

$$\psi_0(p_i) = p_{i,1}^2 + p_{i,2}^2 \;\; \psi_1(p_i) = -2p_{i,1} \;\; \psi_2(p_i) = -2p_{i,2} \;\; \psi_3(p_i) = 1$$
$$\varphi_1(x) = x_1 \quad \varphi_2(x) = x_2 \quad \varphi_3(x) = x_1^2 + x_2^2$$

By Theorem 4.4, we can compute a relaxed-ε-kernel for the dual space via Algorithm 1 in $\mathbb{R}^4$ and map back to relaxed-ε-kernel for $\mathcal{F}'$, $\mathcal{Q}_\varepsilon$. Then $\mathcal{Q}_{\varepsilon,1/r}$ is a relaxed-ε-kernel for $\mathcal{F}$ by Theorem A.5. Computing $\min_{x\in\mathbb{R}^2} \mathcal{E}_{\mathcal{Q}_{\varepsilon,1/r}}(x)$ as well as $\operatorname{argmin}_{x\in\mathbb{R}^2}\mathcal{E}_{\mathcal{Q}_{\varepsilon,1/r}}(x)$ outputs the width and center of the minimum enclosing annulus, respectively.

A.3 Proofs details

In this section, we will provide the missing proofs from the main text.

A.3.1 Proofs from Section 3

The following lemma will be important to show that relaxed ε-kernels can approximate well-behaved measurements of the original point set P.

Lemma A.6. *Suppose Q is a relaxed-ε-kernel of P. Let $\hat{P} = P \cup Q$. Then (a) Q is a ε-approximation of $\hat{P}$ and (b) P is an ε-approximation of $\hat{P}$.*

Proof of Lemma A.6 Let $u \in \mathbf{S}^{d-1}$. To show that Q is an ε-approximation of $\hat{P}$, we must show that

$$\max_{q\in Q}\langle q,u\rangle - \varepsilon \mathsf{w}_u(Q) \leq \max_{\hat{p}\in\hat{P}}\langle \hat{p},u\rangle \leq \max_{q\in Q}\langle q,u\rangle + \varepsilon \mathsf{w}_u(Q)$$

and

$$\min_{q\in Q}\langle q,u\rangle - \varepsilon \mathsf{w}_u(Q) \leq \min_{\hat{p}\in\hat{P}}\langle \hat{p},u\rangle \leq \min_{q\in Q}\langle q,u\rangle + \varepsilon \mathsf{w}_u(Q)$$

We know that $\max_{\hat{p}\in\hat{P}}\langle \hat{p},u\rangle = \max\{\max_{p\in P}\langle p,u\rangle, \max_{q\in Q}\langle q,u\rangle\}$. We know that $\max_{q\in Q}\langle q,u\rangle - \varepsilon \mathsf{w}_u(Q) \leq \max_{p\in P}\langle u,p\rangle \leq \max_{q\in Q}\langle u,q\rangle + \varepsilon \mathsf{w}_u(Q)$ because Q is an ε-relaxed-kernel of P. Clearly, $\max_{q\in Q}\langle q,u\rangle - \varepsilon \mathsf{w}_u(Q) \leq \max_{q\in Q}\langle q,u\rangle \leq \max_{q\in Q}\langle q,u\rangle + \varepsilon \mathsf{w}_u(Q)$ so

$$\max_{q\in Q}\langle q,u\rangle - \varepsilon \mathsf{w}_u(Q) \leq \max\{\max_{p\in P}\langle p,u\rangle, \max_{q\in Q}\langle q,u\rangle\} = \max_{\hat{p}\in\hat{P}}\langle \hat{p},u\rangle \leq \max_{q\in Q}\langle q,u\rangle + \varepsilon \mathsf{w}_u(Q).$$

We can do something similar for $\min_{q\in Q}\langle q,u\rangle$ and $\min_{\hat{p}\in\hat{P}}\langle \hat{p},u\rangle$.

The same argument will hold for (b).

Proof of Theorem 3.2. Let $\widehat{P} = P \cup Q$. Let μ be a faithful measure and let c be the constant in for the faithful measure, μ. By Lemma A.6 (a), Q is ε-kernel of $\widehat{P}$, meaning Q is a $c\varepsilon$-coreset of $\widehat{P}$. By Lemma A.6 (b), P is ε-kernel of $\widehat{P}$, meaning P is a $c\varepsilon$-coreset of $\widehat{P}$. It then follows that

$$\frac{1-c\varepsilon}{1+c\varepsilon}\mu(Q) \leq \mu(P) \leq \frac{1+c\varepsilon}{1-c\varepsilon}\mu(Q).$$

For $c\varepsilon < 1/3$, it is easy to verify that this implies

$$(1-3c\varepsilon)\mu(Q) \leq \mu(P) \leq (1+3c\varepsilon)\mu(Q),$$

hence the theorem holds with $c' = 3c$.

Proof of Theorem 3.3 First, we make two important observations regarding the points in the output relaxed-ε-kernels, Q, computed by Algorithm 1 and their relationship to the set of chosen directions Ω. First, suppose we are given $\varepsilon > 0$ and $A = \{a_1, \ldots, a_N\} \subseteq \mathbb{R}$ such that $a_i = \langle u, p_i\rangle$, let $\mathbf{a} = [a_1, \ldots, a_N]^T$. Recall from Algorithm 1, ρ_ε is defined as

$$\rho_\varepsilon(\mathbf{a}) = \begin{pmatrix} \mathrm{ReLU}(a_1 + \varepsilon \cdot w(A) - M_A) \\ \mathrm{ReLU}(a_2 + \varepsilon \cdot w(A) - M_A) \\ \vdots \\ \mathrm{ReLU}(a_n + \varepsilon \cdot w(A) - M_A) \end{pmatrix}$$

where $M_A = \max(A)$ and $w(A) = \max(A) - \min(A)$. Note $\mathrm{ReLU}(a_i + \varepsilon \cdot w(A) - M_A) > 0$ only when a_i is within $\varepsilon \cdot w(A)$ of the maximum value, M_A. Recall our modified softmax normalization from Algorithm 1 given $x \in \mathbb{R}^n$:

$$\sigma(x) = \left[\frac{e^{x_1}-1}{\sum_{i=1}^n (e^{x_i}-1)} \cdots \frac{e^{x_n}-1}{\sum_{i=1}^n (e^{x_i}-1)}\right].$$

Notice that $\sigma(x)_i > 0$ only when $x_i > 0$. Hence, we can see $\sigma(\rho_\varepsilon(\mathbf{a}))$ as a probability vector over $\mathbf{a}$ which only has non-zero values corresponding to those a_i that are within $\varepsilon \cdot w(A)$ of M_A. If we take $\sigma(\rho_\varepsilon(\mathbf{a}))^T\mathbf{a}$, we observe that $\sigma(\rho_\varepsilon(\mathbf{a}))^T\mathbf{a}$ is a convex combination of the points in A.

Thus, given $u \in \Omega$ and $q_u \in Q$, we make the following important observations about q_u.

Observation A.7. *Given $u \in \Omega$, $q_u \in Q$ is the convex combination of a subset of points $p_{I_1}, \ldots, p_{I_{r_u}}$. For each such point p_{I_i}, $\langle u, p_{I_i} \rangle \in [\max_{p \in P} \langle u, p \rangle - \varepsilon \mathsf{w}_u(P), \max_{p \in P} \langle u, p \rangle]$.*

Observation A.8. *Given $u \in \Omega$, $\langle u, q_u \rangle \in [\max_{p \in P} \langle u, p \rangle - \varepsilon \mathsf{w}_u(P), \max_{p \in P} \langle u, p \rangle]$.*

Our goal is to show that for any $u \in \mathbf{S}^{d-1}$, the u-projection $\overrightarrow{\mathsf{w}}_u(Q)$ is an ε-approximation of the interval (u-projection) $\overrightarrow{\mathsf{w}}_u(P)$. First, note that by construction, each point in Q is a convex combination of a subset of points in P so $Q \subseteq \mathrm{CH}(P)$. This implies that $\overrightarrow{\mathsf{w}}_u(Q) \subseteq \overrightarrow{\mathsf{w}}_u(P)$. What remains is to show that $\mathsf{w}_u(Q) \geq (1 - 3\varepsilon)\mathsf{w}_u(P)$. If $u \in \Omega$, then this holds as

$$\begin{aligned}
\max_{q \in Q} \langle u, q \rangle - \min_{q \in Q} \langle u, q \rangle &\geq \langle u, q_u \rangle - \langle -u, q_{-u} \rangle \\
&\geq \max_{p \in P} \langle u, p \rangle - \varepsilon \mathsf{w}_u(P) - \min_{p \in P} \langle u, p \rangle - \varepsilon \mathsf{w}_u(P) \quad \text{due to Observation 2} \\
&\geq \mathsf{w}_u(P) - 2\varepsilon \mathsf{w}_u(P) \\
&\geq (1 - 3\varepsilon)\mathsf{w}_u(P)
\end{aligned}$$

Consider when $u \notin \Omega$ and let $\lambda = \frac{\alpha\varepsilon}{4\sqrt{d}}$. Then there is a $u' \in \Omega$ such that $\|u - u'\| \leq \lambda$ due to the construction of Ω and $-u' \in \Omega$. Then

$$\begin{aligned}
\mathsf{w}_{u'}(Q) &= \max_{q \in Q} \langle u', q \rangle - \min_{q \in Q} \langle u', q \rangle \\
&\geq \langle u', q_{u'} \rangle - \min_{q \in Q} \langle u', q \rangle \\
&\geq \langle u', \mathrm{argmax}_{p \in P} \langle u', p \rangle \rangle - \varepsilon \mathsf{w}_{u'}(P) - \min_{q \in Q} \langle u', q \rangle \quad \text{(Observation 2)} \\
&= \langle u', \mathrm{argmax}_{p \in P} \langle u', p \rangle \rangle - \varepsilon \mathsf{w}_{u'}(P) - \max_{q \in Q} \langle -u', q \rangle \\
&= \max_{p \in P} \langle u', p \rangle - \varepsilon \mathsf{w}_{u'}(P) - \langle -u', q_{-u'} \rangle \\
&\geq \max_{p \in P} \langle u', p \rangle - \varepsilon \mathsf{w}_{u'}(P) - (\langle -u', \mathrm{argmax}_{p \in P} \langle -u', p \rangle \rangle - \varepsilon \mathsf{w}_{-u'}(P)) \\
&= \max_{p \in P} \langle u', p \rangle - \min_{p \in P} \langle u', p \rangle - 2\varepsilon \mathsf{w}_{u'}(P) = (1 - 2\varepsilon)\mathsf{w}_{u'}(P)
\end{aligned}$$

By Lemma A.2,

$$\begin{aligned}
\mathsf{w}_u(Q) &\geq \mathsf{w}_{u'}(Q) - 2\lambda\sqrt{d} \\
&\geq (1 - 2\varepsilon)\mathsf{w}_{u'}(P) \\
&\geq (1 - 2\varepsilon)(\mathsf{w}_u(P) - 2\lambda\sqrt{d}) - 2\lambda\sqrt{d} \\
&= (1 - 2\varepsilon)\mathsf{w}_u(P) - 2\lambda\sqrt{d}(1 - 2\varepsilon + 1) \\
&= (1 - 2\varepsilon)\mathsf{w}_u(P) - 4\lambda\sqrt{d}(1 - \varepsilon)
\end{aligned}$$

Therefore, by Lemma A.1,

$$\begin{aligned}
\frac{\mathsf{w}_u(Q)}{\mathsf{w}_u(P)} &\geq 1 - 2\varepsilon - \frac{4\lambda\sqrt{d}(1 - \varepsilon)}{\mathsf{w}_u(P)} \\
&\geq 1 - 2\varepsilon - \frac{4\lambda\sqrt{d}(1 - \varepsilon)}{\alpha} \quad \text{due to } \alpha\text{-fatness of } P \\
&\geq 1 - 2\varepsilon - \varepsilon(1 - \varepsilon) \\
&\geq 1 - 3\varepsilon
\end{aligned}$$

and we get our desired result i.e. $\mathsf{w}_u(Q) \geq (1 - 3\varepsilon)\mathsf{w}_u(P)$

Proof of Theorem 3.4. Let $k(\varepsilon) \geq O\Big(\frac{1}{(\frac{\alpha\varepsilon/3}{4\sqrt{d}})^{d-1}}\Big)$ and let Ω be a fixed set of directions such that $|\Omega| = k(\varepsilon)$. Notice that here, since $k(\varepsilon) \geq O\Big(\frac{1}{(\frac{\alpha\varepsilon/3}{4\sqrt{d}})^{d-1}}\Big)$, by Theorem 3.3, the output of

Algorithm 1 would be a relaxed-ε-kernel. Let $F_{\text{inner}} : \mathcal{X} \to \mathbb{R}^{k(\varepsilon)}$ such that

$$F_{\text{inner}}(S) = \begin{pmatrix} \max_{x \in S} \langle u_1, x \rangle \\ \vdots \\ \max_{s \in S} \langle u_{k(\varepsilon)}, x \rangle \end{pmatrix}$$

Additionally, let $F_{\text{outer},1} : \mathbb{R}^d \times \mathbb{R}^d \to \mathbb{R}^{k(\varepsilon)}$ such

$$F_{\text{outer},1}(x) = \begin{pmatrix} \langle x, u_1 \rangle \\ \langle x, u_2 \rangle \\ \vdots \\ \langle x, u_{k(\varepsilon)} \rangle \end{pmatrix}$$

and $F_{\text{outer},2} : \mathbb{R}^{k(\varepsilon)} \times \mathbb{R}^{k(\varepsilon)} \to \mathbb{R}^{k(\varepsilon)}$ be defined as $F_{\text{outer},2}(x, y) = \text{ReLU}(x + y)$. Given $x \in \mathbb{R}^d$ and $y \in \mathbb{R}^{k(\varepsilon)}$, let $F_{\text{outer}}(x, y) = F_{\text{outer},2}(F_{\text{outer},1}(x) + y)$.

First, we note that ℓ_p-norms converge to the ℓ_∞-norm so there is a p such that for any $x \in \mathbb{R}^N$, $|\|x\|_p - \|x\|_\infty| < \frac{\varepsilon\alpha}{2}$. F_{inner} can be approximated to within $\frac{\varepsilon\alpha}{2}$ via a sum-decomposition by first mapping each $s \in S$ to $\phi_1(s) = [\langle u_1, s \rangle^p, \ldots, \langle u_{k(\varepsilon)}, s \rangle^p]^T \in \mathbb{R}^{k(\varepsilon)}$ and then taking $\sum(\phi_1(s))^{1/p}$ where the $1/p$-power is taken elementwise. Thus, by the universal approximation property of MLPs, there are multilayer perceptrons MLP_1 and MLP_2 such that

$$\left\| F_{\text{inner}}(S) - \text{MLP}_1 \left(\sum_{s \in S} \text{MLP}_2(s) \right) \right\| < \varepsilon\alpha.$$

This means that $F_{\text{inner}}(S)_i$ is within $\varepsilon\alpha$ for $\max_{s \in S} \langle u_i, s \rangle$ for any $S \in \mathcal{X}_\alpha$. Because each set in $\mathcal{X}_\alpha$ is α-fat, $\forall u \in S^{d-1}$, $F_{\text{inner}}(S)_i$ is within $\varepsilon \mathsf{w}_u(S)$ of the maximum value. In other words,

$$\left| \text{MLP}_1 \left(\sum_{s \in S} \text{MLP}_2(s) \right)_i - F_{\text{inner}}(S)_i \right| \leq \varepsilon \cdot \alpha \leq \varepsilon \cdot \mathsf{w}_{u_i}(S).$$

We can implement $F_{\text{outer},1}$ with MLP_3 i.e. $F_{\text{outer},1}(x) = \text{MLP}_3(x)$ where MLP_3 can realize $F_{\text{outer},1}$ by choosing its weight matrix to be diagonal with entries $[u_1, \ldots, u_{k(\varepsilon)}]$ along the diagonal. Similarly, $F_{\text{outer},2}$ can be exactly represented by

$$F_{\text{outer},2}(x, y) = \text{MLP}_4(x + y)$$

where MLP_4 represents the identity function followed by a ReLU activation. F_{outer} can be represented by a neural network ψ such that $\psi(x, y) = \text{MLP}_4(\text{MLP}_3(x) + y)$. Given $P \in \mathcal{X}_\alpha$ and $p_i \in P$,

$$\psi \left(p_i + \text{MLP}_1 \left(\sum_{s \in S} \text{MLP}_2(s) \right) \right) = \begin{pmatrix} \text{ReLU}(\langle u_1, p_i \rangle + \varepsilon \mathsf{w}_{u_i}(P) - \max_{p \in P} \langle u_1, p \rangle) \\ \vdots \\ \text{ReLU}(\langle u_{k(\varepsilon)}, p_i \rangle + \varepsilon \mathsf{w}_{u_i}(P) - \max_{p \in P} \langle u_{k(\varepsilon)}, p \rangle) \end{pmatrix}$$

This is exactly the point-wise update computed in a SumFormer architecture so if we instantiate a SumFormer $\mathcal{S}_\varepsilon$ with the MLPs described above and each MLP in $\mathcal{S}_\varepsilon$ mapping to an intermediate dimension of $k(\varepsilon)$, $Q_{\mathcal{S}_\varepsilon} = \sigma_{\text{col}}(\mathcal{S}_\varepsilon(P))^T P$ is a relaxed-ε-kernel by Theorem 3.3. Additionally, note that each MLP used to approximate $Q_{\mathcal{S}_\varepsilon}$ maps to $\mathbb{R}^k(\varepsilon)$ where k is *independent of the size of the input set and only dependent on the input dimension d, the fatness of the point set α, and the desired approximation error ε.*

Proof of Corollary 3.5 From Theorem 3.4, we know that $Q_\varepsilon = L_{1,\text{col}}(\mathcal{S}_\varepsilon(P))^T P$ is a relaxed ε-kernel for P. By Theorem 3.2, since Q_ε is a relaxed ε-kernel, it is $3c\varepsilon$-coreset for P. Then $(1-3c\varepsilon)\mu(P) \leq \mu(Q_\varepsilon) \leq (1+3c\varepsilon)\mu(P)$. By the universality of DeepSets, $\mathcal{N}_{\text{deepset}}$ can approximate μ to arbitrary accuracy for any point set in $\mathcal{X}_\alpha$. Thus, there is a $\mathcal{N}_{\text{deepset}}$ architecture such that

$$|\mathcal{N}_{\text{deepset}}(Q_\varepsilon) - \mu(Q_\varepsilon)| < \varepsilon$$

and we get the desired result.

A.3.2 Proofs from Section 4

Proof of Theorem 4.3 Note that the non-relaxed version is also given in [2]. For completeness, we prove this theorem for the relaxed case which essentially just follows from the definitions of duality.

First for any point $x \in \mathbb{R}^{d-1}$, let $\hat{x} = [x, 1]$ denote the point in $\mathbb{R}^d$ with the last coordinate being 1. Let $\phi(x) := \hat{x}/\|\hat{x}\| \in \mathbf{S}^{d-1}$ be the unit vector in direction x. Let $\mathbf{S}^{d-1}_+$ be the positive semi-sphere. It is easy to see that ϕ is bijective from $\mathbb{R}^{d-1}$ to $\mathbf{S}^{d-1}_+$. Note that for any $x \in \mathbb{R}^{d-1}$, $\langle \hat{x}, f^* \rangle$ and for any set of functions $\mathcal{H}$,

$$L_{\mathcal{H}}(x) = \min_{h \in \mathcal{H}} h(x) = \|x\| \min_{h \in \mathcal{H}} \langle \phi(x), h^* \rangle \quad \text{and}$$
$$U_{\mathcal{H}}(x) = \max_{h \in \mathcal{H}} h(x) = \|x\| \max_{h \in \mathcal{H}} \langle \phi(x), h^* \rangle.$$

Then

$$\mathcal{E}_{\mathcal{H}}(x) = \|x\| \cdot \mathsf{w}_{\phi(x)}(\mathcal{H}^*)$$

where $\mathcal{H}^*$ is the dual point set of $\mathcal{H}$.

If $\mathcal{G} = \{g_1, \ldots, g_k\}$ is a relaxed ε-kernel for $\mathcal{F}$. Then for any $x \in \mathbb{R}^d$, we have that $L_{\mathcal{F}}(x) \geq L_{\mathcal{G}}(x) - \varepsilon \mathcal{E}_{\mathcal{F}}(x)$ and $U_{\mathcal{F}}(x) \leq U_{\mathcal{G}}(x) + \varepsilon \mathcal{E}_{\mathcal{F}}(x)$. It then follows that for any $x \in \mathbb{R}^{d-1}$,

$$\min_{f^* \in \mathcal{F}^*} \langle \phi(x), f^* \rangle \geq \min_{g^* \in \mathcal{G}^*} \langle \phi(x), g^* \rangle - \varepsilon \mathsf{w}_{\phi(x)}(\mathcal{F}^*) \quad \text{and}$$
$$\max_{f^* \in \mathcal{F}^*} \langle \phi(x), f^* \rangle \leq \max_{g^* \in \mathcal{G}^*} \langle \phi(x), g^* \rangle + \varepsilon \mathsf{w}_{\phi(x)}(\mathcal{F}^*)$$

That is, for any $u \in \mathbf{S}^{d-1}_+$, $\overrightarrow{\mathsf{w}}_u(\mathcal{G}^*)$ ε-approximates $\overrightarrow{\mathsf{w}}_u(\mathcal{F}^*)$. Given that $\langle -u, p \rangle = -\langle u, p \rangle$ for any point p, this means that $\overrightarrow{\mathsf{w}}_u(\mathcal{G}^*)$ ε-approximates $\overrightarrow{\mathsf{w}}_u(\mathcal{F}^*)$ holds for any $u \in \mathbf{S}^{d-1}_+ \cup \mathbf{S}^{d-1}_-$. Hence the only directions left are $u \in \mathbf{S}^{d-1} \cap \{x \in \mathbb{R}^d, x_d = 0\}$. However, given that each term above is continuous, this holds due to continuity.

The other direction follows easily from the fact that ϕ being bijective.

Proof of Theorem 4.4 Suppose $\mathcal{F}$ admits a linearization of dimension m. For any $x \in \mathbb{R}^d$, we will show first that $\overrightarrow{\mathcal{E}}_{\mathcal{Q}_\varepsilon}(x) \subseteq \overrightarrow{\mathcal{E}}_{\mathcal{F}}(x)$. Then we will show that $\mathcal{E}_{\mathcal{Q}_\varepsilon}(x) \geq (1-\varepsilon)\mathcal{E}_{\mathcal{F}}(x)$. If we use Algorithm 1 to compute a relaxed-ε-kernel of the dual $\mathcal{F}^*$, we know that each $q_i^* \in \mathcal{Q}_\varepsilon^*$ is

$$q_i^* = \alpha_1^i \Psi(a_1) + \cdots + \alpha_N^i \Psi(a_N)$$

where $\sum_{\ell=1}^N \alpha_\ell^i = 1$. Additionally, we will let $k = |\mathcal{Q}_\varepsilon^*|$. Then we know there is a $q_i \in \mathcal{Q}_\varepsilon$ where

$$q_i(x) = (\alpha_1^i \ldots \alpha_N^i) \begin{pmatrix} \psi_0(a_1) \\ \vdots \\ \psi_0(a_N) \end{pmatrix} + (\alpha_1^i \ldots \alpha_N^i) \begin{pmatrix} \psi_1(a_1) \\ \vdots \\ \psi_1(a_N) \end{pmatrix} \varphi_1(x) + \cdots + (\alpha_1^i \ldots \alpha_N^i) \begin{pmatrix} \psi_m(a_1) \\ \vdots \\ \psi_m(a_N) \end{pmatrix} \varphi_m(x)$$

To ease notation, for any $j \in \{0, \ldots, m\}$ and $i \in [k]$, we write

$$\tilde{\Psi}_j = \begin{pmatrix} \psi_j(a_1) \\ \vdots \\ \psi_j(a_N) \end{pmatrix} \in \mathbb{R}^N \quad \boldsymbol{\alpha}^i = \begin{pmatrix} \alpha_1^i \\ \vdots \\ \alpha_N^i \end{pmatrix} \in \mathbb{R}^N$$

so $q_i(x) = (\boldsymbol{\alpha}^i)^T \tilde{\Psi}_0 + (\boldsymbol{\alpha}^i)^T \tilde{\Psi}_1 \varphi_1(x) + \cdots + (\boldsymbol{\alpha}^i)^T \tilde{\Psi}_m \varphi_m(x)$. We can re-write q_i as a convex combination of elements in $\mathcal{F}$:

$$\begin{aligned} q_i(x) &= \alpha_1^i \Psi(a_1)^T \Phi(x) + \cdots + \alpha_N^i \Psi(a_N)^T \Phi(x) \\ &= \alpha_1^i f_1(x) + \cdots + \alpha_N^i f_N(x) \end{aligned}$$

Let $x \in \mathbb{R}^d$ and let $f^* = \operatorname{argmin}_{f \in \mathcal{F}} f(x)$. Then for any $q_i \in \mathcal{Q}$,

$$q_i(x) = \alpha_1^i f_1(x) + \cdots \alpha_N^i f_N(x) \geq \alpha_1^i f^*(x) + \cdots + \alpha_N^i f^*(x) = f^*(x)$$

Therefore, $L_{\mathcal{Q}_\varepsilon} = \min_{q \in \mathcal{Q}_\varepsilon} q(x) \geq L_{\mathcal{F}}(x) = \min_{f \in \mathcal{F}} f(x)$. A similar argument shows that $U_{\mathcal{Q}_\varepsilon}(x) \leq U_{\mathcal{F}}(x)$.

Table 3: **Dataset details for approximating relaxed-ε-kernels.** $|P_{\text{train}}|$ and $|P_{\text{test}}|$ refer to the size of the train and test point clouds, respectively. The first four columns describe synthetic datasets while the last two columns describe two real datasets. For the 'Uniform ball' dataset, we sample point clouds uniformly from a d-dimensional ball. Note that for the 'Uniform ball' and 'Uniform Ellipse' in $\mathbb{R}^{10}$, we use point clouds of size 700 to train and test. For 'Uniform Ball', we will sometimes call it 'Uniform Disk' for point clouds in $\mathbb{R}^2$. For 'Ellipse', we sample from a randomly scaled and rotated point cloud. For 'Single Gaussians', we sample point clouds from a Gaussian with a random standard deviation and 'Gaussian Mixture' refers to point clouds sampled from two to five randomly placed Gaussian clusters. Note that for ModelNet, we apply random scaling to the point cloud so that the bounds are between $[-5, 5]$. See [43] and [26] for more details regarding SQUID and ModelNet, respectively.

	Synthetic				Real	
	Uniform Ball	Ellipse	Single Gaussian	Gaussian Mixture	ModelNet	SQUID
$\lvert P_{\text{train}}\rvert$	500, 700 (for $\mathbb{R}^{10}$)	500, 700 (for $\mathbb{R}^{10}$)	500	500	200	350
$\lvert P_{\text{test}}\rvert$	500, 700 (for $\mathbb{R}^{10}$)	500, 700 (for $\mathbb{R}^{10}$)	500	500	200	350
# train point clouds	3000	3000	3000	3000	2048	774
# test point clouds	750	750	750	750	2048	332
Input dim.	2,3,5,10	2,3,5,10	2,3,5	2,3,5	3	2
Bounds	$[-5, 5]$	$[-5, 5]$	$[-5, 5]$	$[-5, 5]$	$[-5, 5]$	$[0, 450]$

Now we will show that $\mathcal{E}_{\mathcal{Q}_\varepsilon}(x) \geq (1-\varepsilon)\mathcal{E}_{\mathcal{F}}(x)$ for any $x \in \mathbb{R}^d$. Given $x \in \mathbb{R}^d$, we know that $\Phi(x) = (1, \varphi_1(x), \ldots, \varphi_m(x)) \in \mathbb{R}^{m+1}$. Define $\mathcal{F}^{\text{Lin}}$ and $\mathcal{Q}_\varepsilon^{\text{Lin}}$ to be a set of linear functions

$$\mathcal{F}^{\text{Lin}} = \left\{ f_i^{\text{Lin}}(x_1, \ldots, x_m) = \Psi(a_j)^T \begin{pmatrix} 1 \\ x_1 \\ \vdots \\ x_m \end{pmatrix} : a_j \in A \right\}$$

$$\mathcal{Q}_\varepsilon^{\text{Lin}} = \left\{ ((\boldsymbol{\alpha}^i)^T \tilde{\Psi}_0 \cdots (\boldsymbol{\alpha}^i)^T \tilde{\Psi}_m) \begin{pmatrix} 1 \\ x_1 \\ \vdots \\ x_m \end{pmatrix} : i \in [m] \right\}.$$

First, notice that $(\mathcal{F}^{\text{Lin}})^* = \mathcal{F}^*$ and $(\mathcal{Q}_\varepsilon^{\text{Lin}})^* = \mathcal{Q}_\varepsilon^*$. We know that $\mathcal{Q}_\varepsilon^*$ is a relaxed-ε-kernel of $\mathcal{F}^*$ so by Theorem 4.3, $\mathcal{Q}_\varepsilon^{\text{Lin}}$ is a relaxed-ε-kernel for $\mathcal{F}^*$. Given any $x \in \mathbb{R}^d$, we know that $f_i(x) = f_i^{\text{Lin}}(\Phi(x))$ so

$$\mathcal{E}_{\mathcal{F}}(x) = \mathcal{E}_{\mathcal{F}^{\text{Lin}}}(\Phi(x)).$$

Similarly, we know that $q_j(x) = q_j^{\text{Lin}}(x)$ so

$$\mathcal{E}_{\mathcal{Q}_\varepsilon}(x) = \mathcal{E}_{\mathcal{Q}_\varepsilon^{\text{Lin}}}(\Phi(x)).$$

Since $\mathcal{Q}_\varepsilon^{\text{Lin}}$ is a relaxed-ε-kernel for $\mathcal{F}^*$,

$$\mathcal{E}_{\mathcal{Q}_\varepsilon}(x) \geq (1-\varepsilon)\mathcal{E}_{\mathcal{F}}(x).$$

A.4 Additional experimental details and results

All models are implemented in PyTorch and trained on 8 NVIDIA RTX A6000 GPUs. Our code is publically available[1]. Additionally, all models are trained using the ADAM optimizer [20] provided in PyTorch and trained using a learning rate of 0.001. Relaxed-ε-kernel networks are trained for 200 epochs while all extent-measure models are trained for 500 epochs. Additionally, for the processor for

[1] https://github.com/chens5/coreset-nn

Table 4: **Dataset details for extent measure approximation tasks.** $|P_{\text{train}}|$ and $|P_{\text{test}}|$ refer to the size of the train and test point clouds, respectively. The 'Uniform Ball' dataset is used for the minimum enclosing ball task and consists of point clouds randomly sampled from a d-dimensional ball. The 'Uniform Ellipse' dataset is used for the minimum enclosing ellipse task and consists of point clouds sampled from randomly scaled and rotated ellipses. The 'Uniform Annulus' dataset is used for the minimum enclosing annulus task and consists of point clouds sampled from annuli with widths from 0.1 to 3. See [43] and [26] for more details regarding SQUID and ModelNet, respectively.

	Synthetic			Real	
	Uniform Ball	Uniform Ellipse	Uniform Annulus	ModelNet	SQUID
$\lvert P_{\text{train}}\rvert$	200	100	100	200	350
$\lvert P_{\text{test}}\rvert$	200	100	100	200	350
# train point clouds	3000	3000	3000	2048	774
# test point clouds	3000	3000	3000	2048	332
Input dim.	2, 3	2	2	3	2
Bounds	$[-5, 5]$	$[-5, 5]$	$[-5, 5]$	$[-5, 5]$	$[0, 450]$

the encode-decode-process models (used for extent measure tasks), we fix the processor to take input from $\mathbb{R}^5$, have three blocks (either SumFormer or Transformer) and output 150 points from $\mathcal{N}_{\phi_\varepsilon}$. We choose this configuration as these hyperparameters had the best performance on the relaxed-ε-coreset task in $\mathbb{R}^5$. Additionally, for the frozen training regime, the processor networks ($\mathcal{N}_{\phi_\varepsilon}$) take input of a point cloud $\widehat{P}$ in $\mathbb{R}^5$ (which could contain arbitrary number of points), output $k = 150$ points, and are pre-trained on the 'Mixed Synthetic' data in $\mathbb{R}^5$. Detailed dataset specifications for the relaxed-ε-kernel experiments are given in Table 3 and those for extent-measure tasks are given Table 4. All code (including models, hyperparameter settings, and synthetic dataset generation) is available.

Size generalization for extent measures. Here we described the train and test set details for the size generalization experiments on the extent measure tasks described in Section 5, Figure 6 as well in our motivating example in Section 2. Each model used for our size generalization experiment is trained on the synthetic $\mathbb{R}^2$ datasets detailed in Table 4. For the minimum enclosing ball (MEB) task, test point clouds have sizes $N \in 500, 1000, \ldots, 17000$, with the bounding box from which test points are sampled defined as $[-N/500, N/500]^2$. For the minimum enclosing ellipse (MEE) and minimum enclosing annulus (MEA) tasks, test point clouds have sizes $N \in 100, 200, \ldots, 3000$, and the bounding box scales as $[-N/100, N/100]^2$.

Hyperparameter details. For our hyperparameter search on the relaxed-ε-kernel, we chose the depth of the network from $\{2, 3, 4\}$, the hidden dimension from $\{128, 256, 512, 1024\}$, and the embedding dimension from $16, 32$. All results in our paper are reported on the best performing models from our hyperparameter search. For the extent-measure models, we fix the hyperparameters of the processor based on the best configuration from the ε-kernel task and search over the hyperparameters (width/depth) of the encoder and decoder networks. The depth of both the encoder and decoder MLPs are sampled from $\{2, 3, 4\}$ and the width from $\{64, 128, 256\}$. Finally, we also tune the number of epochs trained and chose to test the models trained for 200 epochs as they had the best validation loss. We note that we did not observe the transformer OOD performance to improve with longer training times.

Loss functions. Here, we list all loss functions used to train each task given an input point set P.

- **Relaxed-ε-kernel:** To train a model to approximate relaxed-ε-kernel, at each epoch t, we first sample a random set of 100 directions Ω_t. We then compute the difference between the max projection of P and $\mathcal{N}_{\phi_\varepsilon}(P)$ for $d \in \Omega_t$ as well as the difference between the min

projection of P and $\mathcal{N}_{\phi_\varepsilon}(P)$ for $d \in D_t$:

$$\mathcal{L}_\varepsilon(P, \mathcal{N}_{\phi_\varepsilon}(P), D_t) = \frac{1}{|D_t|} \sum_{u \in \Omega_t} \left(|\max_{p \in P} \langle u, p \rangle - \max_{q \in \mathcal{N}_{\phi_\varepsilon}(P)} \langle u, q \rangle| + |\min_{p \in P} \langle u, p \rangle - \min_{q \in \mathcal{N}_{\phi_\varepsilon}(P)} \langle u, q \rangle| \right)$$

- **Minimum enclosing ball:** We aim to approximate the radius of the minimum enclosing ball. In order to validate that we have actually learned the ball, we also predict the center of ball. Therefore, given an input point set in $\mathbb{R}^d$, we configure $\mathcal{N}_{\text{extent}}$ such that $\mathcal{N}_{\text{extent}}(P) \in \mathbb{R}^{d+1}$ where the first d coordinates, $\mathcal{N}_{\text{extent}}(P)_{1:d}$ represent the center and the last coordinate $\mathcal{N}_{\text{extent}}(P)_{d+1}$ represents the radius. Given the ground truth center $c \in \mathbb{R}^d$ and radius $r \in \mathbb{R}$, the loss function we use to train $\mathcal{N}_{\text{extent}}$ is

$$\mathcal{L}(c, r, \mathcal{N}_{\text{extent}}(P)) = \|c - \mathcal{N}_{\text{extent}}(P)_{1:d}\| + (r - \mathcal{N}_{\text{extent}}(P)_{d+1})^2$$

- **Minimum enclosing ellipse:** Recall that we aim to predict the minimum area enclosing ellipse. First, we note that we center all data at the origin for the minimum enclosing ellipse. Unlike the minimum enclosing ball, we do not predict the center for the ellipse. Given an input point set $P \subseteq \mathbb{R}^d$, we configure $\mathcal{N}_{\text{extent}}$ such that $\mathcal{N}_{\text{extent}}(P) \in \mathbb{R}^3$ where $\mathcal{N}_{\text{extent}}(P)_1$ represents the major radius, $\mathcal{N}_{\text{extent}}(P)_2$ represents the minor radius, and $\mathcal{N}_{\text{extent}}(P)_3$ represents the angle of rotation. Given the ground truth major radius $r_{\text{maj}} \in \mathbb{R}$, minor radius $r_{\text{min}} \in \mathbb{R}$ and angle of rotation $\theta \in \mathbb{R}$, the loss function we use to train $\mathcal{N}_{\text{extent}}$ is

$$\begin{aligned}\mathcal{L}(r_{\text{maj}}, r_{\text{min}}, \theta, \mathcal{N}_{\text{extent}}(P)) = (r_{\text{maj}} - \mathcal{N}_{\text{extent}}(P)_1)^2 + (r_{\text{min}} - \mathcal{N}_{\text{extent}}(P)_2)^2 \\ + (\sin(\theta) - \sin(\mathcal{N}_{\text{extent}}(P)_3))^2 + (\cos(\theta) - \cos(\mathcal{N}_{\text{extent}}(P)_3))^2\end{aligned}$$

- **Minimum enclosing annulus:** We aim to predict the minimum width of the minimum enclosing annulus, which can be computed by predicting the inner and outer radii of the annulus and then taking their difference. Given an input point set $P \subseteq \mathbb{R}^d$, $\mathcal{N}_{\text{extent}}(P) \in \mathbb{R}^2$ where $\mathcal{N}_{\text{extent}}(P)_{d+1}$ represents the inner radius and $\mathcal{N}_{\text{extent}}(P)_{d+2}$ represents the outer radius. Then given the ground truth inner radius $r_{\text{inner}} \in \mathbb{R}$ and outer radius $r_{\text{outer}} \in \mathbb{R}$, the loss function we use to train $\mathcal{N}_{\text{extent}}$ is

$$\mathcal{L}(c, r_{\text{inner}}, r_{\text{outer}}, \mathcal{N}_{\text{extent}}(P)) = \frac{|r_{\text{inner}} - \mathcal{N}_{\text{extent}}(P)_1|}{r_{\text{inner}}} + \frac{|r_{\text{outer}} - \mathcal{N}_{\text{extent}}(P)_2|}{r_{\text{outer}}}$$

A.4.1 Additional experiments for approximating relaxed-ε-kernels

First, we note that we include all complete tables from the main text with error bars in Table 5 and Table 6. We additionally include results on datasets in higher-dimensional synthetic datasets in $\mathbb{R}^5$ in Table 7 and $\mathbb{R}^{10}$ in Table 8. We see largely the same trends, where the $\mathcal{S}_\varepsilon$ performs comparably to $\mathcal{T}_\varepsilon$ on in-distribution data and then $\mathcal{S}_\varepsilon$ performs much better than $\mathcal{T}_\varepsilon$ on out of distribution data. Although the classical ε-kernel algorithm sometimes has lower directional error than $\mathcal{S}_\varepsilon$, we compare the runtime of the ε-kernel algorithm with all neural approaches in Figure 11 and show that our neural models are generally much more efficient at inference time than algorithmic approaches. We also provide more extensive results in Tables 9, 10, and 11, where we detail the performance of each neural approach on different types of synthetic and real datasets.

For the relaxed-ε-kernel tasks, we also provide several sensitivity analyses showing the effect of input dimension, fatness of point sets, and the size of relaxed-ε-kernel on the direction error ($\mathcal{E}_{\text{dir}}$). For each of these sensitivity analyses, we also provide a baseline comparison to the relaxed-ε-kernel algorithm described in Algorithm 1 given $\varepsilon = 0.1$ in order to analyze the behavior of the neural network with respect to its aligned algorithm. In all cases, the data-driven way of learning the relaxed-ε-kernel presents significantly more accurate (in terms of directional error) coresets than the baseline algorithmic implementation.

Effect of input dimension. From Theorem 3.4, we know that the accuracy of the approximation of the relaxed-ε-kernel will depend on the dimension of the input point cloud. We verify this empirically in Figure 7 across different sizes of ε-kernels. For this experiment, we train and test each model on the point clouds with 500 points sampled uniformly from a ball in $\mathbb{R}^D$ where $D \in \{2, 3, 5\}$. We can see in Figure 7 that $\mathcal{E}_{\text{dir}}$ increases as the input dimension of the point cloud increases.

Effect of α-fatness. Similar to the relationship between error and input point cloud dimension, we know from Theorem 3.4 that the accuracy of the approximation of the relaxed-ε-kernel will depend on the α-fatness of the input point set. To verify this, we train both the SumFormer and Transformer model on point clouds with 500 points sampled uniformly from a balls in $\mathbb{R}^3$ and $\mathbb{R}^2$ (disks in the case of $\mathbb{R}^2$). We then test on point clouds of 100 points sampled from ellipsoids which have their minor axes scaled to simulate point clouds with a range of α-fatness. The results are reported in Figure 8. Indeed, we see that as α increases (i.e. the point cloud becomes fatter) the accuracy of our approach increases.

Effect of output size. In order to examine the effect of the output relaxed-ε-kernel size for the quality of the approximation, we plot the normalized output size (i.e. number of relaxed-ε-kernel points/total number of input points) against the directional width error. See Figure 9. As expected, we see that the error decreases as the output size increases.

Effect of input point set size. We also examine the out-of-distribution capabilities of the models in terms of generalizing to larger point sets. For this experiment, we train each model on the point clouds with 500 points sampled uniformly from a ball in $\mathbb{R}^D$ where $D \in \{2, 3, 5\}$ and then test the models on much larger point clouds (up to 1000 points per cloud) sampled from the uniform ball. The results are reported in Figure 10 and we find that the SumFormer model generalizes especially well to out-of-distribution point set sizes (maintains low error).

A.4.2 Additional experiments for approximation of extent measures

We include the full results from the main text (which include the percentage of points excluded from each covering object). The full results each extent measure task are included in Tables 12, 13, 14, and 15 for minimum enclosing ball in $\mathbb{R}^2$, minimum enclosing ball in $\mathbb{R}^3$, minimum enclosing ellipse in $\mathbb{R}^2$, and minimum enclosing annulus $\mathbb{R}^2$, respectively. We also include comparisons to classical algorithmic approximations in our full experimental tables. In particular, we evaluate the standard pipeline of first computing an ε-kernel and then applying the exact algorithm to the resulting coreset. For MEB and MEE, we use Welzl's algorithm as the exact solver; for MEA, we use the quadratic programming formulation implemented in the Computational Geometry Algorithms Library (CGAL) [35]. Additionally, Figure 12 reports the inference times of the neural models alongside the runtimes of the corresponding algorithmic approaches.

First, note that our ε-kernel–aligned model, the frozen $\mathcal{S}_{\text{extent}}$, misses a much smaller proportion of points than other models (even those with lower radius or width prediction error) indicating that its predicted shape more accurately captures the true enclosing object. Notice that while classical algorithms can achieve higher accuracy in some cases, our neural models outperform them on the minimum enclosing annulus task, which is more challenging than the other extent measure tasks as it is unfaithful and non LP-type. Moreover, as shown in Figure 12, our neural approaches are substantially faster than all algorithmic baselines (both the exact and the approximation), particularly for the minimum enclosing annulus. Finally, as emphasized in the main text, neural approximations offer a key conceptual advantage over classical algorithms beyond gains in speed: they do not require explicit knowledge of the underlying optimization objective. To train our neural models, only labeled data and the knowledge that the problem belongs to the general family of extent-measure tasks are needed. In contrast, classical algorithmic methods require full specification of the objective and often the design of a custom algorithm to solve each specific problem.

Finally, Figure 13 presents additional results for the size-generalization experiment shown in Figure 6, where we record the proportion of points excluded as the number of points per cloud increases. Not only does the frozen $\mathcal{S}_{\text{extent}}$ model outperform all other neural baselines in terms of size generalization and the error (as seen in Figure 6 but also the predicted output from the frozen $\mathcal{S}_{\text{extent}}$ model misses a low proportion of points. Notably, models that exclude fewer points than the frozen $\mathcal{S}\text{extent}$ tend to exhibit higher width or radius error, indicating an overestimate of the enclosing object. This can also be seen in visualizations of the predicted output from each model in Figure 14, where we see that the frozen $\mathcal{S}_{\text{extent}}$ model can better adapt to out-of-distribution input data.

A.5 Figures and Tables

Table 5: $\mathcal{E}_{\text{dir}}$ on datasets in $\mathbb{R}^2$ for an output relaxed-ε-kernel of 16 points. We compare Sumformer and Transformer neural approaches across three different test sets for each train set. Note that 'Mixed Synthetic' has no 'OOD, Synthetic' because the train set contains all types of synthetic data. Boldface indicates the lower error per row.

		Test Sets		
			OOD	
Train Set	**Method**	In-dist.	Synthetic	SQUID
Ellipse	$\mathcal{S}_\varepsilon$	0.060 ± 0.026	$\mathbf{0.044 \pm 0.042}$	$\mathbf{0.127 \pm 0.111}$
	$\mathcal{T}_\varepsilon$	$\mathbf{0.029 \pm 0.013}$	0.098 ± 0.056	0.275 ± 0.112
	$\mathcal{S}_{\varepsilon,B}$	0.131 ± 0.029	0.354 ± 0.172	0.993 ± 0.002
	$\mathcal{T}_{\varepsilon,B}$	0.117 ± 0.045	0.63 ± 0.115	0.976 ± 0.007
Gaussian Mixture	$\mathcal{S}_\varepsilon$	$\mathbf{0.014 \pm 0.013}$	$\mathbf{0.043 \pm 0.040}$	$\mathbf{0.028 \pm 0.043}$
	$\mathcal{T}_\varepsilon$	0.027 ± 0.024	0.097 ± 0.049	0.218 ± 0.101
	$\mathcal{S}_{\varepsilon,\text{B}}$	0.146 ± 0.062	0.146 ± 0.057	0.962 ± 0.011
	$\mathcal{T}_{\varepsilon,\text{B}}$	0.19 ± 0.087	0.383 ± 0.067	0.94 ± 0.015
SQUID	$\mathcal{S}_\varepsilon$	$\mathbf{0.028 \pm 0.022}$	0.504 ± 0.114	$\mathbf{0.028 \pm 0.022}$
	$\mathcal{T}_\varepsilon$	0.061 ± 0.052	$\mathbf{0.40 \pm 0.109}$	0.061 ± 0.052
	$\mathcal{S}_{\varepsilon,\text{B}}$	0.421 ± 0.511	7.137 ± 3.892	0.421 ± 0.511
	$\mathcal{T}_{\varepsilon,\text{B}}$	0.228 ± 0.207	14.561 ± 6.632	0.228 ± 0.207
Mixed Synthetic	$\mathcal{S}_\varepsilon$	$\mathbf{0.027 \pm 0.018}$	–	$\mathbf{0.065 \pm 0.071}$
	$\mathcal{T}_\varepsilon$	0.032 ± 0.024	–	0.296 ± 0.113
	$\mathcal{S}_{\varepsilon,\text{B}}$	0.094 ± 0.058	-	0.971 ± 0.008
	$\mathcal{T}_{\varepsilon,\text{B}}$	0.203 ± 0.181	-	0.939 ± 0.017
Algorithmic Baselines	$\mathcal{B}_{\varepsilon,R}$	-	0.180 ± 0.079	0.228 ± 0.139
	$\mathcal{B}_{\varepsilon,E}$	-	0.040 ± 0.049	0.062 ± 0.095

Table 6: $\mathcal{E}_{\text{dir}}$ for predicted relaxed-ε-kernels of 64 points in $\mathbb{R}^3$. We compare Sumformer and Transformer neural approaches across three different test sets for each train set. Note that 'Mixed Synthetic' has no 'OOD, Synthetic' because the train set contains all types of synthetic data. Boldface indicates the lower error per row.

		Test Sets		
			OOD	
Train Set	**Method**	In-Dist.	Synthetic	ModelNet
Ellipse	$\mathcal{S}_\varepsilon$	$\mathbf{0.049 \pm 0.019}$	$\mathbf{0.032 \pm 0.024}$	$\mathbf{0.066 \pm 0.053}$
	$\mathcal{T}_\varepsilon$	0.055 ± 0.021	0.106 ± 0.076	0.147 ± 0.077
	$\mathcal{S}_{\varepsilon,\text{B}}$	0.221 ± 0.039	0.462 ± 0.098	4.736 ± 3.49
	$\mathcal{T}_{\varepsilon,\text{B}}$	0.243 ± 0.056	0.555 ± 0.063	3.603 ± 5.454
Gaussian Mixture	$\mathcal{S}_\varepsilon$	$\mathbf{0.047 \pm 0.027}$	$\mathbf{0.039 \pm 0.026}$	$\mathbf{0.064 \pm 0.050}$
	$\mathcal{T}_\varepsilon$	0.054 ± 0.027	0.066 ± 0.033	0.250 ± 0.125
	$\mathcal{S}_{\varepsilon,\text{B}}$	0.274 ± 0.049	0.289 ± 0.029	1.949 ± 3.49
	$\mathcal{T}_{\varepsilon,\text{B}}$	0.357 ± 0.146	0.851 ± 0.104	4.486 ± 5.514
ModelNet	$\mathcal{S}_\varepsilon$	$\mathbf{0.041 \pm 0.037}$	$\mathbf{0.099 \pm 0.077}$	$\mathbf{0.041 \pm 0.037}$
	$\mathcal{T}_\varepsilon$	0.049 ± 0.044	0.265 ± 0.118	0.049 ± 0.044
	$\mathcal{S}_{\varepsilon,\text{B}}$	0.378 ± 0.621	0.542 ± 0.069	0.379 ± 0.621
	$\mathcal{T}_{\varepsilon,\text{B}}$	0.542 ± 0.952	0.658 ± 0.142	0.542 ± 0.952
Mixed Synthetic	$\mathcal{S}_\varepsilon$	$\mathbf{0.035 \pm 0.029}$	–	$\mathbf{0.055 \pm 0.048}$
	$\mathcal{T}_\varepsilon$	0.042 ± 0.038	–	0.117 ± 0.071
	$\mathcal{S}_{\varepsilon,\text{B}}$	0.174 ± 0.054	-	1.518 ± 2.288
	$\mathcal{T}_{\varepsilon,\text{B}}$	0.289 ± 0.179	-	4.356 ± 5.257
Algorithmic Baselines	$\mathcal{B}_{\varepsilon,R}$	-	1.016 ± 9.988	2.176 ± 2.849
	$\mathcal{B}_{\varepsilon,E}$	-	0.062 ± 0.040	0.050 ± 0.047

Table 7: $\mathcal{E}_{\text{dir}}$ for predicted relaxed-ε-kernels of 200 points in $\mathbb{R}^5$. We compare Sumformer and Transformer neural approaches for in-distribution and out-of-distribution synthetic test sets. Note that there are no real datasets in $\mathbb{R}^5$ so the only test sets here are synthetic.

Train Set	**Method**	In-Distribution	OOD, Synthetic
Uniform Ball	$\mathcal{S}_\varepsilon$	$\mathbf{0.084 \pm 0.016}$	$\mathbf{0.091 \pm 0.041}$
	$\mathcal{T}_\varepsilon$	0.118 ± 0.022	0.29 ± 0.117
	$\mathcal{S}_{\varepsilon,\text{B}}$	0.238 ± 0.029	0.694 ± 0.234
	$\mathcal{T}_{\varepsilon,\text{B}}$	0.35 ± 0.043	0.575 ± 0.249
Ellipse	$\mathcal{S}_\varepsilon$	0.085 ± 0.025	$\mathbf{0.077 \pm 0.027}$
	$\mathcal{T}_\varepsilon$	$\mathbf{0.084 \pm 0.024}$	0.196 ± 0.133
	$\mathcal{S}_{\varepsilon,\text{B}}$	0.399 ± 0.108	0.589 ± 0.256
	$\mathcal{T}_{\varepsilon,\text{B}}$	0.343 ± 0.096	0.614 ± 0.167
Single Gaussian	$\mathcal{S}_\varepsilon$	$\mathbf{0.065 \pm 0.018}$	$\mathbf{0.10 \pm 0.033}$
	$\mathcal{T}_\varepsilon$	0.065 ± 0.022	0.183 ± 0.053
	$\mathcal{S}_{\varepsilon,\text{B}}$	0.352 ± 0.048	3.75 ± 0.154
	$\mathcal{T}_{\varepsilon,\text{B}}$	0.333 ± 0.044	3.941 ± 0.112
Gaussian Mixture	$\mathcal{S}_\varepsilon$	$\mathbf{0.084 \pm 0.028}$	$\mathbf{0.087 \pm 0.027}$
	$\mathcal{T}_\varepsilon$	0.091 ± 0.025	0.109 ± 0.032
	$\mathcal{S}_{\varepsilon,\text{B}}$	0.717 ± 0.021	0.465 ± 0.184
	$\mathcal{T}_{\varepsilon,\text{B}}$	0.757 ± 0.278	1.488 ± 0.344
Mixed Synthetic	$\mathcal{S}_\varepsilon$	$\mathbf{0.075 \pm 0.025}$	-
	$\mathcal{T}_\varepsilon$	0.087 ± 0.032	-
	$\mathcal{S}_{\varepsilon,\text{B}}$	0.347 ± 0.188	-
	$\mathcal{T}_{\varepsilon,\text{B}}$	0.879 ± 0.599	-
Algorithmic Baselines	$\mathcal{B}_{\varepsilon,R}$	-	0.653 ± 0.366
	$\mathcal{B}_{\varepsilon,E}$	-	0.083 ± 0.033

Table 8: $\mathcal{E}_{\text{dir}}$ for predicted relaxed-ε-kernels of 200 points in $\mathbb{R}^{10}$. We compare Sumformer and Transformer neural approaches for in-distribution and out-of-distribution synthetic test sets. Note that there are no real datasets in $\mathbb{R}^5$ so the only test sets here are synthetic.

Train Set	**Method**	In-Distribution	OOD, Synthetic
Uniform Ball	$\mathcal{S}_\varepsilon$	0.367 ± 0.0289	0.301 ± 0.074
	$\mathcal{T}_\varepsilon$	$\mathbf{0.259 \pm 0.0227}$	$\mathbf{0.292 \pm 0.044}$
	$\mathcal{S}_{\varepsilon,\text{B}}$	0.290 ± 0.033	0.459 ± 0.214
	$\mathcal{T}_{\varepsilon,\text{B}}$	0.266 ± 0.029	0.435 ± 0.208
Ellipse	$\mathcal{S}_\varepsilon$	$\mathbf{0.222 \pm 0.037}$	$\mathbf{0.275 \pm 0.062}$
	$\mathcal{T}_\varepsilon$	0.251 ± 0.042	0.276 ± 0.041
	$\mathcal{S}_{\varepsilon,\text{B}}$	0.693 ± 0.166	0.518 ± 0.209
	$\mathcal{T}_{\varepsilon,\text{B}}$	0.777 ± 0.192	0.582 ± 0.281
Mixed Synthetic	$\mathcal{S}_\varepsilon$	$\mathbf{0.241 \pm 0.036}$	-
	$\mathcal{T}_\varepsilon$	0.258 ± 0.034	-
	$\mathcal{S}_{\varepsilon,\text{B}}$	0.530 ± 0.281	-
	$\mathcal{T}_{\varepsilon,\text{B}}$	0.535 ± 0.287	-
Algorithmic Baselines	$\mathcal{B}_{\varepsilon,R}$	-	0.621 ± 0.225
	$\mathcal{B}_{\varepsilon,E}$	-	0.199 ± 0.034

Table 9: Directional error across 2D datasets for various ϵ-kernel sizes. Note that we already report performance for the mixed synthetic data in the tables in the main text so we do not report the performance here.

Train Set	ϵ	Method	Uniform Disk	Ellipse	Single Gaussian	Gaussian Mixture	SQUID
Uniform Disk	16	$\mathcal{S}_\varepsilon$	0.040 ± 0.013	0.109 ± 0.081	0.125 ± 0.057	0.074 ± 0.059	0.101 ± 0.065
		$\mathcal{T}_\varepsilon$	0.040 ± 0.013	0.200 ± 0.094	0.370 ± 0.078	0.346 ± 0.144	0.297 ± 0.110
		$\mathcal{S}_{\varepsilon,B}$	0.237 ± 0.009	0.544 ± 0.159	0.767 ± 0.017	0.712 ± 0.115	0.995 ± 0.002
		$\mathcal{T}_{\varepsilon,B}$	0.061 ± 0.007	0.456 ± 0.167	0.720 ± 0.019	0.512 ± 0.159	0.973 ± 0.008
	64	$\mathcal{S}_\varepsilon$	0.009 ± 0.004	0.065 ± 0.051	0.214 ± 0.057	0.061 ± 0.053	0.264 ± 0.093
		$\mathcal{T}_\varepsilon$	0.007 ± 0.004	0.158 ± 0.079	0.385 ± 0.058	0.287 ± 0.123	0.236 ± 0.099
		$\mathcal{S}_{\varepsilon,B}$	0.062 ± 0.008	0.443 ± 0.165	0.703 ± 0.020	0.561 ± 0.123	0.975 ± 0.007
		$\mathcal{T}_{\varepsilon,B}$	0.044 ± 0.011	0.456 ± 0.186	0.702 ± 0.020	0.534 ± 0.134	0.972 ± 0.009
	200	$\mathcal{S}_\varepsilon$	0.006 ± 0.003	0.069 ± 0.057	0.128 ± 0.062	0.097 ± 0.099	0.174 ± 0.085
		$\mathcal{T}_\varepsilon$	0.005 ± 0.003	0.199 ± 0.110	0.465 ± 0.041	0.262 ± 0.110	0.427 ± 0.109
		$\mathcal{S}_{\varepsilon,B}$	0.111 ± 0.008	0.473 ± 0.165	0.721 ± 0.019	0.589 ± 0.103	0.982 ± 0.005
		$\mathcal{T}_{\varepsilon,B}$	0.123 ± 0.010	0.484 ± 0.167	0.739 ± 0.018	0.599 ± 0.144	0.975 ± 0.008
Ellipse	16	$\mathcal{S}_\varepsilon$	0.045 ± 0.013	0.058 ± 0.026	0.042 ± 0.039	0.067 ± 0.057	0.130 ± 0.109
		$\mathcal{T}_\varepsilon$	0.031 ± 0.010	0.029 ± 0.013	0.093 ± 0.056	0.050 ± 0.041	0.272 ± 0.108
		$\mathcal{S}_{\varepsilon,B}$	0.110 ± 0.012	0.131 ± 0.029	0.458 ± 0.039	0.495 ± 0.271	0.993 ± 0.002
		$\mathcal{T}_{\varepsilon,B}$	0.715 ± 0.061	0.119 ± 0.046	0.601 ± 0.035	0.575 ± 0.247	0.975 ± 0.007
	64	$\mathcal{S}_\varepsilon$	0.011 ± 0.005	0.015 ± 0.008	0.034 ± 0.050	0.078 ± 0.086	0.088 ± 0.070
		$\mathcal{T}_\varepsilon$	0.013 ± 0.005	0.012 ± 0.006	0.116 ± 0.057	0.033 ± 0.032	0.241 ± 0.087
		$\mathcal{S}_{\varepsilon,B}$	0.121 ± 0.010	0.146 ± 0.029	0.438 ± 0.039	0.456 ± 0.210	0.976 ± 0.007
		$\mathcal{T}_{\varepsilon,B}$	0.674 ± 0.049	0.101 ± 0.040	0.613 ± 0.031	0.593 ± 0.231	0.978 ± 0.007
	200	$\mathcal{S}_\varepsilon$	0.004 ± 0.002	0.005 ± 0.003	0.033 ± 0.046	0.057 ± 0.077	0.118 ± 0.073
		$\mathcal{T}_\varepsilon$	0.010 ± 0.004	0.008 ± 0.005	0.030 ± 0.027	0.034 ± 0.033	0.197 ± 0.079
		$\mathcal{S}_{\varepsilon,B}$	0.098 ± 0.011	0.118 ± 0.025	0.445 ± 0.038	0.435 ± 0.215	0.989 ± 0.003
		$\mathcal{T}_{\varepsilon,B}$	0.217 ± 0.028	0.076 ± 0.030	0.436 ± 0.038	0.583 ± 0.413	0.961 ± 0.011
Gaussian	16	$\mathcal{S}_\varepsilon$	0.056 ± 0.015	0.097 ± 0.052	0.032 ± 0.020	0.071 ± 0.049	0.091 ± 0.069
		$\mathcal{T}_\varepsilon$	0.062 ± 0.017	0.069 ± 0.029	0.019 ± 0.014	0.080 ± 0.052	0.206 ± 0.095
		$\mathcal{S}_{\varepsilon,B}$	0.924 ± 0.031	1.174 ± 0.604	0.108 ± 0.030	1.256 ± 0.638	0.946 ± 0.015
		$\mathcal{T}_{\varepsilon,B}$	2.417 ± 0.109	2.376 ± 1.023	0.246 ± 0.053	2.200 ± 1.126	0.922 ± 0.024
	64	$\mathcal{S}_\varepsilon$	0.029 ± 0.009	0.050 ± 0.029	0.011 ± 0.010	0.039 ± 0.032	0.078 ± 0.068
		$\mathcal{T}_\varepsilon$	0.052 ± 0.015	0.056 ± 0.027	0.005 ± 0.007	0.083 ± 0.058	0.241 ± 0.100
		$\mathcal{S}_{\varepsilon,B}$	0.884 ± 0.032	1.102 ± 0.612	0.101 ± 0.032	1.314 ± 0.741	0.949 ± 0.015
		$\mathcal{T}_{\varepsilon,B}$	2.374 ± 0.102	2.209 ± 0.941	0.152 ± 0.044	2.147 ± 1.089	0.879 ± 0.028
	200	$\mathcal{S}_\varepsilon$	0.017 ± 0.007	0.057 ± 0.060	0.003 ± 0.004	0.056 ± 0.048	0.067 ± 0.058
		$\mathcal{T}_\varepsilon$	0.047 ± 0.015	0.049 ± 0.020	0.004 ± 0.006	0.071 ± 0.049	0.220 ± 0.099
		$\mathcal{S}_{\varepsilon,B}$	0.927 ± 0.031	1.131 ± 0.617	0.114 ± 0.030	1.316 ± 0.703	0.944 ± 0.019
		$\mathcal{T}_{\varepsilon,B}$	2.456 ± 0.125	2.151 ± 0.946	0.144 ± 0.041	2.216 ± 1.116	0.910 ± 0.024
Gaussian Mixture	16	$\mathcal{S}_\varepsilon$	0.024 ± 0.008	0.033 ± 0.015	0.071 ± 0.059	0.013 ± 0.013	0.028 ± 0.037
		$\mathcal{T}_\varepsilon$	0.040 ± 0.011	0.034 ± 0.011	0.063 ± 0.050	0.027 ± 0.024	0.214 ± 0.100
		$\mathcal{S}_{\varepsilon,B}$	0.067 ± 0.010	0.087 ± 0.025	0.188 ± 0.043	0.128 ± 0.058	0.967 ± 0.011
		$\mathcal{T}_{\varepsilon,B}$	0.686 ± 0.051	0.485 ± 0.075	0.272 ± 0.047	0.190 ± 0.086	0.944 ± 0.015
	64	$\mathcal{S}_\varepsilon$	0.015 ± 0.006	0.018 ± 0.010	0.107 ± 0.067	0.006 ± 0.006	0.015 ± 0.013
		$\mathcal{T}_\varepsilon$	0.032 ± 0.011	0.017 ± 0.008	0.026 ± 0.033	0.009 ± 0.010	0.156 ± 0.082
		$\mathcal{S}_{\varepsilon,B}$	0.062 ± 0.010	0.084 ± 0.024	0.179 ± 0.046	0.121 ± 0.052	0.963 ± 0.011
		$\mathcal{T}_{\varepsilon,B}$	1.031 ± 0.050	0.609 ± 0.105	0.316 ± 0.046	0.164 ± 0.075	0.947 ± 0.015
	200	$\mathcal{S}_\varepsilon$	0.005 ± 0.003	0.009 ± 0.007	0.100 ± 0.047	0.003 ± 0.004	0.012 ± 0.018
		$\mathcal{T}_\varepsilon$	0.030 ± 0.012	0.011 ± 0.006	0.032 ± 0.033	0.006 ± 0.007	0.149 ± 0.084
		$\mathcal{S}_{\varepsilon,B}$	0.086 ± 0.010	0.103 ± 0.026	0.193 ± 0.046	0.138 ± 0.067	0.966 ± 0.011
		$\mathcal{T}_{\varepsilon,B}$	1.706 ± 0.082	0.815 ± 0.140	0.356 ± 0.052	0.191 ± 0.103	0.940 ± 0.014
SQUID	16	$\mathcal{S}_\varepsilon$	0.548 ± 0.012	0.528 ± 0.027	0.547 ± 0.040	0.395 ± 0.183	0.029 ± 0.021
		$\mathcal{T}_\varepsilon$	0.434 ± 0.041	0.403 ± 0.060	0.390 ± 0.081	0.368 ± 0.163	0.066 ± 0.051
		$\mathcal{S}_{\varepsilon,B}$	10.061 ± 0.191	9.954 ± 3.629	2.875 ± 0.296	10.191 ± 4.073	0.283 ± 0.276
		$\mathcal{T}_{\varepsilon,B}$	19.858 ± 0.815	18.238 ± 6.542	5.490 ± 0.519	16.164 ± 6.500	0.231 ± 0.224
	64	$\mathcal{S}_\varepsilon$	0.287 ± 0.014	0.289 ± 0.032	0.411 ± 0.047	0.274 ± 0.173	0.009 ± 0.008
		$\mathcal{T}_\varepsilon$	0.373 ± 0.025	0.376 ± 0.039	0.409 ± 0.057	0.350 ± 0.149	0.062 ± 0.042
		$\mathcal{S}_{\varepsilon,B}$	16.621 ± 0.499	16.123 ± 4.591	6.463 ± 0.608	12.393 ± 5.642	0.224 ± 0.202
		$\mathcal{T}_{\varepsilon,B}$	22.050 ± 1.050	19.865 ± 7.018	5.916 ± 0.611	16.114 ± 7.801	0.234 ± 0.241
	200	$\mathcal{S}_\varepsilon$	0.368 ± 0.013	0.339 ± 0.034	0.378 ± 0.048	0.255 ± 0.190	0.009 ± 0.009
		$\mathcal{T}_\varepsilon$	0.322 ± 0.059	0.346 ± 0.069	0.463 ± 0.081	0.379 ± 0.140	0.047 ± 0.036
		$\mathcal{S}_{\varepsilon,B}$	5.683 ± 0.144	5.374 ± 2.142	1.582 ± 0.179	6.337 ± 4.633	0.199 ± 0.199
		$\mathcal{T}_{\varepsilon,B}$	15.879 ± 0.788	15.438 ± 4.420	4.426 ± 0.487	13.109 ± 5.951	0.261 ± 0.243
Mixed	16	$\mathcal{S}_\varepsilon$	0.038 ± 0.012	0.052 ± 0.024	0.019 ± 0.015	0.031 ± 0.026	0.064 ± 0.073
		$\mathcal{T}_\varepsilon$	0.035 ± 0.011	0.046 ± 0.023	0.017 ± 0.014	0.040 ± 0.033	0.307 ± 0.112
		$\mathcal{S}_{\varepsilon,B}$	0.046 ± 0.008	0.057 ± 0.016	0.069 ± 0.017	0.124 ± 0.058	0.971 ± 0.008
		$\mathcal{T}_{\varepsilon,B}$	0.577 ± 0.0509	0.646 ± 0.267	0.220 ± 0.059	0.512 ± 0.329	0.939 ± 0.017
	64	$\mathcal{S}_\varepsilon$	0.010 ± 0.004	0.013 ± 0.008	0.002 ± 0.004	0.008 ± 0.008	0.023 ± 0.030
		$\mathcal{T}_\varepsilon$	0.016 ± 0.007	0.014 ± 0.006	0.001 ± 0.003	0.014 ± 0.017	0.183 ± 0.080
		$\mathcal{S}_{\varepsilon,B}$	0.109 ± 0.010	0.136 ± 0.031	0.108 ± 0.029	0.138 ± 0.065	0.967 ± 0.010
		$\mathcal{T}_{\varepsilon,B}$	1.339 ± 0.094	0.877 ± 0.265	0.320 ± 0.073	0.561 ± 0.368	0.922 ± 0.024
	200	$\mathcal{S}_\varepsilon$	0.006 ± 0.003	0.008 ± 0.005	0.001 ± 0.002	0.005 ± 0.006	0.014 ± 0.022
		$\mathcal{T}_\varepsilon$	0.014 ± 0.008	0.012 ± 0.008	0.001 ± 0.003	0.013 ± 0.014	0.144 ± 0.062
		$\mathcal{S}_{\varepsilon,B}$	0.251 ± 0.012	0.285 ± 0.121	0.261 ± 0.049	0.391 ± 0.222	0.949 ± 0.015
		$\mathcal{T}_{\varepsilon,B}$	1.428 ± 0.064	1.133 ± 0.366	0.238 ± 0.055	0.468 ± 0.289	0.913 ± 0.024

Table 10: $\mathcal{E}_{\text{dir}}$ across all 3D datasets for various ϵ-kernel sizes. Note that we already report performance for the mixed synthetic data in the tables in the main text so we do not report the performance here.

Dataset	ϵ	Architecture	Uniform Ball	Ellipse	Single Gaussian	Gaussian Mixture	ModelNet
Uniform Ball	16	$\mathcal{S}_\varepsilon$	0.180 ± 0.030	0.239 ± 0.069	0.159 ± 0.045	0.180 ± 0.072	0.161 ± 0.094
		$\mathcal{T}_\varepsilon$	0.180 ± 0.032	0.358 ± 0.085	0.553 ± 0.030	0.421 ± 0.123	0.426 ± 0.130
		$\mathcal{S}_{\varepsilon,B}$	0.251 ± 0.031	0.620 ± 0.214	0.774 ± 0.014	0.643 ± 0.128	2.887 ± 4.045
		$\mathcal{T}_{\varepsilon,B}$	0.149 ± 0.019	0.569 ± 0.2	0.757 ± 0.015	0.623 ± 0.133	3.547 ± 5.67
	64	$\mathcal{S}_\varepsilon$	0.046 ± 0.012	0.051 ± 0.018	0.029 ± 0.014	0.050 ± 0.028	0.067 ± 0.057
		$\mathcal{T}_\varepsilon$	0.041 ± 0.010	0.198 ± 0.079	0.389 ± 0.047	0.257 ± 0.093	0.361 ± 0.111
		$\mathcal{S}_{\varepsilon,B}$	0.161 ± 0.018	0.582 ± 0.204	0.759 ± 0.015	0.673 ± 0.086	5.920 ± 7.937
		$\mathcal{T}_{\varepsilon,B}$	0.149 ± 0.019	0.569 ± 0.2	0.757 ± 0.015	0.623 ± 0.133	3.547 ± 5.67
	200	$\mathcal{S}_\varepsilon$	0.021 ± 0.007	0.020 ± 0.008	0.007 ± 0.007	0.029 ± 0.021	0.053 ± 0.047
		$\mathcal{T}_\varepsilon$	0.014 ± 0.005	0.158 ± 0.065	0.332 ± 0.055	0.237 ± 0.097	0.361 ± 0.111
		$\mathcal{S}_{\varepsilon,B}$	0.152 ± 0.019	0.572 ± 0.203	0.755 ± 0.015	0.670 ± 0.080	6.110 ± 7.866
		$\mathcal{T}_{\varepsilon,B}$	0.103 ± 0.017	0.543 ± 0.195	0.746 ± 0.016	0.603 ± 0.141	2.817 ± 3.886
Ellipse	16	$\mathcal{S}_\varepsilon$	0.178 ± 0.029	0.244 ± 0.074	0.159 ± 0.045	0.187 ± 0.076	0.149 ± 0.093
		$\mathcal{T}_\varepsilon$	0.176 ± 0.027	0.244 ± 0.078	0.235 ± 0.063	0.235 ± 0.111	0.232 ± 0.114
		$\mathcal{S}_{\varepsilon,B}$	0.188 ± 0.014	0.221 ± 0.036	0.562 ± 0.027	0.602 ± 0.191	3.180 ± 3.799
		$\mathcal{T}_{\varepsilon,B}$	0.257 ± 0.041	0.232 ± 0.048	0.600 ± 0.035	0.898 ± 0.466	3.276 ± 4.107
	64	$\mathcal{S}_\varepsilon$	0.043 ± 0.010	0.049 ± 0.019	0.028 ± 0.013	0.051 ± 0.029	0.065 ± 0.053
		$\mathcal{T}_\varepsilon$	0.047 ± 0.011	0.050 ± 0.018	0.196 ± 0.068	0.075 ± 0.051	0.163 ± 0.089
		$\mathcal{S}_{\varepsilon,B}$	0.187 ± 0.014	0.221 ± 0.039	0.517 ± 0.030	0.659 ± 0.262	3.510 ± 4.736
		$\mathcal{T}_{\varepsilon,B}$	0.425 ± 0.046	0.243 ± 0.055	0.625 ± 0.027	0.615 ± 0.117	3.603 ± 5.454
	200	$\mathcal{S}_\varepsilon$	0.021 ± 0.007	0.021 ± 0.009	0.008 ± 0.007	0.030 ± 0.021	0.049 ± 0.045
		$\mathcal{T}_\varepsilon$	0.019 ± 0.006	0.019 ± 0.009	0.039 ± 0.050	0.087 ± 0.074	0.250 ± 0.121
		$\mathcal{S}_{\varepsilon,B}$	0.177 ± 0.022	0.219 ± 0.058	0.531 ± 0.030	0.677 ± 0.285	3.848 ± 4.900
		$\mathcal{T}_{\varepsilon,B}$	0.198 ± 0.042	0.219 ± 0.070	0.512 ± 0.032	0.907 ± 0.523	3.609 ± 5.109
Single Gaussian	16	$\mathcal{S}_\varepsilon$	0.180 ± 0.030	0.252 ± 0.076	0.156 ± 0.043	0.183 ± 0.073	0.200 ± 0.087
		$\mathcal{T}_\varepsilon$	0.239 ± 0.037	0.232 ± 0.051	0.146 ± 0.040	0.227 ± 0.082	0.363 ± 0.121
		$\mathcal{S}_{\varepsilon,B}$	1.85 ± 0.068	2.332 ± 0.891	0.248 ± 0.04	2.314 ± 0.78	7.204 ± 8.48
		$\mathcal{T}_{\varepsilon,B}$	2.742 ± 0.080	3.300 ± 1.244	0.252 ± 0.044	3.480 ± 1.063	20.436 ± 24.422
	64	$\mathcal{S}_\varepsilon$	0.057 ± 0.013	0.080 ± 0.034	0.033 ± 0.016	0.063 ± 0.032	0.075 ± 0.052
		$\mathcal{T}_\varepsilon$	0.078 ± 0.016	0.110 ± 0.044	0.037 ± 0.015	0.123 ± 0.054	0.257 ± 0.124
		$\mathcal{S}_{\varepsilon,B}$	2.883 ± 0.092	3.565 ± 1.341	0.29 ± 0.048	2.6 ± 1.09	9.931 ± 11.224
		$\mathcal{T}_{\varepsilon,B}$	2.762 ± 0.083	3.249 ± 1.199	0.261 ± 0.041	3.179 ± 0.951	15.886 ± 17.536
	200	$\mathcal{S}_\varepsilon$	0.034 ± 0.009	0.039 ± 0.017	0.013 ± 0.010	0.040 ± 0.024	0.059 ± 0.047
		$\mathcal{T}_\varepsilon$	0.069 ± 0.016	0.075 ± 0.026	0.014 ± 0.010	0.088 ± 0.044	0.219 ± 0.100
		$\mathcal{S}_{\varepsilon,B}$	1.179 ± 0.052	1.791 ± 0.716	0.17 ± 0.032	2.17 ± 0.712	10.473 ± 14.457
		$\mathcal{T}_{\varepsilon,B}$	2.707 ± 0.079	3.286 ± 1.236	0.263 ± 0.042	2.997 ± 0.903	16.368 ± 19.089
Gaussian Mixture	16	$\mathcal{S}_\varepsilon$	0.183 ± 0.031	0.231 ± 0.062	0.163 ± 0.046	0.179 ± 0.072	0.154 ± 0.092
		$\mathcal{T}_\varepsilon$	0.176 ± 0.027	0.204 ± 0.047	0.176 ± 0.049	0.178 ± 0.069	0.209 ± 0.099
		$\mathcal{S}_{\varepsilon,B}$	0.215 ± 0.015	0.2145 ± 0.039	0.292 ± 0.041	0.259 ± 0.069	1.880 ± 2.784
		$\mathcal{T}_{\varepsilon,B}$	2.175 ± 0.103	1.408 ± 0.223	0.392 ± 0.049	0.425 ± 0.179	5.125 ± 6.170
	64	$\mathcal{S}_\varepsilon$	0.054 ± 0.013	0.061 ± 0.020	0.032 ± 0.019	0.047 ± 0.027	0.065 ± 0.053
		$\mathcal{T}_\varepsilon$	0.060 ± 0.013	0.059 ± 0.016	0.054 ± 0.027	0.054 ± 0.027	0.250 ± 0.127
		$\mathcal{S}_{\varepsilon,B}$	0.261 ± 0.015	0.266 ± 0.036	0.343 ± 0.035	0.274 ± 0.049	1.941 ± 3.493
		$\mathcal{T}_{\varepsilon,B}$	1.222 ± 0.065	0.952 ± 0.198	0.378 ± 0.048	0.357 ± 0.146	4.485 ± 5.514
	200	$\mathcal{S}_\varepsilon$	0.027 ± 0.008	0.030 ± 0.013	0.010 ± 0.009	0.023 ± 0.014	0.042 ± 0.037
		$\mathcal{T}_\varepsilon$	0.032 ± 0.010	0.029 ± 0.012	0.021 ± 0.019	0.030 ± 0.019	0.232 ± 0.098
		$\mathcal{S}_{\varepsilon,B}$	0.179 ± 0.015	0.215 ± 0.047	0.276 ± 0.040	0.284 ± 0.100	2.111 ± 3.048
		$\mathcal{T}_{\varepsilon,B}$	1.550 ± 0.086	1.220 ± 0.212	0.352 ± 0.045	0.416 ± 0.185	4.501 ± 7.400
ModelNet	16	$\mathcal{S}_\varepsilon$	0.209 ± 0.035	0.268 ± 0.075	0.199 ± 0.058	0.206 ± 0.082	0.149 ± 0.098
		$\mathcal{T}_\varepsilon$	0.448 ± 0.029	0.408 ± 0.073	0.683 ± 0.053	0.486 ± 0.126	0.150 ± 0.096
		$\mathcal{S}_{\varepsilon,B}$	0.255 ± 0.017	0.384 ± 0.088	0.660 ± 0.023	0.627 ± 0.124	0.363 ± 0.538
		$\mathcal{T}_{\varepsilon,B}$	0.589 ± 0.048	0.775 ± 0.373	0.793 ± 0.019	0.664 ± 0.122	0.533 ± 0.814
	64	$\mathcal{S}_\varepsilon$	0.113 ± 0.022	0.148 ± 0.043	0.182 ± 0.052	0.106 ± 0.084	0.041 ± 0.038
		$\mathcal{T}_\varepsilon$	0.303 ± 0.027	0.217 ± 0.051	0.332 ± 0.060	0.274 ± 0.124	0.048 ± 0.040
		$\mathcal{S}_{\varepsilon,B}$	0.322 ± 0.019	0.434 ± 0.093	0.693 ± 0.023	0.65 ± 0.127	0.379 ± 1.459
		$\mathcal{T}_{\varepsilon,B}$	0.593 ± 0.058	0.703 ± 0.229	0.249 ± 0.036	0.476 ± 0.235	4.355 ± 5.257
	200	$\mathcal{S}_\varepsilon$	0.037 ± 0.015	0.047 ± 0.029	0.021 ± 0.015	0.043 ± 0.033	0.024 ± 0.030
		$\mathcal{T}_\varepsilon$	0.169 ± 0.022	0.183 ± 0.040	0.466 ± 0.046	0.286 ± 0.105	0.030 ± 0.025
		$\mathcal{S}_{\varepsilon,B}$	0.388 ± 0.021	0.451 ± 0.062	0.701 ± 0.024	0.608 ± 0.118	0.379 ± 0.988
		$\mathcal{T}_{\varepsilon,B}$	0.494 ± 0.047	0.708 ± 0.312	0.791 ± 0.019	0.668 ± 0.114	0.512 ± 0.833
Mixed	16	$\mathcal{S}_\varepsilon$	0.179 ± 0.030	0.238 ± 0.069	0.157 ± 0.043	0.180 ± 0.075	0.150 ± 0.093
		$\mathcal{T}_\varepsilon$	0.189 ± 0.031	0.245 ± 0.071	0.162 ± 0.043	0.189 ± 0.075	0.235 ± 0.106
		$\mathcal{S}_{\varepsilon,B}$	0.157 ± 0.017	0.259 ± 0.089	0.207 ± 0.029	0.345 ± 0.135	1.611 ± 2.038
		$\mathcal{T}_{\varepsilon,B}$	0.416 ± 0.050	0.521 ± 0.187	0.217 ± 0.037	0.477 ± 0.224	5.080 ± 18.203
	64	$\mathcal{S}_\varepsilon$	0.040 ± 0.010	0.047 ± 0.019	0.020 ± 0.012	0.042 ± 0.025	0.055 ± 0.049
		$\mathcal{T}_\varepsilon$	0.044 ± 0.010	0.055 ± 0.024	0.025 ± 0.014	0.066 ± 0.042	0.117 ± 0.068
		$\mathcal{S}_{\varepsilon,B}$	0.148 ± 0.013	0.183 ± 0.062	0.16 ± 0.024	0.278 ± 0.102	1.518 ± 2.288
		$\mathcal{T}_{\varepsilon,B}$	0.593 ± 0.058	0.703 ± 0.229	0.249 ± 0.036	0.476 ± 0.235	4.355 ± 5.257
	200	$\mathcal{S}_\varepsilon$	0.017 ± 0.006	0.017 ± 0.009	0.004 ± 0.005	0.022 ± 0.016	0.032 ± 0.032
		$\mathcal{T}_\varepsilon$	0.023 ± 0.007	0.023 ± 0.012	0.005 ± 0.006	0.035 ± 0.029	0.112 ± 0.063
		$\mathcal{S}_{\varepsilon,B}$	0.154 ± 0.012	0.178 ± 0.035	0.159 ± 0.023	0.244 ± 0.067	1.631 ± 2.385
		$\mathcal{T}_{\varepsilon,B}$	0.625 ± 0.082	0.726 ± 0.219	0.216 ± 0.037	0.451 ± 0.212	5.681 ± 7.941

Table 11: $\mathcal{E}_{\text{dir}}$ across all 5D datasets for various ϵ-kernel sizes. Note that we already report performance for the mixed synthetic data in the tables in the main text so we do not report the performance here.

Train dataset	ϵ	Method	Uniform Ball	Ellipse	Single Gaussian	Gaussian Mixture
Uniform Ball	16	$\mathcal{S}_\varepsilon$	0.431 ± 0.043	0.562 ± 0.086	0.426 ± 0.067	0.524 ± 0.102
		$\mathcal{T}_\varepsilon$	0.464 ± 0.048	0.514 ± 0.069	0.676 ± 0.038	0.599 ± 0.092
		$\mathcal{S}_{\varepsilon,B}$	0.440 ± 0.047	0.742 ± 0.248	0.803 ± 0.012	0.725 ± 0.111
		$\mathcal{T}_{\varepsilon,B}$	0.352 ± 0.044	0.684 ± 0.202	0.816 ± 0.011	0.741 ± 0.099
	64	$\mathcal{S}_\varepsilon$	0.188 ± 0.025	0.247 ± 0.057	0.159 ± 0.033	0.232 ± 0.058
		$\mathcal{T}_\varepsilon$	0.197 ± 0.027	0.366 ± 0.066	0.538 ± 0.033	0.362 ± 0.092
		$\mathcal{S}_{\varepsilon,B}$	0.242 ± 0.027	0.621 ± 0.177	0.796 ± 0.011	0.695 ± 0.133
		$\mathcal{T}_{\varepsilon,B}$	0.248 ± 0.033	0.633 ± 0.199	0.791 ± 0.011	0.702 ± 0.113
	200	$\mathcal{S}_\varepsilon$	0.084 ± 0.016	0.112 ± 0.038	0.058 ± 0.023	0.103 ± 0.038
		$\mathcal{T}_\varepsilon$	0.118 ± 0.023	0.202 ± 0.052	0.369 ± 0.047	0.356 ± 0.113
		$\mathcal{S}_{\varepsilon,B}$	0.238 ± 0.03	0.63 ± 0.198	0.79 ± 0.011	0.669 ± 0.105
		$\mathcal{T}_{\varepsilon,B}$	0.23 ± 0.029	0.625 ± 0.193	0.786 ± 0.012	0.704 ± 0.118
Ellipse	16	$\mathcal{S}_\varepsilon$	0.547 ± 0.066	0.549 ± 0.072	0.554 ± 0.089	0.609 ± 0.107
		$\mathcal{T}_\varepsilon$	0.534 ± 0.066	0.534 ± 0.072	0.577 ± 0.054	0.553 ± 0.102
		$\mathcal{S}_{\varepsilon,B}$	0.351 ± 0.032	0.394 ± 0.070	0.844 ± 0.017	1.035 ± 0.295
		$\mathcal{T}_{\varepsilon,B}$	0.370 ± 0.047	0.514 ± 0.158	0.758 ± 0.029	0.872 ± 0.216
	64	$\mathcal{S}_\varepsilon$	0.193 ± 0.024	0.213 ± 0.043	0.168 ± 0.033	0.187 ± 0.048
		$\mathcal{T}_\varepsilon$	0.313 ± 0.051	0.302 ± 0.063	0.543 ± 0.034	0.417 ± 0.095
		$\mathcal{S}_{\varepsilon,B}$	0.356 ± 0.043	0.498 ± 0.125	0.894 ± 0.011	0.825 ± 0.157
		$\mathcal{T}_{\varepsilon,B}$	0.351 ± 0.054	0.548 ± 0.174	0.702 ± 0.026	0.902 ± 0.280
	200	$\mathcal{S}_\varepsilon$	0.091 ± 0.017	0.085 ± 0.024	0.069 ± 0.017	0.094 ± 0.031
		$\mathcal{T}_\varepsilon$	0.092 ± 0.018	0.084 ± 0.024	0.369 ± 0.042	0.239 ± 0.091
		$\mathcal{S}_{\varepsilon,B}$	0.257 ± 0.031	0.399 ± 0.108	0.695 ± 0.02	0.814 ± 0.161
		$\mathcal{T}_{\varepsilon,B}$	0.35 ± 0.043	0.343 ± 0.096	0.721 ± 0.024	0.77 ± 0.188
Gaussian	16	$\mathcal{S}_\varepsilon$	0.488 ± 0.066	0.529 ± 0.072	0.448 ± 0.075	0.565 ± 0.142
		$\mathcal{T}_\varepsilon$	0.728 ± 0.061	0.722 ± 0.068	0.467 ± 0.073	0.631 ± 0.095
		$\mathcal{S}_{\varepsilon,B}$	3.627 ± 0.169	4.249 ± 1.076	0.436 ± 0.064	2.446 ± 0.675
		$\mathcal{T}_{\varepsilon,B}$	3.601 ± 0.171	4.290 ± 1.114	0.410 ± 0.052	3.043 ± 0.677
	64	$\mathcal{S}_\varepsilon$	0.204 ± 0.027	0.250 ± 0.050	0.163 ± 0.033	0.196 ± 0.049
		$\mathcal{T}_\varepsilon$	0.471 ± 0.055	0.452 ± 0.064	0.205 ± 0.045	0.411 ± 0.099
		$\mathcal{S}_{\varepsilon,B}$	3.122 ± 0.109	4.051 ± 1.045	0.291 ± 0.035	2.106 ± 0.666
		$\mathcal{T}_{\varepsilon,B}$	3.434 ± 0.127	4.332 ± 1.130	0.354 ± 0.050	3.225 ± 0.734
	200	$\mathcal{S}_\varepsilon$	0.095 ± 0.017	0.116 ± 0.038	0.065 ± 0.019	0.102 ± 0.032
		$\mathcal{T}_\varepsilon$	0.177 ± 0.026	0.170 ± 0.041	0.065 ± 0.022	0.165 ± 0.056
		$\mathcal{S}_{\varepsilon,B}$	3.46 ± 0.12	4.421 ± 1.108	0.352 ± 0.048	2.069 ± 0.718
		$\mathcal{T}_{\varepsilon,B}$	3.297 ± 0.112	4.206 ± 1.096	0.333 ± 0.044	3.018 ± 0.59
Gaussian Mixture	16	$\mathcal{S}_\varepsilon$	0.546 ± 0.066	0.539 ± 0.074	0.460 ± 0.079	0.501 ± 0.098
		$\mathcal{T}_\varepsilon$	0.622 ± 0.060	0.571 ± 0.071	0.516 ± 0.081	0.504 ± 0.098
		$\mathcal{S}_{\varepsilon,B}$	0.342 ± 0.030	0.413 ± 0.078	0.438 ± 0.039	0.573 ± 0.194
		$\mathcal{T}_{\varepsilon,B}$	1.097 ± 0.141	1.314 ± 0.329	0.434 ± 0.040	1.002 ± 0.433
	64	$\mathcal{S}_\varepsilon$	0.193 ± 0.025	0.213 ± 0.041	0.164 ± 0.032	0.170 ± 0.045
		$\mathcal{T}_\varepsilon$	0.197 ± 0.025	0.205 ± 0.039	0.182 ± 0.036	0.174 ± 0.046
		$\mathcal{S}_{\varepsilon,B}$	0.427 ± 0.025	0.409 ± 0.044	0.465 ± 0.035	0.444 ± 0.113
		$\mathcal{T}_{\varepsilon,B}$	1.731 ± 0.143	1.925 ± 0.391	0.447 ± 0.035	0.860 ± 0.395
	200	$\mathcal{S}_\varepsilon$	0.093 ± 0.017	0.103 ± 0.030	0.073 ± 0.019	0.084 ± 0.028
		$\mathcal{T}_\varepsilon$	0.097 ± 0.018	0.093 ± 0.025	0.084 ± 0.025	0.091 ± 0.032
		$\mathcal{S}_{\varepsilon,B}$	0.487 ± 0.045	0.541 ± 0.121	0.366 ± 0.046	0.717 ± 0.207
		$\mathcal{T}_{\varepsilon,B}$	2.154 ± 0.122	1.953 ± 0.287	0.356 ± 0.042	0.757 ± 0.278
Mixed	16	$\mathcal{S}_\varepsilon$	0.562 ± 0.065	0.544 ± 0.073	0.485 ± 0.085	0.512 ± 0.101
		$\mathcal{T}_\varepsilon$	0.602 ± 0.063	0.559 ± 0.071	0.477 ± 0.078	0.524 ± 0.095
		$\mathcal{S}_{\varepsilon,B}$	0.349 ± 0.031	0.412 ± 0.097	0.360 ± 0.037	0.675 ± 0.217
		$\mathcal{T}_{\varepsilon,B}$	1.883 ± 0.188	2.458 ± 0.684	0.391 ± 0.049	1.525 ± 0.572
	64	$\mathcal{S}_\varepsilon$	0.194 ± 0.026	0.220 ± 0.045	0.162 ± 0.032	0.177 ± 0.047
		$\mathcal{T}_\varepsilon$	0.202 ± 0.025	0.228 ± 0.046	0.168 ± 0.034	0.188 ± 0.051
		$\mathcal{S}_{\varepsilon,B}$	0.265 ± 0.032	0.351 ± 0.087	0.285 ± 0.04	0.592 ± 0.224
		$\mathcal{T}_{\varepsilon,B}$	0.977 ± 0.102	1.632 ± 0.448	0.336 ± 0.042	1.276 ± 0.455
	200	$\mathcal{S}_\varepsilon$	0.085 ± 0.017	0.076 ± 0.022	0.060 ± 0.020	0.079 ± 0.031
		$\mathcal{T}_\varepsilon$	0.094 ± 0.018	0.094 ± 0.028	0.064 ± 0.020	0.096 ± 0.047
		$\mathcal{S}_{\varepsilon,B}$	0.195 ± 0.017	0.294 ± 0.079	0.257 ± 0.034	0.551 ± 0.216
		$\mathcal{T}_{\varepsilon,B}$	3.092 ± 0.164	2.999 ± 0.699	0.314 ± 0.041	1.575 ± 0.424

Table 12: Results for minimum enclosing ball (2D). We report the relative error for the predicted radius (w.r.t to ground truth radius) ($\mathcal{E}_{\mathrm{r}}$) and percentage of points excluded from the predicted enclosing ball ($\mathcal{E}_{\mathrm{p}}$). All processors are configured to output a coarsened set of 16 points and frozen processors are trained on mixed synthetic data. Boldface indicates the best performing method while underlines denote best performing *neural* method.

Train Set	Architecture	$\mathcal{E}_{\mathbf{r}}$	$\mathcal{E}_{\mathbf{p}}(\%)$
Uniform Disk	$\mathcal{S}_{\mathrm{extent}}$ (Frozen)	$\underline{0.009 \pm 0.008}$	1.9 ± 1.3
	$\mathcal{S}_{\mathrm{extent}}$ (E2E)	0.023 ± 0.019	2.3 ± 1.9
	$\mathcal{T}_{\mathrm{extent}}$ (Frozen)	0.099 ± 0.050	$\underline{0.1 \pm 0.3}$
	$\mathcal{T}_{\mathrm{extent}}$ (E2E)	0.024 ± 0.020	1.4 ± 1.8
	$\mathcal{S}_{\mathrm{Baseline}}$ (E2E)	0.048 ± 0.028	0.5 ± 1.0
	$\mathcal{T}_{\mathrm{Baseline}}$ (E2E)	0.030 ± 0.024	0.3 ± 3.0
	$\mathcal{S}_{\mathrm{Direct}}$	0.012 ± 0.006	3.2 ± 1.3
	$\mathcal{T}_{\mathrm{Direct}}$	0.022 ± 0.018	7.1 ± 3.8
	ε-kernel + Exact	$\mathbf{0.000002 \pm 0.00009}$	$\mathbf{0 \pm 0}$
SQUID	$\mathcal{S}_{\mathrm{extent}}$ (Frozen)	0.020 ± 0.200	2.0 ± 3.0
	$\mathcal{S}_{\mathrm{extent}}$ (E2E)	$\underline{0.010 \pm 0.010}$	2.0 ± 3.0
	$\mathcal{T}_{\mathrm{extent}}$ (Frozen)	0.068 ± 0.045	$\underline{1.6 \pm 3.2}$
	$\mathcal{T}_{\mathrm{extent}}$ (E2E)	0.190 ± 0.090	4.0 ± 5.0
	$\mathcal{S}_{\mathrm{Baseline}}$ (E2E)	0.027 ± 0.025	2.8 ± 2.5
	$\mathcal{T}_{\mathrm{Baseline}}$ (E2E)	0.039 ± 0.034	4.5 ± 3.8
	$\mathcal{S}_{\mathrm{Direct}}$	0.058 ± 0.046	3.3 ± 4.4
	$\mathcal{T}_{\mathrm{Direct}}$	0.685 ± 0.065	83.3 ± 10.7
	ε-kernel + Exact	$\mathbf{0.00004 \pm 0.0006}$	$\mathbf{0 \pm 0}$

Table 13: Results for minimum enclosing ball (3D). We report the relative error for the predicted radius ($\mathcal{E}_{\mathrm{r}}$) and the percentage of points which excluded from the estimated ball ($\mathcal{E}_{\mathrm{p}}(\%)$). All frozen processors are trained on mixed synthetic data. Boldface indicates the best performing method while underlines denote best performing *neural* method.

Train Set	Architecture	$\mathcal{E}_{\mathbf{r}}$	$\mathcal{E}_{\mathbf{p}}(\%)$
Uniform Ball	$\mathcal{S}_{\mathrm{extent}}$ (Frozen)	0.030 ± 0.020	$\underline{0.7 \pm 1.0}$
	$\mathcal{S}_{\mathrm{extent}}$ (E2E)	0.035 ± 0.028	2.8 ± 3.4
	$\mathcal{T}_{\mathrm{extent}}$ (Frozen)	0.020 ± 0.018	4.6 ± 3.8
	$\mathcal{T}_{\mathrm{extent}}$ (E2E)	0.076 ± 0.051	2.0 ± 4.0
	$\mathcal{S}_{\mathrm{Baseline}}$ (E2E)	0.056 ± 0.031	1.8 ± 2.5
	$\mathcal{T}_{\mathrm{Baseline}}$ (E2E)	0.035 ± 0.032	8.6 ± 6.5
	$\mathcal{S}_{\mathrm{Direct}}$	$\underline{0.014 \pm 0.011}$	1.6 ± 1.5
	$\mathcal{T}_{\mathrm{Direct}}$	0.028 ± 0.017	1.7 ± 5.9
	ε-kernel + Exact	$\mathbf{0.001 \pm 0.003}$	$\mathbf{0 \pm 0}$
ModelNet	$\mathcal{S}_{\mathrm{extent}}$ (Frozen)	0.100 ± 0.070	$\underline{0.2 \pm 0.7}$
	$\mathcal{S}_{\mathrm{extent}}$ (E2E)	0.060 ± 0.050	0.2 ± 0.9
	$\mathcal{T}_{\mathrm{extent}}$ (Frozen)	0.077 ± 0.072	0.6 ± 1.3
	$\mathcal{T}_{\mathrm{extent}}$ (E2E)	$\underline{0.029 \pm 0.032}$	3.3 ± 4.4
	$\mathcal{S}_{\mathrm{Baseline}}$ (E2E)	0.053 ± 0.058	1.6 ± 2.5
	$\mathcal{T}_{\mathrm{Baseline}}$ (E2E)	0.858 ± 0.289	57.3 ± 39.6
	$\mathcal{S}_{\mathrm{Direct}}$	0.214 ± 0.179	8.1 ± 9.7
	$\mathcal{T}_{\mathrm{Direct}}$	0.033 ± 0.02	3.6 ± 3.8
	ε-kernel + Exact	$\mathbf{0.0005 \pm 0.0023}$	$\mathbf{0.27 \pm 2.67}$

Table 14: Minimum enclosing ellipse error for point clouds in $\mathbb{R}^2$ on in-distribution test data, comparing frozen and end-to-end (E2E) training procedures. All frozen processors are trained on mixed synthetic data. We report the relative error in major ($\mathcal{E}_{\mathrm{r,maj}}$) and minor radii ($\mathcal{E}_{\mathrm{r,min}}$) and the percentage of points excluded ($\mathcal{E}_{\mathrm{p}}(\%)$). Boldface indicates the best performing method while underlines denote best performing *neural* method.

Train Set	**Architecture**	$\mathcal{E}_{\mathrm{r,min}}$	$\mathcal{E}_{\mathrm{r,maj}}$	$\mathcal{E}_{\mathrm{p}}$ (%)
Synthetic Ellipses	$\mathcal{S}_{\mathrm{extent}}$ (Frozen)	0.037 ± 0.037	$\underline{0.022 \pm 0.018}$	$\underline{5.1 \pm 5.2}$
	$\mathcal{S}_{\mathrm{extent}}$ (E2E)	0.056 ± 0.047	0.047 ± 0.035	9.1 ± 5.4
	$\mathcal{T}_{\mathrm{extent}}$ (Frozen)	0.041 ± 0.040	0.027 ± 0.020	7.5 ± 5.4
	$\mathcal{T}_{\mathrm{extent}}$ (E2E)	0.038 ± 0.033	0.022 ± 0.019	6.5 ± 5.3
	$\mathcal{S}_{\mathrm{Baseline}}$ (E2E)	0.378 ± 0.234	0.426 ± 0.387	27.7 ± 25.1
	$\mathcal{T}_{\mathrm{Baseline}}$ (E2E)	0.071 ± 0.660	0.047 ± 0.038	8.8 ± 7.2
	$\mathcal{S}_{\mathrm{Direct}}$	$\underline{0.033 \pm 0.025}$	0.039 ± 0.022	9.8 ± 4.4
	$\mathcal{T}_{\mathrm{Direct}}$	0.035 ± 0.03	0.025 ± 0.019	6.6 ± 4.9
	ε-kernel + Exact	$\mathbf{0.0004 \pm 0.003}$	$\mathbf{0.0001 \pm 0.0009}$	$\mathbf{3.3 \pm 1.3}$
SQUID	$\mathcal{S}_{\mathrm{extent}}$ (Frozen)	$\underline{0.056 \pm 0.047}$	0.047 ± 0.035	6.6 ± 5.4
	$\mathcal{S}_{\mathrm{extent}}$ (E2E)	0.078 ± 0.065	0.050 ± 0.038	13.9 ± 7.2
	$\mathcal{T}_{\mathrm{extent}}$ (Frozen)	0.058 ± 0.051	$\underline{0.032 \pm 0.026}$	12.5 ± 6.6
	$\mathcal{T}_{\mathrm{extent}}$ (E2E)	0.093 ± 0.074	0.045 ± 0.034	14.4 ± 7.7
	$\mathcal{S}_{\mathrm{Baseline}}$ (E2E)	0.322 ± 0.365	0.250 ± 0.262	32.0 ± 16.6
	$\mathcal{T}_{\mathrm{Baseline}}$ (E2E)	0.357 ± 0.550	0.049 ± 0.041	16.8 ± 18.4
	$\mathcal{S}_{\mathrm{Direct}}$	0.684 ± 0.729	0.049 ± 0.039	$\underline{0 \pm 0}$
	$\mathcal{T}_{\mathrm{Direct}}$	1.483 ± 1.287	0.128 ± 0.064	1.8 ± 0.7
	ε-kernel + Exact	$\mathbf{0.004 \pm 0.028}$	$\mathbf{0.002 \pm 0.014}$	$\mathbf{7.7 \pm 5.34}$

Table 15: Minimum enclosing annulus error on in-distribution test data, comparing frozen and end-to-end (E2E) training procedures. All frozen processors are trained on mixed synthetic data. We report the relative error in the width of the annuli and the proportion of points excluded

Train Set	**Architecture**	$\mathcal{E}_{\mathrm{w}}$	$\mathcal{E}_{\mathrm{p}}$ (%)
Synthetic Annuli	$\mathcal{S}_{\mathrm{extent}}$ (Frozen)	0.050 ± 0.070	$\underline{\mathbf{4.26 \pm 4.94}}$
	$\mathcal{S}_{\mathrm{extent}}$ (E2E)	$\underline{0.038 \pm 0.042}$	5.55 ± 4.64
	$\mathcal{T}_{\mathrm{extent}}$ (Frozen)	0.077 ± 0.104	11.39 ± 8.02
	$\mathcal{T}_{\mathrm{extent}}$ (E2E)	0.083 ± 0.087	12.53 ± 4.64
	$\mathcal{S}_{\mathrm{Baseline}}$	0.128 ± 0.263	5.27 ± 5.27
	$\mathcal{T}_{\mathrm{Baseline}}$	0.417 ± 0.574	4.39 ± 8.22
	$\mathcal{S}_{\mathrm{Direct}}$	0.141 ± 0.117	4.99 ± 6.95
	$\mathcal{T}_{\mathrm{Direct}}$	0.076 ± 0.120	4.43 ± 6.25
	ε-kernel + Exact	$\mathbf{0.022 \pm 0.07}$	4.32 ± 5.9
SQUID	$\mathcal{S}_{\mathrm{extent}}$ (Frozen)	0.073 ± 0.110	$\underline{6.31 \pm 4.15}$
	$\mathcal{S}_{\mathrm{extent}}$ (E2E)	0.087 ± 0.103	8.42 ± 4.64
	$\mathcal{T}_{\mathrm{extent}}$ (Frozen)	0.064 ± 0.084	9.60 ± 4.75
	$\mathcal{T}_{\mathrm{extent}}$ (E2E)	0.104 ± 0.133	6.43 ± 4.21
	$\mathcal{S}_{\mathrm{Baseline}}$ (E2E)	0.191 ± 0.219	7.23 ± 5.04
	$\mathcal{T}_{\mathrm{Baseline}}$ (E2E)	0.118 ± 0.120	11.9 ± 6.86
	$\mathcal{S}_{\mathrm{Direct}}$	$\underline{\mathbf{0.041 \pm 0.079}}$	9.87 ± 6.05
	$\mathcal{T}_{\mathrm{Direct}}$	0.065 ± 0.102	10.2 ± 4.66
	ε-kernel + Exact	0.111 ± 0.095	$\mathbf{0.213 \pm 0.122}$

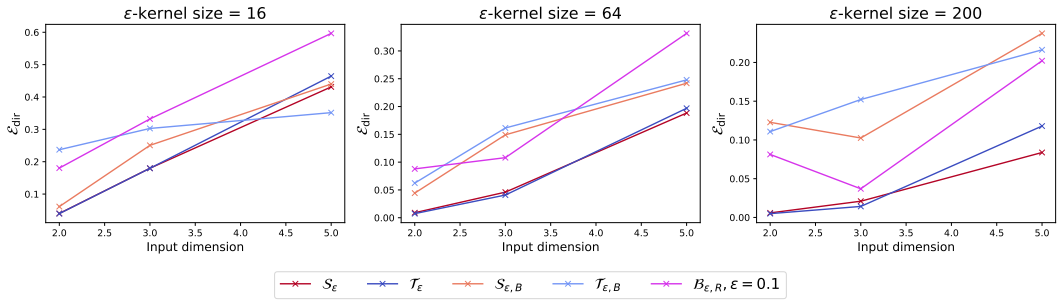

Figure 7: Directional width error ($\mathcal{E}_{\text{dir}}$) vs. the input dimension of the point cloud. We train each model on 'Uniform Ball' datasets in $\mathbb{R}^2$, $\mathbb{R}^3$ and $\mathbb{R}^5$ and test on in-distribution dataset. We notice that all models, as well as the baseline algorithm have increasing directional width error as the input point cloud dimension increases.

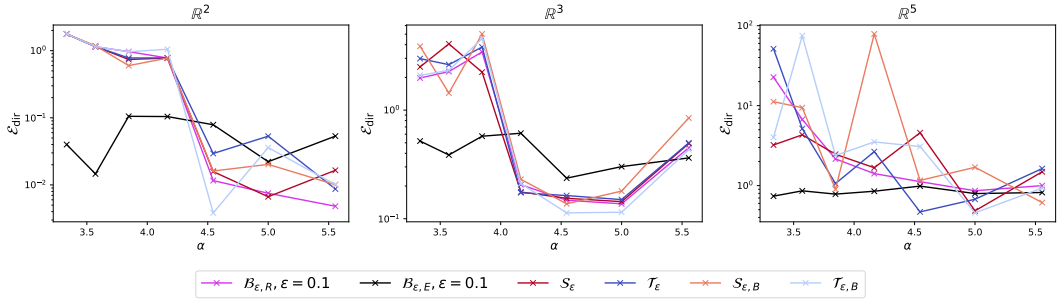

Figure 8: Directional width error ($\mathcal{E}_{\text{dir}}$) vs α-fatness on relaxed-ε-kernel approximation task for $\mathbb{R}^2$ and $\mathbb{R}^3$. We vary the α-fatness of the input data by varying the scale of the minor axes of ellipsoids in $\mathbb{R}^2$ and $\mathbb{R}^3$ and then sampling point clouds from such ellipsoids. Each input point cloud has 100 points and the output ε-kernels are fixed at 64.

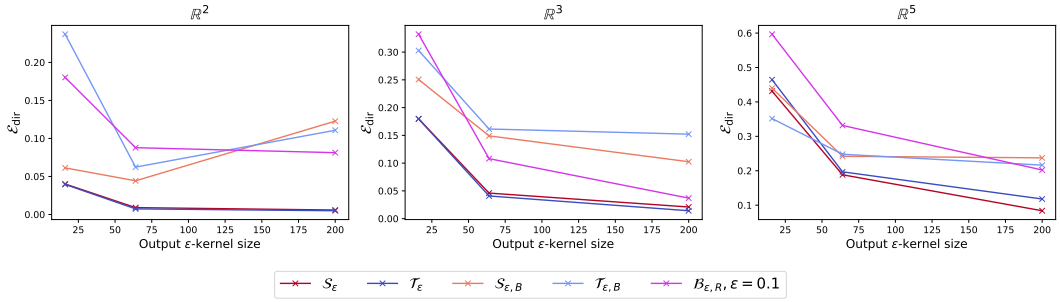

Figure 9: Direction width error $\mathcal{E}_{\text{dir}}$ vs output size of relaxed-ε-kernel size across dimensions. All models are trained and evaluated on point clouds sampled from uniform balls/disks with 500 points per set. Notice that, similar to the baseline algorithm, each model will have better results as we increase output point set size (with SumFormer implementation of $\mathcal{N}_{\phi_\varepsilon}$ still outperforming Transformer).

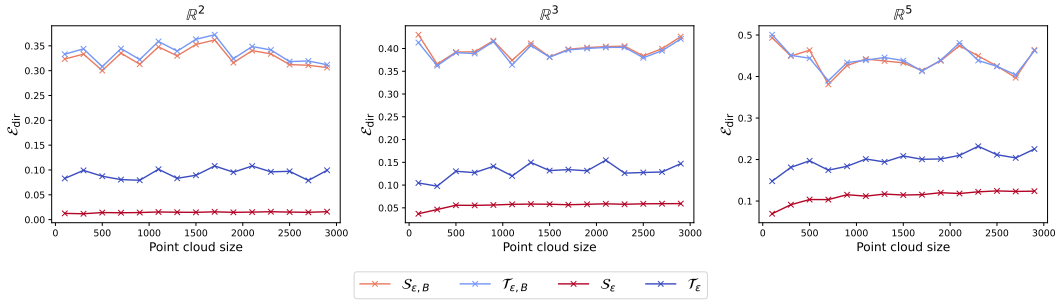

Figure 10: Directional width error $\mathcal{E}_{\text{dir}}$ vs. input point cloud size. All models are trained on the uniform ball/disk dataset and evaluated on uniform ellipses/ellipsoids of varying sizes.

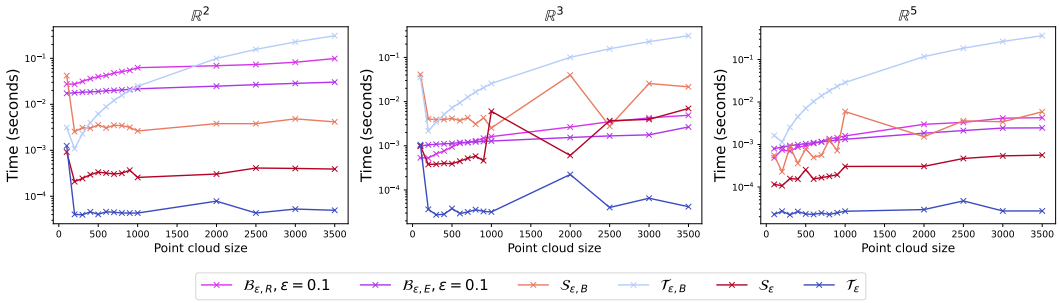

Figure 11: Comparison of inference time for each model along with the runtime of the exact and approximate algorithms for extent measure tasks.

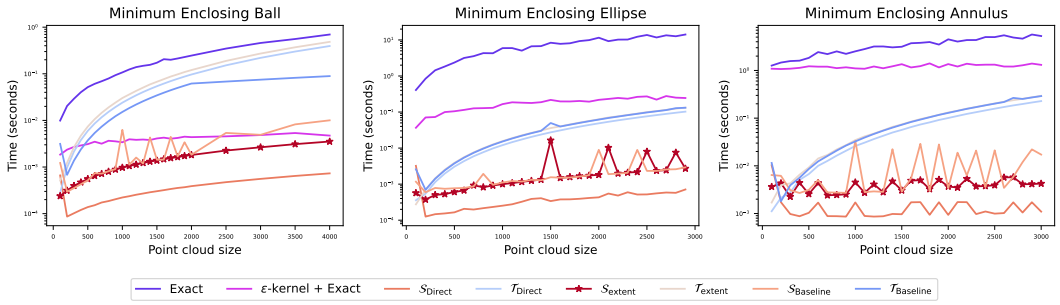

Figure 12: Comparison of inference time for each model along with runtimes of the exact and approximate algorithms for extent measure tasks. Note that our model, $\mathcal{S}_{\text{extent}}$, is significantly faster than all classical algorithmic approaches.

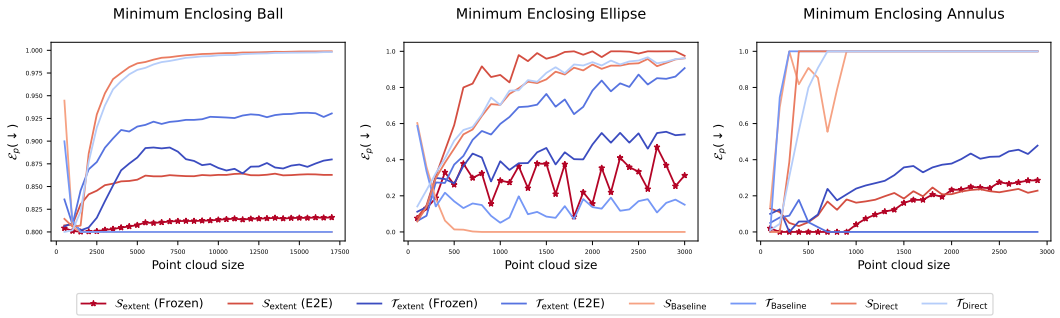

Figure 13: Size generalization across all extent measure tasks. We record the proportion of points missed by the predicted shapes produced by each model on the extent-measure tasks as both the size and bounding box of the input point clouds increase.

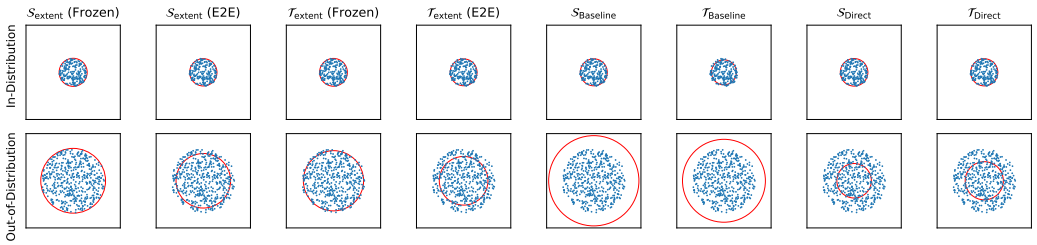

(a) Minimum enclosing ball.

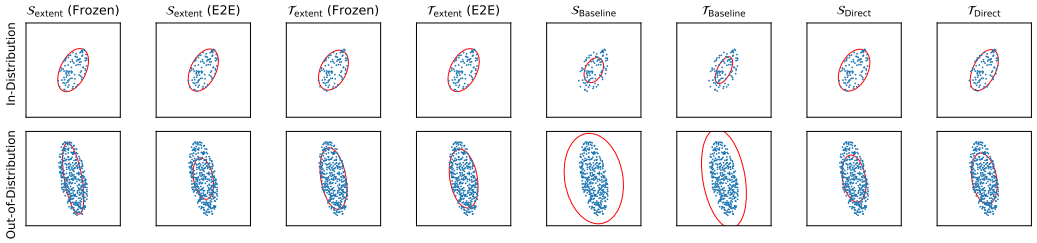

(b) Minimum enclosing ellipse.

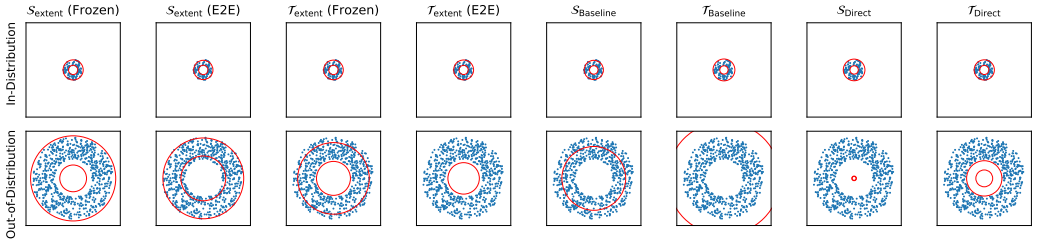

(c) Minimum enclosing annulus.

Figure 14: Visualizations for each extent measure problem. Notice that our frozen model performs much better out-of-distribution than other comparable neural models.